# UNCLASSIFIED

| AD NUMBER |
|---|
| AD241376 |

## LIMITATION CHANGES

**TO:**

Approved for public release; distribution is unlimited.

**FROM:**

Distribution authorized to U.S. Gov't. agencies and their contractors; Administrative/Operational Use; MAR 1960. Other requests shall be referred to U.S. Army Transportation Research Command, Fort Eustis, VA.

## AUTHORITY

THIS PAGE IS UNCLASSIFIED

# UNCLASSIFIED

## AD 241376

# UNCLASSIFIED

# DISCLAIMER NOTICE

THIS DOCUMENT IS BEST QUALITY AVAILABLE. THE COPY FURNISHED TO DTIC CONTAINED A SIGNIFICANT NUMBER OF PAGES WHICH DO NOT REPRODUCE LEGIBLY.
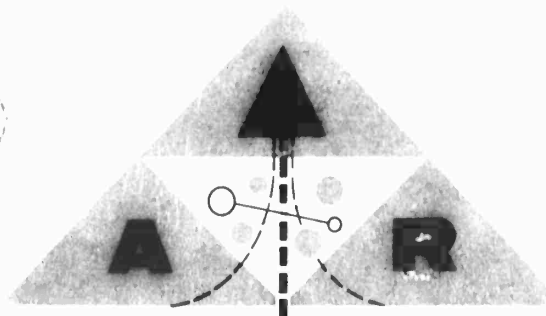
ARD-257

COMPARATIVE PERFORMANCE CHARTS

FOR DUCTED PROPELLERS

Project 9R 38-01-017-24
Contract No. DA-44-177-TC-616

CRD 3460

Project 9R38-01-017-24

Contract DA44-177-TC-616

March 1960


COMPARATIVE PERFORMANCE CHARTS

FOR DUCTED PROPELLERS


Report No. ARD-257


Prepared by:

Aerophysics Department
Advanced Research
Division of Hiller Aircraft Corporation
Palo Alto, California


for


U.S. Army Transportation Research Command
Fort Eustis, Virginia

## TABLE OF CONTENTS

## LIST OF FIGURES

Figure

Figure

# 1. SUMMARY

General comparative performance charts for ducted propellers are presented which show the maximum performance obtained thus far in ducted propeller design. These charts are divided into three basic flight regimes, hovering, axial flow, and non-axial flow.

Visualization water tests of two-dimensional ducted propeller models were conducted. These tests were made to observe what effect various changes in duct diffuser angle, duct chord to diameter ratio and propeller position had on the model wake. The visual results of this program are shown photographically.

Parallel to the water tests, two-dimensional theoretical studies of the shroud and wake shape of a ducted propeller were conducted. These numerical calculations refer to a chord/diameter ratio of one. Similar to the three-dimensional investigations of Reference 4 various combinations of constant and elliptical vorticity distributions along the shroud were assumed. It should be noted that according to the Dickmann-Weissinger theory the location of the propeller in the shroud has no effect on the shroud and wake shap`, which was confirmed by the flow visualization tests.

1

## 2. INTRODUCTION

Improvement in static and low speed axial flow performance of a ducted propeller over that of an open propeller of the same diameter was apparently first found by Luigi Stipa in 1931 (Reference 33). Later Krüger investigated the ducted propeller analytically and experimentally in the axial flow condition from low to high speeds (References 16 and 17). From this work it was found that the increases in performance gained by the ducted propeller at low speeds were not realized at the higher speeds, owing to the drag of the duct.

Numerous experiments with ducted propellers have been made in this and other countries since the above mentioned works were performed. Most of these endeavors have been conducted independently of each other; thus, the total effort in the ducted propeller field shows no continuity, making it extremely difficult to obtain meaningful information for ducted propeller design and performance characteristics. A critical survey of all available information on ducted propellers was conducted by A. H. Sacks and J. A. Burnell of Hiller Aircraft Corporation (Reference 31). This survey was made to give the state of the art regarding the aerodynamics of ducted propellers.

However, the results of the ducted propeller work surveyed in Reference 31 are not in a form that would enable a designer to select a ducted propeller for his immediate application. In order to aid the designer in this respect, the Transportation Research and Engineering Command of the Department of the Army awarded a contract (DA-44-177-TC-616) to the Advanced

Research Division of Hiller Aircraft Corporation for the purpose of
(1) preparing general comparative charts insofar as possible from the
experimental and theoretical information presently available and reviewed
in Reference 31, (2) conducting two-dimensional water experiments to ob-
tain visual data of the ducted propeller flow field as it may be affected
by variations in propeller location, propeller tip clearance, and duct
diffuser angle, and (3) conducting a limited theoretical study of the
shroud and wake shape in the static condition.

The available experimental test data were reduced to non-dimensional
coefficients using the propeller disk area and propeller tip speed as the
reference parameters in all cases. These coefficients were then combined
with appropriate correlation parameters and comparative plots made showing
the test data points and suggested fairing thru these points. The results
of the water tests have been shown in photographs of the wake in each case.
The results of the theoretical study show the theoretical duct shape deter-
mined for zero diffuser exit angle and the associated wake.

## 3. NOTATION

Positive directions for forces, moments, and angles are shown in the following sketch
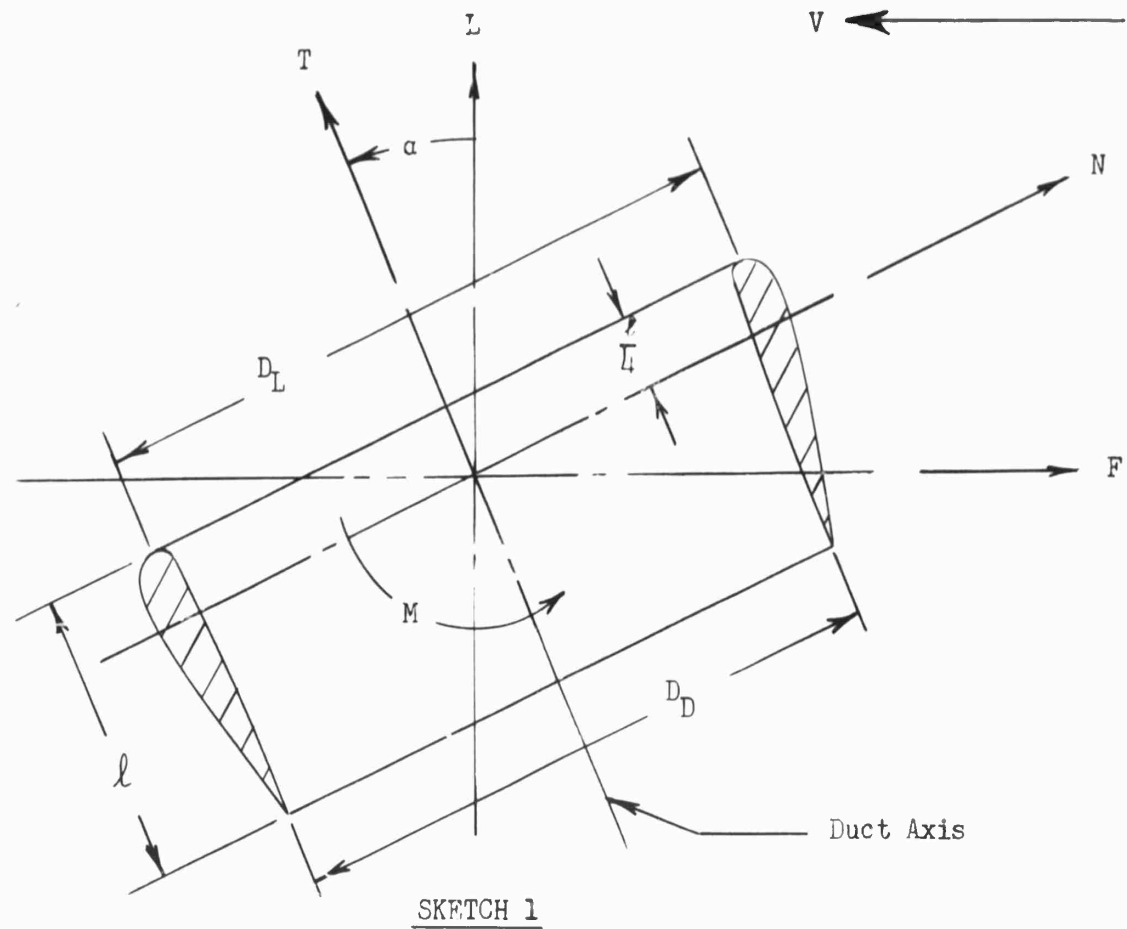


SKETCH 1

$A$      = Propeller disk area, $ft^2$

$c_{.7R}$      = Propeller blade chord at 0.7 radius station, in.

$D$      = Propeller diameter, ft.

$D_{CB}$      = Center body diameter, ft.

$D_D$      = Duct minimum inside diameter, ft.

4

$D_L$      = Duct leading edge diameter, ft. (see Sketch 1)

$D_M$      = Duct maximum outside diameter, ft.

$D_W$      = Wake diameter, ft.

h      = Height of ducted propeller center of gravity above location of assumed single vortex ring, ft.

HP      = Horsepower

$k_F$      = Total propulsive force coefficient, $\dfrac{F}{\rho(\Omega R)^2 A}$

$k_L$      = Total lift coefficient, $\dfrac{L}{\rho(\Omega R)^2 A}$

$k_{M_{\ell/4}}$      = Total pitching moment coefficient about duct quarter chord at duct centerline, $\dfrac{M}{\rho(\Omega R)^2 AR}$

$k_{M_\alpha}$      = $\dfrac{\partial k_M}{\partial \alpha}$ = average angle-of-attack stability derivative over the angle of attack range, per rad.

$k_P$      = Power coefficient, $\dfrac{P}{\rho(\Omega R)^3 A}$

$k_T$      = Total thrust coefficient, $\dfrac{T}{\rho(\Omega R)^2 A}$

L,F      = Components of resultant force vector in wind-axis system:

         L = Lift, positive up, lb.

         F = Propulsive force, positive forward, lb.

$\ell$      = Duct chord, ft.

$\ell_P$      = Position of impeller from duct trailing edge

M      = Figure of merit, $\dfrac{T}{P}\sqrt{\dfrac{T/A}{2\rho}}$    (ideal value = $\sqrt{2}$ with no diffuser according to the simple momentum theory)

M      = Total pitching moment about duct quarter chord at duct centerline, ft-lb. (positive nose-up)

N      = Total number of blades in the propeller drive system, also
         = Normal force

P      = Input power, ft.lb/sec.

r      = Propeller local radius, ft.

R      = Propeller maximum radius, ft.

RPM      = Propeller rotational speed, rev/min.

T,N      = Components of resultant force vector in body-axis system:

         $T$ = Thrust in direction of axis, positive up, lb.
         $N$ = Force normal to T, positive forward, lb.

V      = Free stream velocity, ft/sec.

α      = Duct angle of attack, deg. (Angle between duct axis and the normal
         to free stream velocity, positive when tilted rearward as shown in
         Sketch 1.)

β      = Propeller blade pitch angle at 0.7 radius station, deg.

$\epsilon$      = Equivalent lift/drag ratio, $\quad \epsilon = \dfrac{LV}{P - FV}\quad$ in non-axial flow conditions

η      = Axial flow flight efficiency, $\quad \eta = \dfrac{FV}{P}$

θ      = Duct diffuser half angle, deg.

λ      = Advance ratio, $\quad \dfrac{V}{\Omega R}$

ρ      = Air mass density, $slug/ft^3$

Ω      = Propeller rotational speed, rad/sec.


## Subscripts:

D      = Duct

P      = Propeller

eq      = Equilibrium condition (F = 0)

∞      = At infinity

## 4. COMPARISON OF EXPERIMENTAL TEST DATA

The objective is to establish charts that enable the designer to determine the performance characteristics (lift, propulsive force, pitching moment, and efficiency) of a ducted propeller. The data reviewed in Reference 31 are utilized in this work.

The study is divided into three types of flow, corresponding to the three flight regimes possible for ducted propellers in VTOL vehicles:

1) static operation (hovering flight)

2) axial flow (high-speed flight)

3) non-axial flow (transition flight)

The large number of physical parameters that are possible on a ducted propeller create a problem in selecting geometric parameters for the data correlation. The major variables are:

1. Duct

    a. chord length/propeller diameter ratio

    b. profile thickness/chord ratio

    c. profile camber

    d. leading edge radius

    e. angular chord line orientation relative to the axis

    f. profile trailing edge angle

    g. position of maximum thickness

2. Propeller

    a. solidity

7

b. average pitch setting

c. blade form

d. twist

e. blade profile

3. Duct-propeller combination

a    propeller location within shroud

.    hub diameter/propeller diameter ratio

c    propeller tip clearance

centerbody shape and its location relative to the duct
and propeller

In addition there are the flight parameters for the combination

1. angle of attack

2. advance ratio

3. Reynolds number

4. Mach number

After reviewing the test reports and the various theories and making exploratory plots, the following physical parameters were considered the most important for correlation:

1) the duct chord/propeller diameter ratio, $\ell/D$

2) the duct leading edge diameter/propeller diameter ratio, $D_L/D$

3) the duct maximum outside diameter/propeller diameter ratio, $D_M/D$

4) the duct diffuser half-angle, $\theta$

Since this study is primarily concerned with the ducted propeller per se, those test data of multiple ducts, ducts in wings and compressors are

8

not included in this analysis as well as those tests that have inlet and exit
control vanes (excluding stator vanes) installed in the ducts.

The pertinent physical characteristics of each model tested and utilized
in this analysis are given in Table 1 along with noting what aerodynamic and
power data are available. Also included in this table is a list of symbols
assigned to each model for the purpose of identification on the correlation
plots. Further identification is employed to the following extent:

| $\dfrac{D_M}{D}$ | $\theta$ | Symbol Code |
|---|---|---|
| 1 to 1.16 | $0^o$ | Symbols closed; e.g., ● |
| 1 to 1.16 | $> 0^o$ | Symbols closed and flagged; e.g., ● |
| 1 to 1.16 | $< 0^o$ | Symbols closed and flagged; e.g., ● |
| $> 1.16$ | $0^o$ | Symbols open; e.g., 0 |
| $> 1.16$ | $> 0^o$ | Symbols open and flagged; e.g., 0 |

In addition, where a non-optimum point with respect to $\beta$ or $\lambda$ is used on
an optimum correlation chart (such as the maximum efficiency of the ducted
propeller in axial flow), the symbols for these points are flagged thusly:

  ● ○ , for non-optimum $\beta$'s ;
  ● ○ , for non-optimum $\lambda$'s ; and
  ● ○ , for combined non-optimum $\beta$'s and $\lambda$'s .

The division of the diameter ratio into two parts is somewhat arbitrary.
However, the dividing point 1.16 seems to be boundary at which the various
investigators call their models either high-speed shrouds $\left( 1.0 < \dfrac{D_M}{D} < 1.16 \right)$
or static shrouds $\left( \dfrac{D_M}{D} > 1.16 \right)$ .

9

## 4.1  Static Performance Characteristics ($\alpha = 0^{\circ}$)

In the static operation or hovering flight of a ducted propeller, it is important to obtain as high a thrust per horsepower as possible at a given disk loading. This means that the static figure of merit chosen for this report, namely

$$M = \frac{T}{P} \sqrt{\frac{T/A}{2\rho}}$$

must be a maximum.

It should be noted that in the above equation the figure of merit is defined in such a way that for an ideal open propeller, $M = 1$. The simple momentum theory gives for the ideal non-diffused ducted propeller $M = \sqrt{2}$ which, of course, does not mean that an efficiency larger than 1 is obtained. It is simply a means of comparing a shrouded and non-shrouded propeller by the same yardstick.

### 4.1.1  Figure of Merit

Attempts at trying to correlate the figure of merit with various parameters failed to produce any meaningful results. As an alternative, the maximum figure of merit from each ducted propeller configuration tested is plotted in Figure 1, using T/HP as the ordinate and T/A as the abscissa. The ideal value of the static figure of merit for a non-diffused duct is indicated in the figure as well as the theoretical maximum for open propellers. Data from several open propellers used in the test ducts are also included so that a comparison can be made between the two configurations.

10

It will be noted that non-optimum data points with respect to $\beta$ are included in Figure 1. This is done since a number of cases indicated from rough plots of the data that a maximum figure of merit would have been obtained had the investigation been extended to include another $\beta$ in the test program. Thus, these data points (near maximum points) are included in the plot and are marked as previously described. In certain other cases investigations were made with only one $\beta$ setting as indicated in Table 1. The figures of merit obtained from these tests are also included in Figure 1 and are identified in the same manner as the near maximum data points.

A large range of disk loadings have been investigated (.18 to 108 lbs. per $ft^2$) by the numerous configurations. The maximum figure of merit thus far obtained in the data utilized by this report is 1.4 by a high-speed type duct with diffusion and without an optimum $\beta$ setting.

Conclusions that can be drawn from this plot are: 1) that the ducts with the larger diameter ratios $\frac{D_M}{D}$ 's with and without diffusion generally have the higher figures of merit, and 2) that ducts with a low diameter ratio $\frac{D_M}{D}$ in some cases yield a smaller figure of merit than an open propeller.

## 4.1.2 Division of Thrust in Hovering

The ratio of thrust carried by the duct to the total thrust at the maximum figure of merit is shown in Figure 2. $\frac{T_D}{T}$ is plotted versus the ratio of the duct leading edge diameter to the propeller diameter. The use of this diameter ratio gave the best correlation for the thrust ratio of all the parameters tried. The non-optimum data points are also included in this figure. It can be seen that the thrust carried by the duct increases as the diameter ratio increases and tends to approach an equal distribution of thrust

11

between the duct and propeller as suggested by the simple momentum theory (Reference 31). It is interesting to note that those models having large $\frac{D_M}{D}$ 's but low $\frac{D_L}{D}$ 's (see Table 1) have low thrust ratios $\frac{T_D}{T}$ 's . This indicates that the location of the stagnation pressure point, or more possibly, the separation point (if the flow of the ducts is separated) has a pronounced effect on the thrust developed by a duct in a ducted propeller system. Sufficient investigation has not been made in the various programs to know whether or not the flow around the ducts was separated. In several cases it was well established that separation had occurred on the high-speed type ducts which resulted in lower duct thrust.

It can be seen by comparing symbols in Figures 1 and 2 that, as predicted by theory, the models developing the higher figures of merit also produce the higher duct thrust.

## 4.2 Axial Flow Performance Characteristics ($\alpha = -90^{o}$)

The ducted propeller in the axial flow condition has been treated theoretically in numerous publications (References 17, 18, 20, 34, 35, 37, 38, to mention a few). Of main importance in this speed regime are the maximum propulsion efficiency of ducted propeller and the thrust capability of the duct. The propulsive efficiency in axial flow is given by

$$\eta = \frac{FV}{P}$$

Thus, the maximum efficiency at a given velocity is obtained when the ducted propeller system develops the most net propulsive force per horsepower.

### 4.2.1 Propulsive Efficiency in Axial Flow

The $\eta$'s in axial flow obtained from the experimental data are plotted in Figure 3 versus $\lambda$ for diffused ducts and non-diffused ducts. The best correlation of $\eta$ was obtained when it was multiplied by the ratio of $\dfrac{D_L}{D}$ as shown in the figure. "Non-optimum" points are also included in this figure for the same reasons mentioned previously, with the added problem that the tests in some cases were not conducted over a wide enough $\lambda$ range to obtain a maximum $\lambda$ value for the given pitch setting. These points are indicated as described in Section 4.

Open propeller data for several of the propellers used in the duct testing have been included in Figure 3 to show the change in the propeller maximum efficiency by adding a duct. It can be seen that a diffused duct improves the efficiency of the open propeller in the low-speed regime while there is no improvement in efficiency experienced by the addition of a duct in the higher-speed regime ($\lambda = .4 - .6$ and above). This could be due to the negative propulsive force experienced by ducts as indicated in Figure 4. In addition, diffused ducts yield approximately 17 percent better efficiency than the non-diffused ducts.

### 4.2.2 Division of Thrust in Axial Flow

The fraction of the total thrust carried by the duct in axial flow at the point of maximum efficiency is shown in Figure 4 versus $\lambda$ . Various parameters were investigated in an attempt to obtain a satisfactory corre-lation curve. Finally, the parameters $\dfrac{T_D}{T}$ , $\dfrac{D}{D_L}$ and $\lambda$ were chosen.

13

Although these parameters do not correlate the data to a great degree of satisfaction, they do indicate the approximate percentage of thrust that can be expected to be carried by the duct in axial flow.

Three sets of the experimental data (Krüger's, McNay's and Stipa's, References 17, 22 and 33, respectively) plot far above the other data. The Krüger and Stipa models are considerably different from the rest. Krüger's models were tested with a large nacelle protruding in front of the ducts. The Stipa model is different from the others in that the propeller is located in front of the duct which was comparatively long. McNay's tests were conducted on a full scale model.

It follows from Figures 3 and 4 that maximum propulsive efficiency is obtained at the higher advance ratios even though the duct is developing a negative net propulsive force (drag) at these conditions.

## 4.3  Non-Axial Flow Performance Characteristics $(0^{o} > \alpha < -90^{o})$

The non-axial flow speed regime is subject to the added aerodynamic parameter, angle of attack, which causes non-uniform flow conditions over the duct surface and propeller blades.

To date there have been a few theories developed to predict the performance characteristics of the ducted propeller in non-axial flow (References 21, 24, 25 and 30), but there is no theory available at the present time that can determine the optimum shape or duct propeller combination for maximum performance. An empirical approach was made in Reference 25

14

to determine the ratio of the propulsive force to lift equilibrium tilt angle, and pitching moment of the tilted ducted propeller. In this report both theory and experiments have been utilized to correlate the data.

## 4.3.1 Propulsive Force/Lift Ratios

In References 24 and 25 it is assumed that the induced velocity and resultant force are nearly parallel to the rotor axis and that the turning effect of the duct is small. Upon these assumptions the total drag coefficient (or propulsive coefficient) is written

$$k_F = k_L \tan \alpha + \triangle k_F$$

where $\triangle k_F$ represents the sum of the duct and propeller profile drag and the drag caused by the actual resultant force inclination to the assumed axial direction. Writing this propulsive force in terms of the lift coefficient

$$\frac{k_F}{k_L} = \tan \alpha + \frac{\triangle k_F}{k_L}$$

$\frac{k_F}{k_L}$ is plotted in Figure 5 versus $\lambda/\sqrt{k_L}$ for various angles of attack and propeller blade settings for each $\ell/D$ of the model tested. An attempt was made to correlate $\triangle k_F$ , but it was found to be affected to a great degree by $\alpha$; thus, it was discarded in favor of the total propulsive force coefficient $k_F$ . This data is cross plotted in Figure 6 versus $\ell/D$ at various $\lambda/\sqrt{k_L}$ 's for constant $\alpha$'s. From this figure the propulsive force

15

of a ducted propeller can be determined for a given weight, speed and angle of attack.

### 4.3.2  Equilibrium Angle of Attack

The equilibrium angle of attack for a ducted propeller is that angle of attack at which the propulsive force is zero ($F = 0$).  This angle is plotted in Figure 7 versus $\lambda/\sqrt{k_L}$ for each set of test data exhibiting an equilibrium angle of attack.  A cross plot of these data appears in Figure 8.  The data at the higher $\ell/D$'s peak and start to diminish; the latter effect does not agree with theory and may be influenced by the fact that the shrouds with high $\ell/D$ ratios tested had large diffuser angles.

### 4.3.3  Non-Axial Flow Lifting Efficiency at Equilibrium Angle of Attack

The lifting efficiency of the ducted propeller in non-axial flow is defined by the equivalent lift/drag ratio

$$c = \frac{LV}{P-FV}$$

By definition at the equilibrium angle of attack $F = 0$ and the lifting efficiency simplifies to

$$\varepsilon = \frac{LV}{P}$$

No general correlation of $\varepsilon$ from the test data was found.  However, there is evidence of some correlation at the equilibrium angle of attack.  This data is presented in Figure 9 versus $\lambda/\sqrt{k_L}$.  It should be pointed out that non-optimum points are also plotted in this figure.

16

The data from References 9, 10 and 13 tend to fall off as the speed parameter increases. This is due to the fact that the models are in a very high angle-of-attack range ($-60^{\circ}$ to $-80^{\circ}$) where the model is a poor lifting device. The two lower decreasing curves refer to low speed (bell-mouth type) ducts and would be expected to show a poorer efficiency at high speed. The upper curve which shows a decrease in $\epsilon$ as $\lambda/\sqrt{k_L}$ increases is a high speed duct.

The open propeller data from Reference 5 are also plotted in Figure 9 and are found to be of the same magnitude as the ducted propeller at a given $\lambda/\sqrt{k_L}$.

### 4.3.4 Pitching Moment Coefficient

When the ducted propeller is tilted from a hovering attitude to a forward flight attitude as speed increases, there is a marked difference in the flow characteristics over the front half of the duct compared to the rear half. The flow is such that it causes the ducted propeller to pitch up.

An expression is developed in Reference 30 for the pitching moment coefficient at equilibrium ($F = 0$) as follows:

$$
C_M = \frac{\sqrt{2}\ \frac{\ell}{R}\ C_L}{\sqrt{1 + \sqrt{1 + C_L^2}}} \left[ \frac{C_L^2}{2 + C_L^2 + 2\sqrt{1 + C_L^2}} - \frac{h}{\ell} \right]
$$

This expression is a function of the duct chord to duct radius ratio $\frac{\ell}{R}$,

lift coefficient $C_L$ and height of center of gravity above the assumed location of the single vortex ring $\frac{h}{\ell}$ .

To be of any practical value the location of the vortex ring has to be known. Efforts to determine this quantity were negative. However, the other parameters in the equation were used to correlate the total ducted propeller pitching moment coefficient about the duct quarter chord point at equilibrium angle of attack.

Figure 10 shows the parameter $\dfrac{k_{M_{\ell/4}}}{\ell/D}$ plotted versus $k_L$ and indicates that the pitching moment increases with increasing lift coefficient. There is some evidence of the pitching moment reaching a maximum in a few cases (References 10 and 12), but nothing definite can be concluded in this respect.

## 4.3.4.1 Stability Derivatives

In determining the dynamic stability of a ducted propeller, the angle-of-attack stability and speed stability derivatives are of importance. The outcome of correlating the angle-of-attack stability is shown in Figure 11. At best this chart is only an indication of the relative magnitude of $k_{M_\alpha}$ between the various chord to diameter ratios, due to the wide variation of $k_{M_{\ell/4}}$ with $\beta$ and $\alpha$. A composite plot without test points is shown in Figure 12.

Attempts at obtaining any correlation of the speed stability failed.

18

## 5. EXPERIMENTAL AND THEORETICAL WAKE STUDIES

There are many areas in ducted propeller theory that need a more adequate explanation and understanding. One such area is the ducted propeller flow field characteristics; if the characteristics were known, then the aerodynamic forces, moments and overall efficiency of the ducted propeller could be determined by integrating the pressures over the pertinent surfaces. One segment of this rather large area that is causing difficulties is the wake characteristics of the ducted propeller in a static flight condition. Theories to determine the static efficiency (figure of merit) of the ducted propeller are not quite consistent with each other. The simple momentum theory, for example, assumes that the final wake diameter is equal to the duct exit diameter. On the other hand, it is shown in Reference 31 that the static efficiency depends on the ratio propeller thrust/total thrust which is directly proportional to the area ratio of the propeller disk to that of the final wake. From simple energy considerations it can be concluded that the energy left in the wake is a minimum if the final wake has a uniform velocity distribution and a diameter as large as possible. From these remarks it follows that a better under-standing of the formation of the wake is of prime importance. In order to study these effects, two-dimensional experiments were performed to observe the effect on the wake of changes in duct diffuser angle, duct chord to propeller diameter ratio and propeller position. Also a theoretical study was made to provide a more complete understanding of the flow phenomena.

19

## 5.1 WATER EXPERIMENTS

### 5.1.1 Test Apparatus and Models

The Hiller Aircraft Corporation water tank shown in Figure 13 is constructed of plate glass and angle iron and fabricated in the same manner as an aquarium. The tank is 60 inches long, 30 inches wide and 2.5 inches deep and rests on a supporting structure.

The models were represented by two sections of a duct placed on either side of a thrust developer or propeller. In this test program the propeller was simulated by a 12-bladed impeller whose axis of rotation lay in a plane parallel to the bottom of the water tank. The impeller shaft was supported at its two ends by brackets mounted on the tank support structure. On the end of the impeller shaft was mounted a grooved pulley for a belt drive. The power was supplied by an electric sewing machine motor of 1/16 horsepower at 5000 rpm through a 100 to 1 worm gear reduction and then through a 2 to 1 reducing pulley arrangement. A rheostat was installed in the electrical system so that the impeller could be operated at any desired speed. This drive system was mounted on an independent support, separate from the tank support, in order to eliminate motor and gear vibrations from the tank. The model and impeller are shown in Figure 13 installed in the water tank.

The models selected for these tests had an inlet contour of a lemniscate curve, straight sides between the inlet and diffuser and variable diffuser half-angles ($\theta$ = 0, 3, 6, 9, 12, 15, and 18 degrees). That is, there was a common inlet configuration and various exit configurations.

20

See Figure 14 for the duct physical characteristics. Three lengths of impeller blades (1, 2, and 3 inches) were employed. See Figure 15 for the impeller physical characteristics. A water depth of 1.37 inches was used throughout the program. The impeller was operated at 22 rpm for this investigation, resulting in a mean water velocity of approximately 0.5 fps.

Several visualization techniques were tried for observing the flow pattern. The method finally selected utilized bottom fluorescent lighting through a milk plexiglass bottom cover for light diffusion (located on the bottomside of the tank bottom). Red food coloring was injected into the water at approximately half the water depth ahead of and spanning the duct inlet. After the coloring had been pulled through the duct a sufficient distance, a photograph was then taken of the wake pattern with a Polaroid Land camera.

## 5.1.2 Test results

The photographic results of the wake patterns of the various models in combination with the various impellers are shown in Figures 16 thru 18. Although the wake is not precisely definable, it can be seen that the wake expands as the diffuser angle is increased. A curve of the diameter ratios, $\frac{D_W}{D}$, at 2 diameters downstream of the trailing edge is obtained by arbitrarily drawing a line from the duct trailing edge along the sides of what appears to be the main wake in each picture. The diameter

ratios are shown in Figure 19 versus diffuser angle for the three impeller
blades. These curves at best indicate that the wake expands as the dif-
fuser angle increases until a maximum diameter ratio is reached at approx-
imately 18 degrees diffuser angle. However, there are two main reasons
to doubt the magnitude of the wake size from these tests. For one, the
coloring does get mixed to a certain extent into the upper portions of
the water due to the impeller rotating up and out of the water. The
other is the presence of small surface waves generated by the impeller
blades leaving the water, causing distortion of the wake due to light
refraction.

The position of the propeller within a non-diffused duct is shown in
Figure 20 to have negligible effect on the wake diameter as predicted in
Reference 4; however, due to the reasons given in the preceding paragraph,
this verification cannot be considered too reliable.

The wake pattern of the theoretical duct determined in Section 5.2
is shown in Figure 21. It appears from this figure that the wake does
not expand for this duct shape.

5.2   THEORETICAL TWO-DIMENSIONAL STUDIES (Static Condition)

5.2.1   Introduction

This section deals with preliminary two-dimensional theoretical studies of the duct and wake.  The objective is to calculate for a given vorticity distribution the proper shroud and the corresponding wake where main emphasis is placed on the final wake diameter.  Similar to the three-dimensional investigations conducted in Reference 4, for the shroud a combination of the classical Birnbaum distributions $\gamma_0$ and $\gamma_2$ has been assumed where $\gamma_0$ denotes the constant and $\gamma_2$ the elliptical component.  The constant part $\gamma_0$ continues on both sides along the wake boundary line from the duct trailing edge to infinity.  See Figure 22.

The mathematical problem can be stated as follows:  Given are the basic $\gamma$-distributions $(\gamma_0, \gamma_2)$ in x-direction, the slope of the vortex sheet[*] at the duct trailing edge, and the exit diameter.  Calculate the duct form and wake boundary line defined in such a way that velocity components normal to duct and wake boundary line are zero.

As the problem cannot be solved analytically in a closed form, an iteration process is used starting with a cylindrical duct and wake.  The following steps are taken:

---

[*]The term "vortex sheet" is used here in a general sense, not restricted to a straight line or plane.

23

a)  Calculation of the shroud shape for a cylindrical wake

b)  Determination of the wake shape for the shroud shape found
    under a)

c)  Rechecking of the shroud shape for the wake shape found under b)

### 5.2.2  Mathematical Approach

For the mathematical model shown in Figure 22, the following equations
hold for the axial - and radial velocities at the point $P(x_1, y_1)$

$$v_a = \int_0^\infty \frac{\gamma(y - y_1)dx}{2\pi \left[(x_1 - x)^2 + (y_1 - y)^2\right]} + \int_0^\infty \frac{\gamma(y + y_1)dx}{2\pi \left[(x_1 - x)^2 + (y_1 + y)^2\right]} \quad (1)$$

$$v_r = \int_0^\infty \frac{\gamma(x_1 - x)dx}{2\pi \left[(x_1 - x)^2 + (y_1 - y)^2\right]} - \int_0^\infty \frac{\gamma(x_1 - x)dx}{2\pi \left[(x_1 - x)^2 + (y_1 + y)^2\right]} \quad (2)$$

In these integrals which have to be taken over the whole vortex sheet from
the leading edge to infinity, the first term comes from the right vortex
sheet and the second term is the contribution of the left side in Figure
23.  It should be noted that $\gamma$, $y$ and $y_1$ are always considered positive.

The above equations for the induced velocity field can only be solved
by graphical integration.  We are primarily interested in the velocity dis-
tribution on the vortex sheet itself.  In this case,

$$x_1 - x = 0$$
$$y_1 - y = 0 \quad (3)$$

which means that a singular point occurs; i.e., the integrand of the first terms in equations (1) and (2) becomes infinite.

This difficulty can be overcome by splitting off an interval of width $\delta$ to both sides of the singular point and combining the integrands at points symmetrical about x -

$$\int_{x-\delta}^{x+\delta} f(x')dx' = \int_{0}^{\delta} \left[ f(x+h) + f(x-h) \right] dh \tag{4}$$

Another problem arises with regard to the upper limits $(x = \infty)$ of the integrals in equations (1) and (2). This difficulty can be overcome by the introduction of the new variable $\xi = (x)^{-1/n}$ where n is an integer:

$$\int_{x_1}^{x_2} f(x)dx = n \int_{\xi_2}^{\xi_1} f(x)(x)^{\frac{n+1}{n}} (d\xi) \tag{5}$$

(See Reference 19, pp 330/331.)

The following paragraph demonstrates how these mathematical tools have been used to solve the problem by means of an iteration process. As must be expected, the convergence of the iteration process decreases with decreasing free stream velocity. For the static condition investigated in this report, especially the inlet of the shroud is very sensitive to the location of the vortex sheet. In order to save time, a shroud with a duct length/exit diameter ratio equal to 1 was selected. For this specific case the induced velocities for the starting point of the iteration process (cylindrical shroud and wake) have already been calculated and are available

25

for the vorticity distributions considered. See Appendix of Reference 19. The calculations are based on a ratio of duct length to exit diameter of 1.0.

### 5.2.3 Determination of Shroud Shape and Wake

#### a) Shroud Shape

The starting point of the calculations is a cylindrical shroud with a cylindrical wake with the vorticity distribution $\gamma_0, \gamma_2$ described earlier in this report. As a first step, the induced velocities $v_a, v_r$ at the location of the cylindrical shroud are calculated by the method outlined in the previous section. They can be written as, say,

$$v_a = k_1 a_0 + k_2 a_2 \tag{6}$$

$$v_r = k_3 a_0 + k_4 a_2 \tag{7}$$

where the coefficients $k_i$ $(i = 1,2,3,4)$ are constants depending on the abscissa x only. The quantity $v_r/v_a$ represents the slope of the shroud. The ratio $a_2/a_0$ is chosen in such a way that the shroud slope assumes a prescribed value for a given x. In our case the ratio $a_2/a_0$ has been selected in such a way that the slope is zero at the trailing edge $x = \ell$. See Figure 23, which shows in the lower curve the calculated shroud slope versus x. The corresponding shroud shape is obtained by integration, starting from the trailing edge. See upper curve, Figure 23.

For the next iteration step the same vortices are assumed and are then shifted from the cylinder to the shroud shape just found and the process is repeated. As mentioned previously, for the static condition the convergence of this iteration process is somewhat unsatisfactory, especially with regard to the inlet. Unfortunately, the induced velocities at the leading edge

26

change considerably with the inlet contour. To a certain extent this is due to the assumed vorticity distribution. The main difficulty, however, lies in the fact that for zero free stream velocity, the inlet contour is very sensitive even to small changes in the induced velocities.

Therefore, a second series of calculations were started where emphasis was laid on the inlet, or more accurately, on the slope at $x = 0.10$. For several selected inlet contours the calculated direction of flow $v_r/v_a$ at $x = 0.1$ was plotted against the assumed duct slope (see Figure 24). The intersection of the two curves gives the duct shape for which the actual slope coincides with the calculated one. This means that the slope of the shroud coincides with the direction of the flow only at two stations: namely, at $x = 0.1\ell$ and $x = \ell$. From Figure 24 a constant factor (independent of $x$) was derived which was applied to the whole duct. From both methods a duct shape is obtained which is believed to be reasonably accurate. This duct shape has then been frozen to calculate the wake. Fortunately, due to its distance from the wake, any error which may exist at the duct inlet has only a minor effect on the wake velocities, and by that on the formation of the wake itself.

b) Final Wake Diameter

In order to determine the shape of the wake, the flow field behind the duct for several assumed wake shapes was investigated. In all cases the previously determined duct shape was taken. In other words, for various arrangements of the vortex sheet behind the duct, the velocity components along the vortex sheet were calculated. As illustrated in Figure 25, the following parameters have been varied:

27

(1) Ratio of final wake diameter to duct exit diameter, selected
    values 1.2, 1.0 and 0.8.

(2) Abscissa of the point where final wake diameter has developed,
    selected values 0.5, D, 2D behind duct trailing edge.

According to the Dickmann-Weissinger theory, Reference 4, in the three-
dimensional case vortex rings are generated at the duct trailing edge at the
rate

$$\frac{d\Gamma}{dt} = \frac{1}{\rho} \text{ x disk loading} \tag{8}$$

As a first approximation it may be assumed that these vortices are carried
away with the axial velocity dx/dt . From

$$\frac{d\Gamma}{dt} = \frac{d\Gamma}{dx}\frac{dx}{dt} = \text{constant} \tag{9}$$

it follows that the strength of the vortex cylinder (or whatever the contour
may be) is inversely proportional to dx/dt . As dx/dt is practically con-
stant, a vortex sheet with constant vorticity $(\gamma = \gamma_o)$ can be assumed for
the two-dimensional case.

For several combinations of the above listed assumed parameters, the
wake shape was calculated. See Figure 26 which shows for three specific
cases both the assumed vortex sheet (full line) and the calculated wake
shape (dotted line).

By cross-plotting for various x-values, the calculated local wake dia-
meter against the assumed diameter of the vortex sheet and selecting the
values for which $D_{assumed} = D_{calculated}$ , a new wake shape is found. See
Figure 27, the lower graph shows the cross-plots and the upper curve gives
the new wake shape thus established.

28

In the next step, the wake shape for the newly established vortex sheet location is recalculated (See Figure 28). The full line of Figure 28 is identical with the duct shape of Figure 23, the wake of Figure 27 (upper curve) and the individual points shown are the recalculated ordinates of the wake. As can be seen, the agreement is very good.

As a final check, the effect of the modified wake on the duct shape was spot-checked. See Figure 29 which shows for x = 0.5 the recalculated ordinate of the shroud. The agreement is satisfactory. In view of the fact that the inlet of the duct has only a minor effect on the wake, no attempt was made to recalculate or modify the duct inlet shape. The final wake diameter was found to be 0.94 of the duct exit diameter; i.e., there is a slight contraction. The calculated final wake diameter agrees fairly well with the experiments which gave a final wake diameter/duct exit diameter ratio of 1.0; however, due to the uncertainties of the water tests, this verification cannot be considered too reliable. Also shown in Figure 29 is the three-dimensional duct shape calculated by Dickmann-Weissinger for

$$\xi = \frac{\triangle p}{V^2 \rho/2} = 100$$

which is the lowest speed investigated in Reference 4. In the above equation $\triangle p$ is the propeller loading and V the free-stream velocity. At a propeller loading of 50 lb/ft$^2$ the value $\xi = 100$ corresponds to a velocity of approximately 20 ft/sec. Our own investigations refer to the static conditions. However, as according to Figures 8 and 9 of Reference 4, the inlet radius rapidly increases with decreasing free stream velocity, no real conclusions can be drawn from this comparison of the two ducts calculated for different speeds.

## 6. CONCLUSIONS

Available test data and theoretical work on ducted propellers have been reviewed and comparative performance charts constructed. Due to the large number of variables and the previous uncoordinated efforts given to this type of configuration, it was found impossible to correlate all the ducted propeller variables involved into the comparative charts. The effect on the performance of certain parameters such as the ratios of $\frac{D_M}{D}$, $\frac{D_L}{D}$ and $\frac{\ell}{D}$ were more pronounced than others; thus, the major correlation effort has been directed at these parameters.

In hovering flight the ducted propeller is shown to have superior figure of merit to that of an open propeller. Also, it is shown that the ideal figure of merit for ducted propellers $\sqrt{2}$ is approached as the ratio of the maximum duct diameter to propeller diameter is increased, and proper attention given to the inlet shape and propeller configuration. These same ducts carry a higher percentage of the total thrust.

In axial flow it is shown that the propulsive efficiency is a function of duct diffuser angle and advance ratio. The diffused ducts give approximately 17 percent better efficiency than the non-diffused duct and surpasses that of the open propeller in the low speed regime. It is as good as the open propeller up to an advance ratio of approximately 0.4 to 0.6, after which the open propeller appears to have the superior efficiency. It is in this area that the duct net force becomes negative (produces a net drag).

The parameters $\frac{k_F}{k_L}$ and $\alpha_{eq}$ both increase in magnitude as the ratios of $\ell/D$ and $\lambda/\sqrt{k_L}$ increase. Trends of the equivalent lift/drag ratio

30

and the pitching moment coefficient are shown to increase for increasing $\lambda/\sqrt{k_L}$'s and $k_L$'s , respectively. The average angle-of-attack stability derivative is found to increase in magnitude as the advance ratio and duct chord to propeller diameter ratio increases. This parameter $k_{1_\alpha}$ is greatly dependent, in addition to the above parameters, on the angle of attack and propeller blade setting.

It appears that the wake diameter of a two-dimensional ducted propeller increases with increasing duct diffuser angle and decreases in size as the duct chord to propeller diameter ratio decreases. However, due to the uncertainties in the water tests, the above results are not considered conclusive.

31

## 7. REFERENCES

1. Aerophysics Development Corporation: Aerial Jeep Phase I Final Report. Vol. I of II. U.S. Army Contract No. DA-44-177-TC-397. ADC Report No. 520-3/R24/46, December 1, 1957.

2. Allen, H. J., Rogallo, F. M.: Ring-Cowled Propellers. A Thesis submitted in partial fulfillment of the requirements for the degree of Engineer in Mechanical Engineering Aeronautics, Stanford University, June, 1935. (Available from Stanford University Library)

3. Clancy, G., Cowgill, R.: Truck Test Stand Tests of Hiller Airborne Personnel Platform, Phase II. ONR Contract No. Nonr 1357(00). Hiller Helicopters, Engineering Report No. 680.2, September, 1955.

4. Dickmann, H. E., Weissinger, J. Beitrag zur Theorie optimaler Düsenschrauben (Kortdüsen). Jahrbuch der Schiffbautechnischen Gesellschaft, pp. 253-305, Band 49, 1955.

5. Gill, W. J.: Wind Tunnel Tests of Several Ducted Propellers in Non-Axial Flow. ONR Contract No. Nonr 1357(00). Advanced Research Division of Hiller Aircraft Corporation, Report No. ARD-224, April 20, 1959. (ASTIA AD 216 620)

6. Gilmore, A. W., Grahame, W. E.: Research Studies on a Ducted Fan Equipped with Turning Vanes. Grumman Aircraft Engineering Corporation. Presented at the Institute of the Aeronautical Sciences 27th Annual Meeting, New York, New York, January 26-29, 1959. IAS Report No. 59-59.

7. Grose, R. M.: Wind Tunnel Tests of Shrouded Propellers at Mach Numbers from 0 to 0.60. United Aircraft Corporation, Research Department, WADC Technical Report 58-604, December, 1958. (ASTIA AD 205 464)

8. Hansen, M.: Standschubverbesserung durch Dusenring bei einer Modellluftschraube kleiner Steigung. Aerodynamische Versuchsanstalt Göttingen (AVA) Report No. B 43/W/48. Also published as German UM (Untersuchungen und Mitteilungen) No. 3043, 1943.

9. Hoehne, V. O., Wattson, R. K.: Shrouded Propeller Investigations: Wind-Tunnel Tests of a Shrouded Propeller with a 17-Bladed Rotor, Inlet and Exit Stators, and Long Shroud with High-Speed Inlet and No Exit Diffusion. Report No. 213-1, June, 1958. (ASTIA AD 200 434)

10. Hoehne, V. O., Wattson, R. K.: Shrouded Propeller Investigations: Wind-Tunnel Tests of a Shrouded Propeller with a 17-Bladed Rotor, Inlet and Exit Stators, and Long Chord Shroud with Static Inlet and No Diffusion. Report No. 213-2, September, 1958. (ASTIA AD 205 858)

11.  Hoehne, V. O., Wattson, R. K.:  Shrouded Propeller Investigations:
     Static Performance of Two Highly-Loaded Shrouded Propellers as
     Measured in the Walter H. Beech Memorial Wind Tunnel.  Report No.
     213-4, September, 1958.  (ASTIA AD 205 860)

12.  Hoehne, V. O.:  Shrouded Propeller Investigations:  Wind-Tunnel
     Tests of a Shrouded Propeller with a 10-Bladed Propeller, Exit
     Stators, and Long Chord Shroud with High-Speed Inlet and No Exit
     Diffusion.  Report No. 213-5, January, 1959.  (ASTIA AD 210 032)

13.  Hoehne, V. O.:  Shrouded Propeller Investigations:  Wind-Tunnel
     Tests of a Shrouded Propeller with a 10-Bladed Propeller, Exit
     Stators, and Long Cnord Shroud with Static Inlet and No Diffusion.
     Report No. 213-6, January, 1959.  (ASTIA AD 210 033)

14.  Horn, F.:  Beitrag zur theorie ummantelter Schiffsschrauben.
     Jahrbuch 1940 der Schiffbautechnischen Gesellschaft.

15.  Johnson, A. E.:  Preliminary Investigation of the Effect of a
     Leading-Edge Slat on Static Thrust of a Shrouded Propeller.  David
     Taylor Model Basin, Aerodynamics Laboratory, Aero Memorandum 65,
     February, 1958.

16.  Krüger, W.:  Contribution to the problem of the Ducted Airscrew.
     M.A.P. Volkenrode Ref: MPA - VG 86-. T, Translated February 15,
     1946.  (NASA N-12674)

17.  Krüger, W.:  On Wind Tunnel Tests and Computations Concerning the
     Problem of Shrouded Propellers.  Translation of ZWB Forschungsbericht
     Nr. 1949, January 21, 1944 by Mary L. Mahler, NACA.  NACA TM 1202,
     February, 1949.

18.  Küchemann, D.:  Der Einfluss einer Verkleidung auf die Axialkräfte
     an Kühlern und Luftschrauben.  Zentrale für Wissenschaftliches
     Berichtswesen (ZWB), Technische Berichte, Bd. 9, Nr. 1, pp. 19-22,
     April, 1942.  (NASA 6510- TB/1942, V. 9, No. 1.)

19.  Küchemann, D., Weber, J.:  Aerodynamics of Propulsion.  Appendix.
     First Edition, McGraw-Hill Book Company, Inc., New York, 1956.

20.  Küchemann, D., Weber, J.:  The Flow over Annular Aerofoils.  Report
     No. VII - The Shrouded Propeller.  Translated and issued by TPA 3,
     Technical Information Bureau for Chief Scientist, Ministry of Supply,
     Great Britain.  (NASA N-109)

21.  Malavard, L., Hacques, G.:  Problemes de L'Aile Annulaire Resolus
     par Analogie Rheoelectrique.  Laboratoire de Calcul Analogique du
     C.N.R.S., (Centre National de la Recherche Scientifique), Paris, France.

22. McNay, D. E.: Study of the Effects of Various Propeller Configurations on the Flow about a Shroud. A Thesis submitted in partial fulfillment of the requirements for the degree of Master of Science in the Department of Mechanical Engineering, Mississippi State College, January, 1958. (Obtainable from Mississippi State College as Research Report No. 14, February 1, 1958)

23. Morse, A.: Shrouded Propeller Aerodynamic Characteristics in Low Speed, Non-Axial Flow. Contract Noa(s)56-935. Hiller Helicopters Engineering Report No. 58-56, July 15, 1958.

24. Moser, H. H.: Analytic and Experimental Investigation of the Aerodynamics of the Ducted Fan. A Thesis submitted in partial fulfillment of the requirements for the degree of Master of Science at the Massachusetts Institute of Technology, May, 1958. (Available from MIT)

25. Moser, H. H., Livingston, C. L.: Experimental and Analytic Study of the Ducted Fan and Fan-in-Wing in Hovering and Forward Flight. Aeroelastic and Structures Research Laboratory, Massachusetts Institute of Technology, Technical Report 79-1, January, 1959. (ASTIA AD 201 398)

26. Parlett, L. P.: Aerodynamic Characteristics of a Small-Scale Shrouded Propeller at Angles of Attack from 0 - 90 Degrees. NACA TN 3547, November, 1955.

27. Platt, R. J.: Static Tests of a Shrouded and an Unshrouded Propeller. NACA RM L7H25, February, 1948.

28. Regenscheit, B.: Standschubmessungen an zwei ummantelten Luftschrauben. Aerodynamische Versuchsanstalt Göttingen (AVA) Report No. 42/W/32, September 7, 1942. Also published as German UM (Untersuchungen und Mitteilungen) No. 681.

29. Reichert, J. B.: Aerodynamic Report (A) Performance (B) Stability and Control. U.S. Army Contract DA-44-177-TC-351. Doak Aircraft Company, Inc., Report No. DS-203, September 18, 1956.

30. Sacks, A. H.: The Flying Platform as a Research Vehicle for Ducted Propellers. Advanced Research Division of Hiller Aircraft Corporation. Presented at the 26th Annual Meeting, New York, New York, January 27-30, 1958. Preprint No. 832.

31. Sacks, A. H., Burnell, J. A.: Ducted Propellers - A Critical Review of the State of the Art. Contract Nonr 2677(00). Advanced Research Division of Hiller Aircraft Corporation, Report ARD No. 232, June 26, 1959.

32. Soloviev, U. I., Churmack, D. A.: Marine Propulsion Devices. Publ. by Military Publishing House, Ministry of the Armed Forces, Moscow, USSR, 1948. Translated by Rose Jermain, Science Translations Service, University of Alabama, STS-101, March, 1951. (BuShips TR 408)

33. Stipa, L.: Experiments with Intubed Propellers. L'Aerotecnica pp. 923-953, August, 1931. Translated by Dwight M. Miner, NACA. NACA TM 655, January, 1932.

34. Trefftz, E.: Über die Kontraktion kreisförmiger Flussigkeitsstrahlen. Zeitschrift für Mathematik und Physik (ZMP), Bd. 64, pp. 34-61, 1916. (Obtained from Stanford University Library)

35. van Manen, J. D.: Open-Water Test Series with Propellers in Nozzles. Publication No. 115a of the Netherlands Ship Model Basin at Wageningen. Reprinted from International Shipbuilding Progress, Vol. 1, No. 2, 1954.

36. van Manen, J. D.: Recent Research on Propellers in Nozzles. Research Department, Netherlands Ship Model Basin at Wageningen, Journal of Ship Research, pp. 13-46, July, 1957.

37. van Niekerk, C. G.: Ducted Fan Design Theory. Journal of Applied Mechanics, Vol. 25, No. 3, pp. 325-331, September, 1958.

38. Wallis, R. A.: Design, Performance and Analysis of Ducted Axial Flow Fans. Department of Supply, Research and Development Branch, Aeronautical Research Laboratories, Australia. ARL Report No. A. 88, August, 1954. (NASA N-34375)

TABLE I

PHYSICAL CHARACTERISTICS OF EXPERIMENTAL MODELS AND OF MEASURED TEST DATA

| Ref. No. | Symbol | Duct Section | L | t/L | $D_M/D$ | $D_L/D$ | $D_{CB}/L$ | θ | i* | Twist | Tip Clearance %R | Trop Location %l | β | r/P for β | λ | α | HP | T | N | M | $T_t$ or P | $N_t$ or P | $\Sigma_t$ or P | Remarks |
|---|---|---|---|---|---|---|---|---|---|---|---|---|---|---|---|---|---|---|---|---|---|---|---|---|
| 1 | ◇ | A | .4 | .144 | 1.18 | 1.12 | .201 | 0 | 2 | x | .77 | 53 | var | 1.0 | 0,var | var | x | x | x | x | - | - | - | |
| " | ◁ | B | " | .248 | " | " | " | " | " | x | " | 54 | " | " | 0 | 0 | x | x | - | - | - | - | - | |
| " | ▷ | B | " | .248 | " | " | " | " | " | x | " | 80 | " | " | 0 | 0 | x | x | - | - | - | - | - | |
| " | ▷ | C | " | .332 | " | " | " | " | " | x | " | 45 | " | " | 0 | 0 | x | x | - | - | - | - | - | |
| " | ◁ | C | " | .332 | " | " | " | " | " | x | " | 47 | " | " | 0 | 0 | x | x | - | - | - | - | - | |
| " | ▽ | C | " | .332 | " | " | " | " | " | x | " | 62 | " | " | 0 | 0 | x | x | - | - | - | - | - | |
| " | ▽ | D | " | .332 | " | 1.18 | " | " | " | x | " | 42 | " | " | 0 | 0 | x | x | - | - | - | - | - | |
| " | ◁ | D | " | .245 | 1.26 | 1.18 | " | " | " | x | " | 56 | " | " | 0,var | var | x | x | - | - | - | - | - | |
| " | ◁ | F | " | .248 | 1.26 | 1.18 | " | " | " | x | " | 89 | " | " | 0 | 0 | x | x | - | - | - | - | - | |
| " | ◻ | F | " | .248 | 1.24 | 1.17 | " | " | " | x | " | 56 | " | " | 0 | 0 | x | x | - | - | - | - | - | |
| " | ◻ | G | " | .248 | 1.24 | 1.17 | " | " | " | x | " | | " | " | 0 | 0 | x | x | - | - | - | - | - | |
| " | ● | Guard Ring | " | .038 | 1.02 | 1.01 | .086 | 0 | 4 | x | " | 50 | " | " | 0 | 0 | x | x | - | - | - | - | - | |
| 2 | ◉ | Clark Y | 3.01 | .164 | 1.08 | 1.04 | .086 | 20.3 | 2 | x | 1.82 | 22 | var | 2.6 | var | -90 | x | x | x | x | x | x | x | Constant chord Prop |
| 3 | ◇ | Lemniscate | 4.98 | .294 | 1.27 | 1.20 | ~3 | 0 | 4c | x | .83 | 75 avg | 14 | .7 | 0,var | var | Est | x | x | - | x | - | - | |
| " | ● | 6421 | 1.99 | .25 | 1.11 | 1.04 | .201 | 0 | 4c | x | .33 | 73 avg | var | .7 | " | " | x | x | x | x | x | x | x | |
| " | ■ | 6421 | " | " | 1.11 | 1.04 | " | 0 | 6c | x | " | " | " | " | " | " | x | x | x | x | x | x | x | |
| " | ◆ | 0018 | " | " | 1.10 | 1.07 | " | 4.5 | 4c | x | " | " | " | " | " | " | x | x | x | x | x | x | x | |
| " | ■ | 0018 | " | " | 1.10 | 1.07 | " | 6.5 | 6c | x | " | " | " | " | " | " | x | x | x | x | x | x | x | |
| " | ▶ | 0018 | " | " | 1.10 | 1.07 | " | 8.5 | 6c | No | " | " | " | " | " | " | x | x | x | x | x | x | x | |
| " | ○ | Lemniscate | " | " | 1.20 | 1.14 | " | 0 | 4c | x | " | " | " | " | " | " | x | x | x | x | x | x | x | |
| " | ◻ | Lemniscate | " | " | 1.20 | 1.14 | " | " | 4c | x | " | 45 | " | " | " | " | x | x | x | x | x | x | x | |
| " | ◀ | 6421 | " | .15 | 1.07 | 1.03 | " | " | 4c | x | " | 56 | " | " | " | " | x | x | x | x | x | x | x | |
| " | ▶ | 6421 | " | .15 | 1.07 | 1.03 | " | " | 6c | x | " | " | " | " | " | " | x | x | x | x | x | x | x | |
| 4 | ○ | Fan-in-Wing Concept | 2.37 | .25 | 2.21 avg | - | .32 | 4.5 avg | 4 | x | .45 | 51 | 30 | .75 | 0 | 0 | x | x | x | x | x | x | - | Fan-in-Wing Concept |
| 7 | ◇ | Airfoil (Mod) | 2.50 | .50 | 1.27 | 1.23 | .25 | 4.5 avg | 4 | x | 1.46 | 50 | var | .75 | 0 | 0 | x | x | x | x | x | x | - | |
| " | ◆ | Airfoil (Mod) | 2.50 | .50 | 1.12 | 1.05 | .25 | 4.5 avg | 4 | x | 1.46 | 50 | var | .75 | 0,var | var | x | x | x | x | x | x | x | |
| 8 | ○ | Cambered | .552 | .50 | 1.21 | 1.14 | .172 | 25? | 4 | x | .49 | 30 | 13.9 | .7 | 0,var | 0,90 | x | x | x | - | x | - | - | |
| " | ◻ | Cambered | .551 | .50 | 1.21 | 1.14 | .172 | 25? | 4 | x | .56 | 30 | 13.0 | .7 | 0,var | 0,90 | x | x | x | - | x | - | - | |
| 11 | ○ | Airfoil | .617 | .4 | 1.17 | 1.32 | - | 4? | 4 | x | .1 | 44 | 14 | - | 0,var | 0,90 | x | x | - | - | x | - | - | |
| " | ○ | Airfoil | .592 | .734 | 1.36 | 1.32 | - | 14 | 4 | x | 3.4 | 50 | 14 | - | 0 | 0 | x | x | x | - | x | - | - | |
| 15 | ◇ | Airfoil | 1.54 | .443 | 1.05 | 1.04 | .49 | 0 | 4 | x | .33 | 55 | - | - | 0 | 0 | x | x | x | - | x | - | - | Water test |
| " | ◇ | Airfoil | 1.54 | .543 | 1.22 | 1.14 | .49 | 0 | 4 | x | .33 | 44 | - | - | 0 | 0 | x | x | x | - | x | - | - | Water test |
| 17 | ◁ | #₁ Airfoil | .797 | .625 | ~1.29 | 1.22 | .35 | 0 | 8 | x | - | 24 | var | .7 | var | -90 | x | x | x | x | x | x | x | Static test / Hi-Speed Duct / P Prop |
| " | ◁ | #₂ Airfoil | .730 | .625 | ~1.29 | 1.22 | .35 | 0 | 8e | x | - | 24 | var | .7 | var | -90 | x | x | x | - | x | x | x | P Proj |

36

Table I Continued

PHYSICAL CHARACTERISTICS OF EXPERIMENTAL MODELS AND OF MEASURED TEST DATA

| Ref. No. | Symbol | Duct Section | D | t/c | D_x/D | D_L/D | D_CB/D | θ | | Twist | Tip Clearance % P | Prop Location % ℓ | β | r/R for β | λ | σ | HP | T | N | M | T_L or P | D or P | T or P | Remarks |
|---|---|---|---|---|---|---|---|---|---|---|---|---|---|---|---|---|---|---|---|---|---|---|---|---|
| 27 | ◇ | #1 Airfoil | .787 | .625 | ≈1.29 | 1.22 | .35 | 0 | 3 | x | — | 26 | var | .7 | var | -∞ | x | x | — | — | x | — | — | — | #1 ETC. |
| " | ◇ | #1 Airfoil | .787 | .625 | ≈1.29 | 1.22 | .35 | 0 | 8 e | x | — | 26 | " | " | " | " | x | x | — | — | x | — | — | — | #2 Prop |
| " | ◆ | #5c Airfoil | .787 | .312 | ≈1.08 | 1.08 | .35 | 70 | 8 | x | — | 30 | " | " | " | " | x | x | — | — | x | — | — | — | #1 Prop |
| 28 | ◻ | Airfoil-1 | .84 | .5 | ≈1.20 | 1.105 | — | 0 | 4 | x | .8 | 24 | 43.5 | " | " | " | x | x | — | — | — | — | — | — | |
| " | ◻ | Airfoil-2 | " | " | 1.20 | 1.105 | — | 6 | " | x | " | " | " | " | " | " | x | x | — | — | — | — | — | — | |
| " | ◻ | Airfoil-3 | " | " | 1.20 | 1.105 | — | 13.5 | " | x | " | " | " | " | " | " | x | x | — | — | — | — | — | — | |
| " | ◻ | Airfoil-4 | " | " | 1.21 | 1.105 | — | 25 | " | x | " | " | " | " | " | " | x | x | — | — | — | — | — | — | |
| " | ◆ | Airfoil-5 | " | " | 1.15 | 1.055 | — | 6 | " | x | " | 36 | " | " | " | " | x | x | — | — | — | — | — | — | |
| " | ◆ | Airfoil-6 | " | " | 1.14 | 1.07 | — | 6 | " | x | " | 35 | " | " | " | " | x | x | — | — | — | — | — | — | |
| " | ◆ | Airfoil-7 | " | " | 1.15 | 1.06 | — | 6 | " | x | " | 37 | " | " | " | " | x | x | — | — | — | — | — | — | |
| " | ◆ | Airfoil-9 | " | .279 | 1.06 | 1.04 | — | 6 | " | x | " | 27 | " | " | " | " | x | x | — | — | — | — | — | — | |
| 23 | ▲ | 4416 | 5.50 | .215 | 1.1 | 1.07 | .249 | 0 | 2 | x | — | 38 | 17.6 | .7 | 0,var | 0,∞ | x | x | — | — | x | — | — | — | Constant Chord |
| " | ▲ | 4416 | 5.50 | .242 | 1.1 | 1.07 | .249 | 0 | 2 | No | — | 38 | 18 | " | 0,var | 0,∞ | x | x | — | — | x | — | — | — | |
| " | ◻ | — | .833 | .50 | 1.2 | 1.10 | .400 | " | 5 | No | — | 43 | 20 | " | 0 | 0 | x | x | — | — | — | — | — | — | |
| 24 | ◯ | Lemniscate | 1.33 | .229 | 1.19 | 1.14 | .451 | " | 2 | x | .35 | 100 | 10.7 | " | var | var | — | x | — | — | x | — | x | x | |
| " | ● | Lin-½ Size | 1.33 | .229 | 1.14 | 1.09 | .361 | " | " | x | .34 | 100 | 19.7 | " | var | var | — | x | — | — | x | — | x | x | |
| 25 | ◻ | Profiled | 1.50 | .33 | 1.33 | 1.17 | .194 | " | " | ? | .35 | 28 | var | .75 | 0 | 0 | x | x | — | — | — | — | — | — | 24° Washed Out Blade |
| " | ◯ | Profiled | 1.50 | .33 | 1.33 | 1.17 | .194 | " | " | No | .35 | 28 | var | " | 0,var | 0,var | x | x | — | — | x | — | — | — | |
| " | ◯ | Profiled | 1.50 | .33 | 1.33 | 1.17 | .194 | " | " | x | .35 | 28 | var | " | 0 | 0 | x | x | — | — | x | — | — | — | 24° Washed in Blades |
| 26 | ◆ | Cyl + Round Lip | 1.50 | .481 | 1.05 | 1.03 | .33 | " | " | x | .47 | " | 4 | " | 0,var | var | — | x | — | — | — | — | — | — | |
| " | ◢ | Profiled | 1.05 | .471 | 1.17 | 1.10 | .33 | 3.5 | 10 c | x | .2 | 37 avg | var | " | 0 | 0 | x | x | — | — | x | — | — | — | |
| " | ▲ | Profiled | 1.00 | .471 | 1.15 | 1.06 | .33 | 21.8 | 12 c | x | .2 | 37 avg | — | " | 0 | 0 | x | x | — | — | x | — | — | — | |
| " | ▼ | Profiled | 1.00 | .536 | 1.14 | 1.05 | .33 | 7.0 | 12 c | x | .2 | 38 avg | — | " | — | — | x | x | — | — | x | — | — | — | |
| 26 | ◆ | 00C1 | 1.22 | .27 | 1.10 | 1.06 | .198 | -10.4 | 3 | x | .5 | 4 | — | " | — | — | x | x | — | — | x | — | — | — | |
| " | ◈ | 00C1 | 1.21 | .27 | 1.14 | 1.20 | .198 | -4.4 | 3 | x | .50 | 50 | — | " | — | — | x | x | — | — | — | — | — | — | |
| " | ◇ | 00C1 | 1.21 | .27 | 1.17 | 1.14 | .198 | +1.1 | 3 | x | .5 | 50 | — | " | — | — | x | x | — | — | — | — | — | — | |
| " | ◯ | 00C1 | 1.21 | .7 | 1.17 | 1.14 | .199 | 0 | 3 | x | .5 | 8 | — | .7 | — | — | x | x | — | — | — | — | — | — | |
| 29 | ◢ | Profiled | 1.00 | .676 | 1.16 | — | .325 | — | 5 | — | — | — | — | — | — | — | x | x | — | — | x | — | — | — | |
| " | ▲ | Profiled | 4.00 | .676 | 1.14 | — | .395 | — | 14 | — | — | — | — | — | — | — | x | x | — | — | x | — | — | — | |
| 30 | ◻ | Profiled | .557 | .459 | 1.22 | 1.15 | — | 0 | 3 or 4 | x | .18 | 30 | — | — | 0,var | 0,∞ | — | x | — | — | x | — | — | — | Water Tests |
| 33 | ◇ | Venturi Tube | 1.57 | 0.80 | 1.34 | 1.09 | 0 | 4.3 | 2 | x | x | — | — | — | 0,var | 0,∞ | x | x | — | — | x | — | — | — | Water Tests |
| " | ◇ | Venturi Tube | 1.71 | 0.89 | 1.25 | .99 | 0 | 4.3 | 4 | x | x | -2.1 | — | — | 0,var | 0,∞ | x | x | — | — | x | — | — | — | |
| 35 | ◇◇ | 4415-2 | .788 | .47 | 1.32 | 1.29 | .19 | 4.1 | 4 | x | .5 | 50 | var | 1.0 | — | — | x | x | — | — | x | — | — | — | Water Tests |
| " | ◇◇ | 4415-3 | " | .50 | 1.24 | 1.22 | " | 4.1 | " | x | — | " | var | — | — | — | x | x | — | — | x | — | — | — | Prop Tests |

37

TABLE I - Continued

PHYSICAL ... OF EXPERIMENTAL MODELS AND OF MEASURED TEST DATA

Note: (x) indicates propeller twist in Twist Column
(x) indicates measured data presented in literature
(-) indicates data not presented in literature

c - contra-rotating
i - inlet stators
e - exit stators

FIGURE 1: COMPARISON OF STATIC
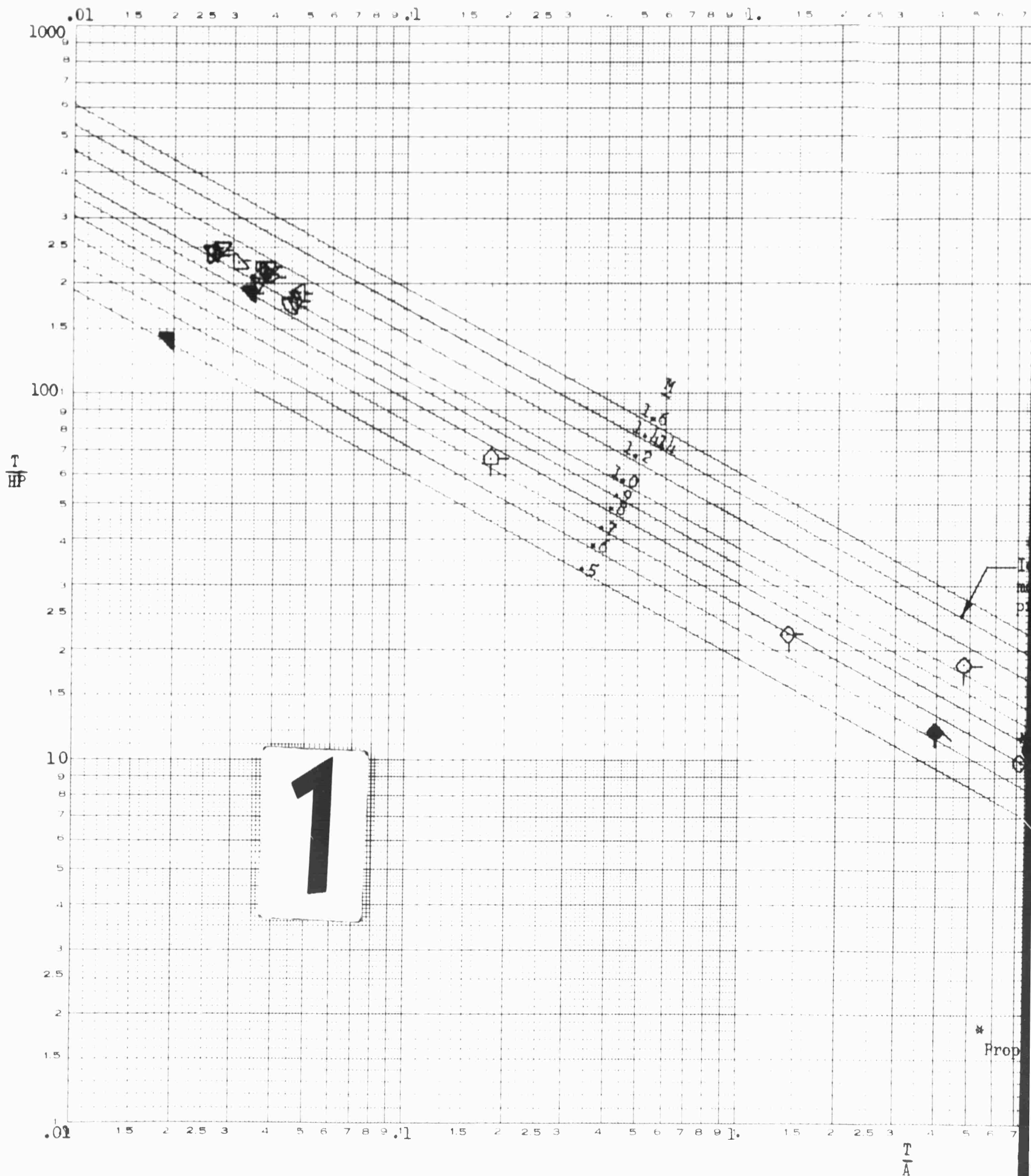
FIGURE 1: COMPARISON OF STATIC FIGURES OF MERIT
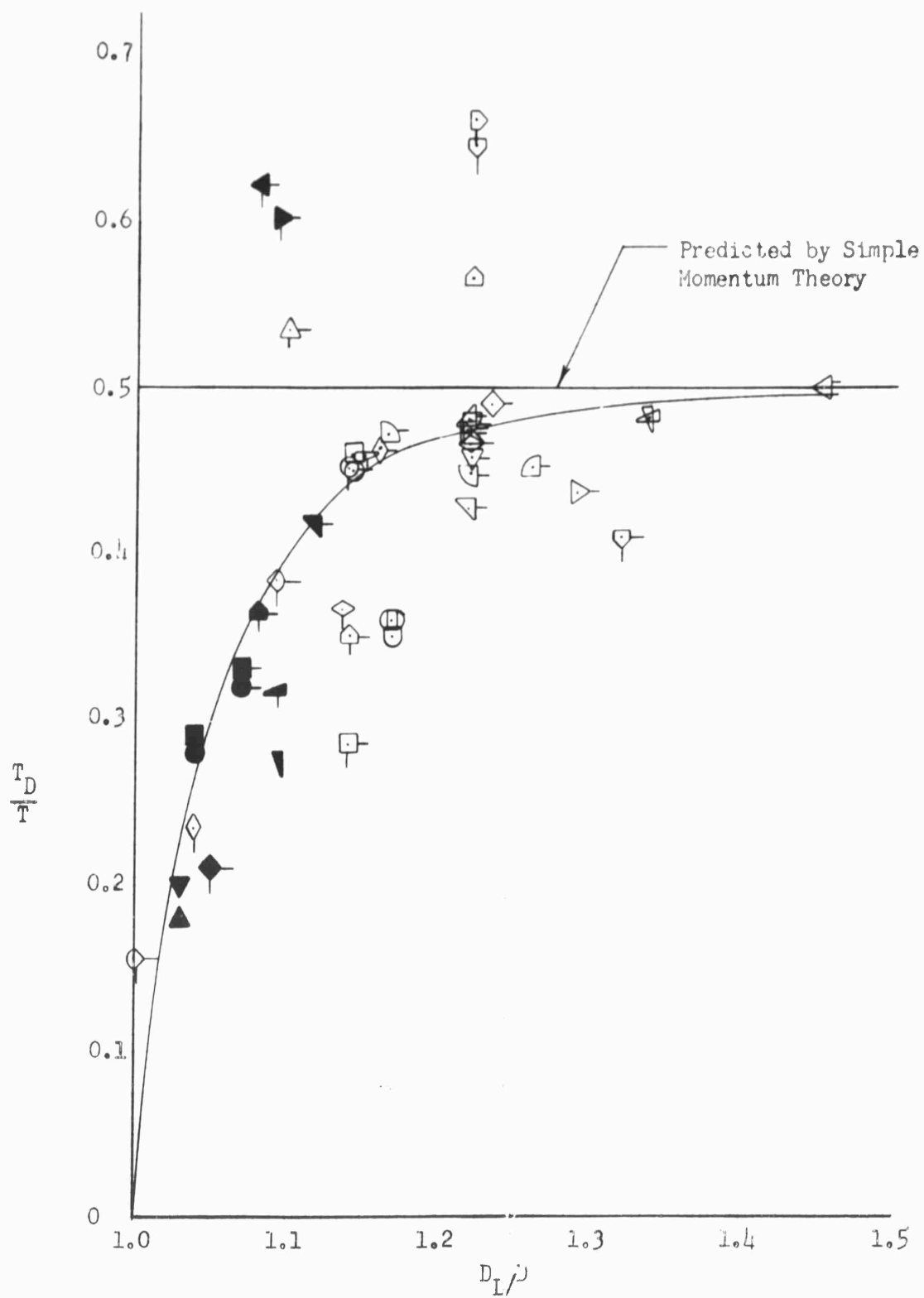
FIGURE 2: COMPARISON OF DUCT THRUST IN HOVERING FLIGHT AT
MAXIMUM FIGURE OF MERIT
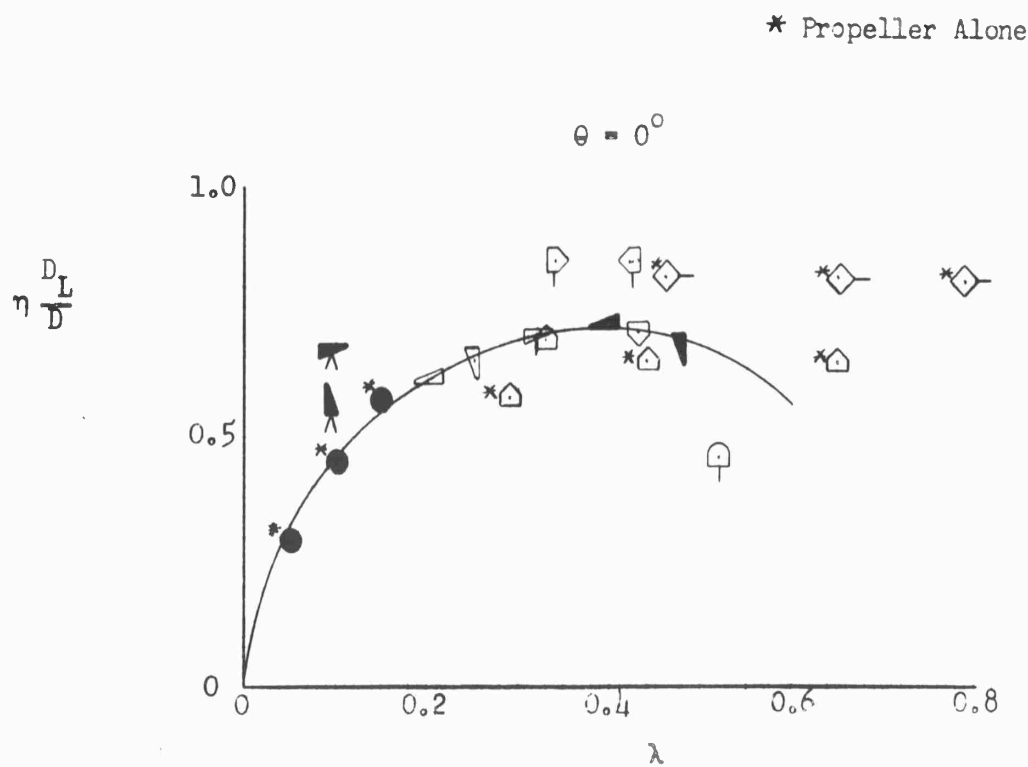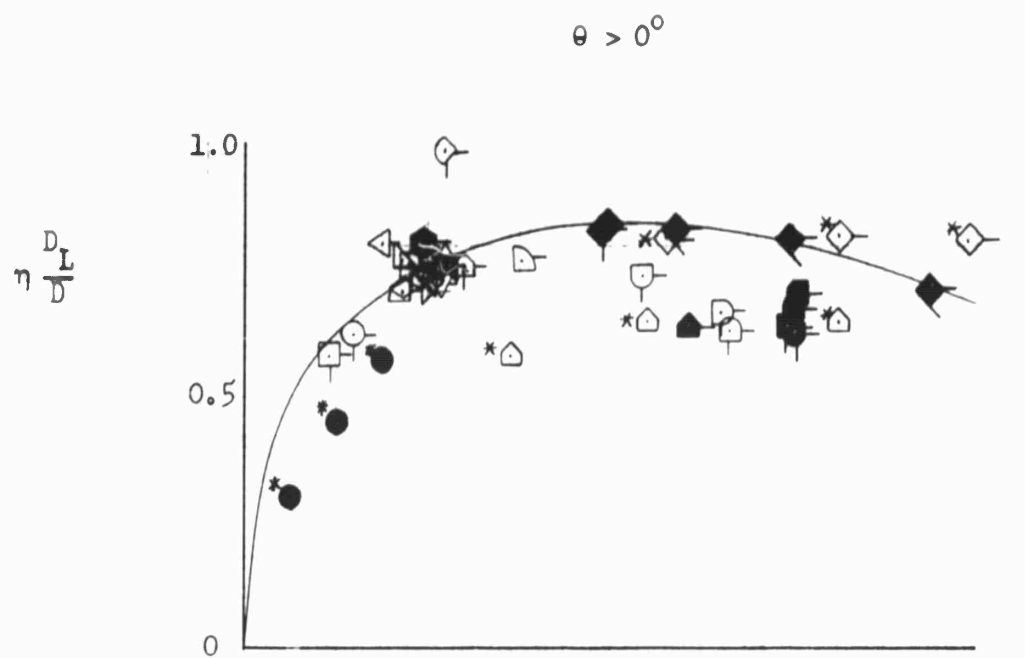
FIGURE 3: COMPARISON OF PROPULSIVE EFFICIENCIES FOR
DIFFUSED AND NON-DIFFUSED DUCTED PROPELLERS
IN AXIAL FLOW
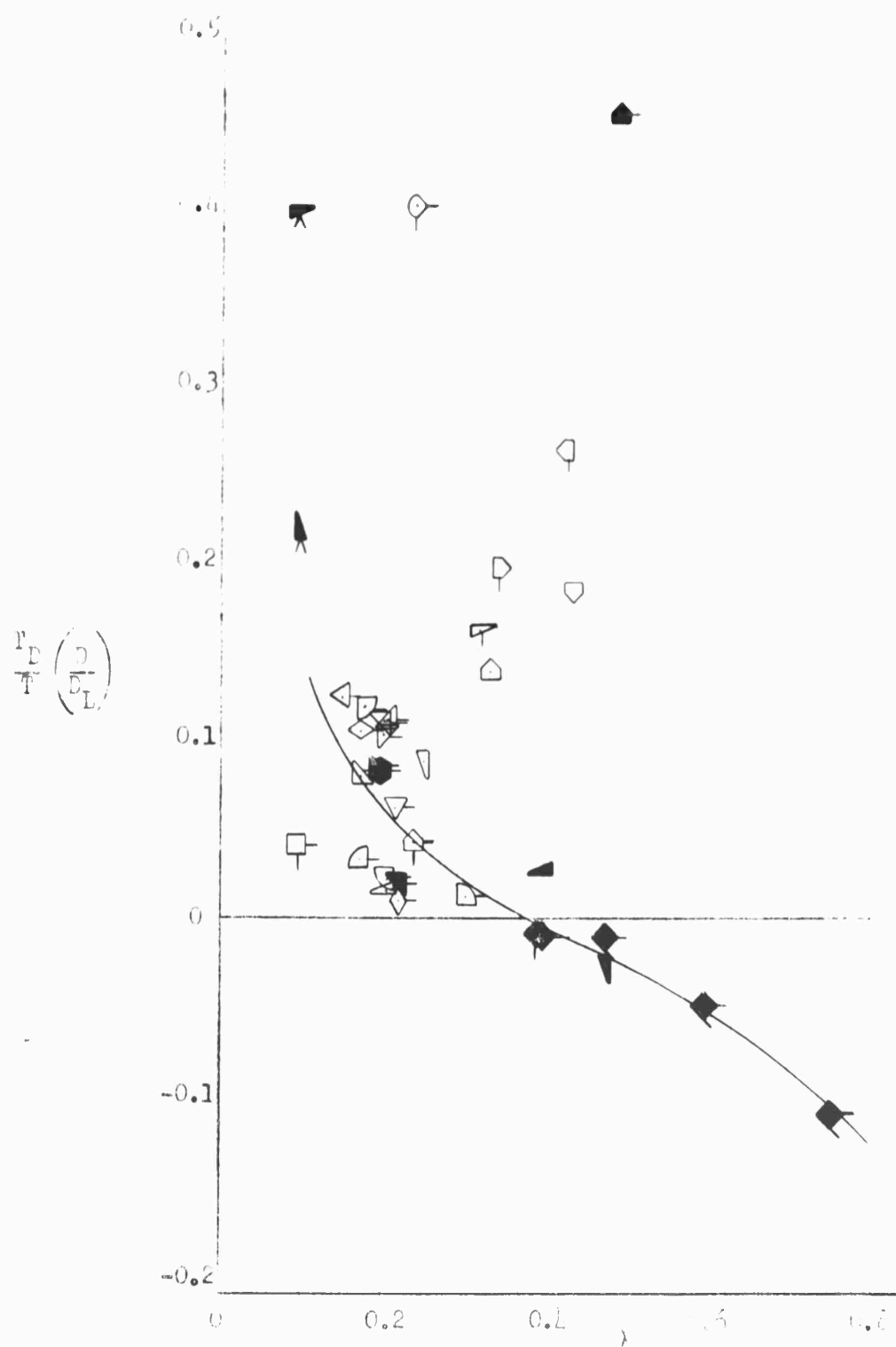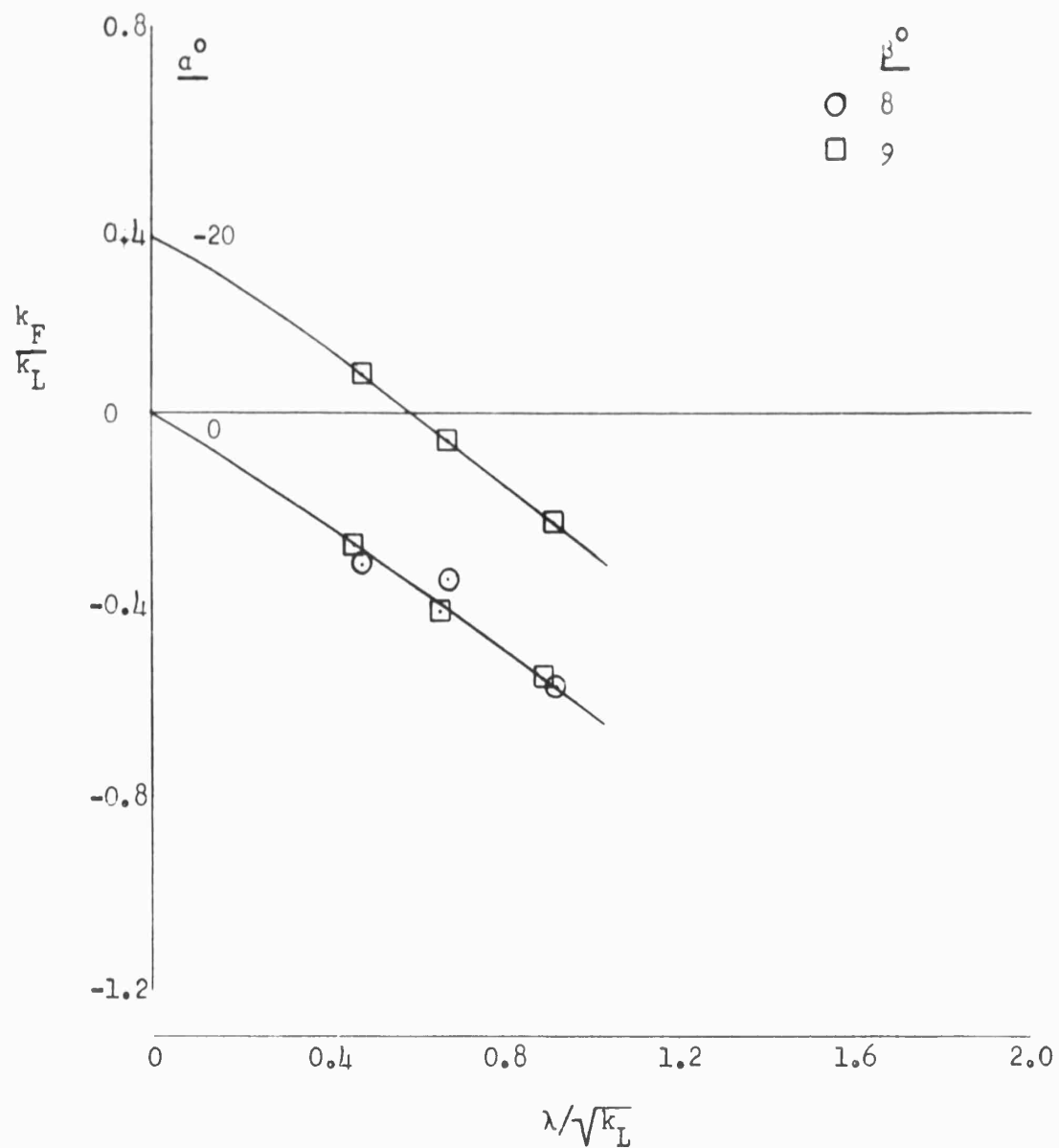
FIGURE 5(a) CORRELATION OF PROPULSIVE FORCE-LIFT RATIO IN NON-AXIAL FLOW
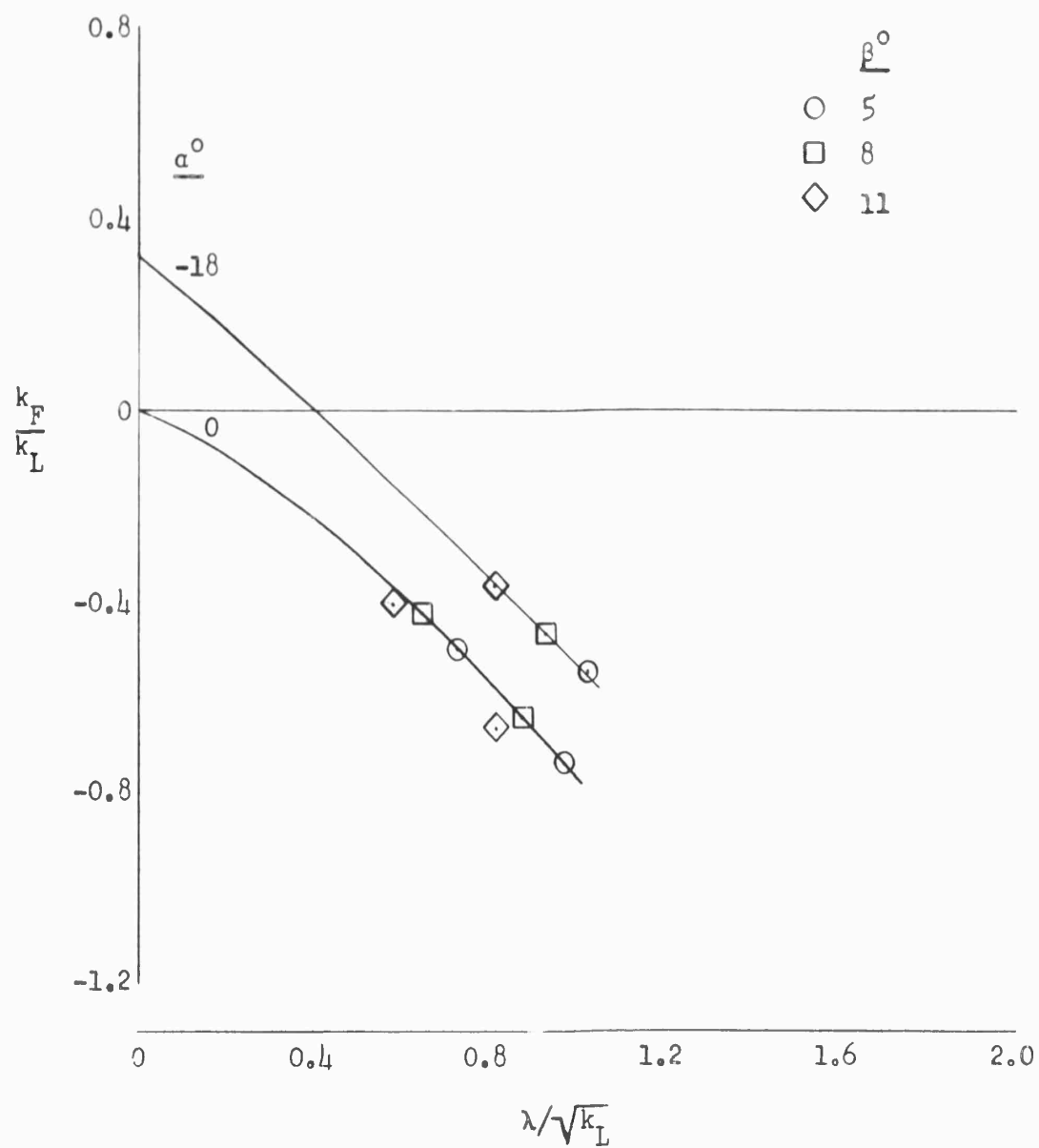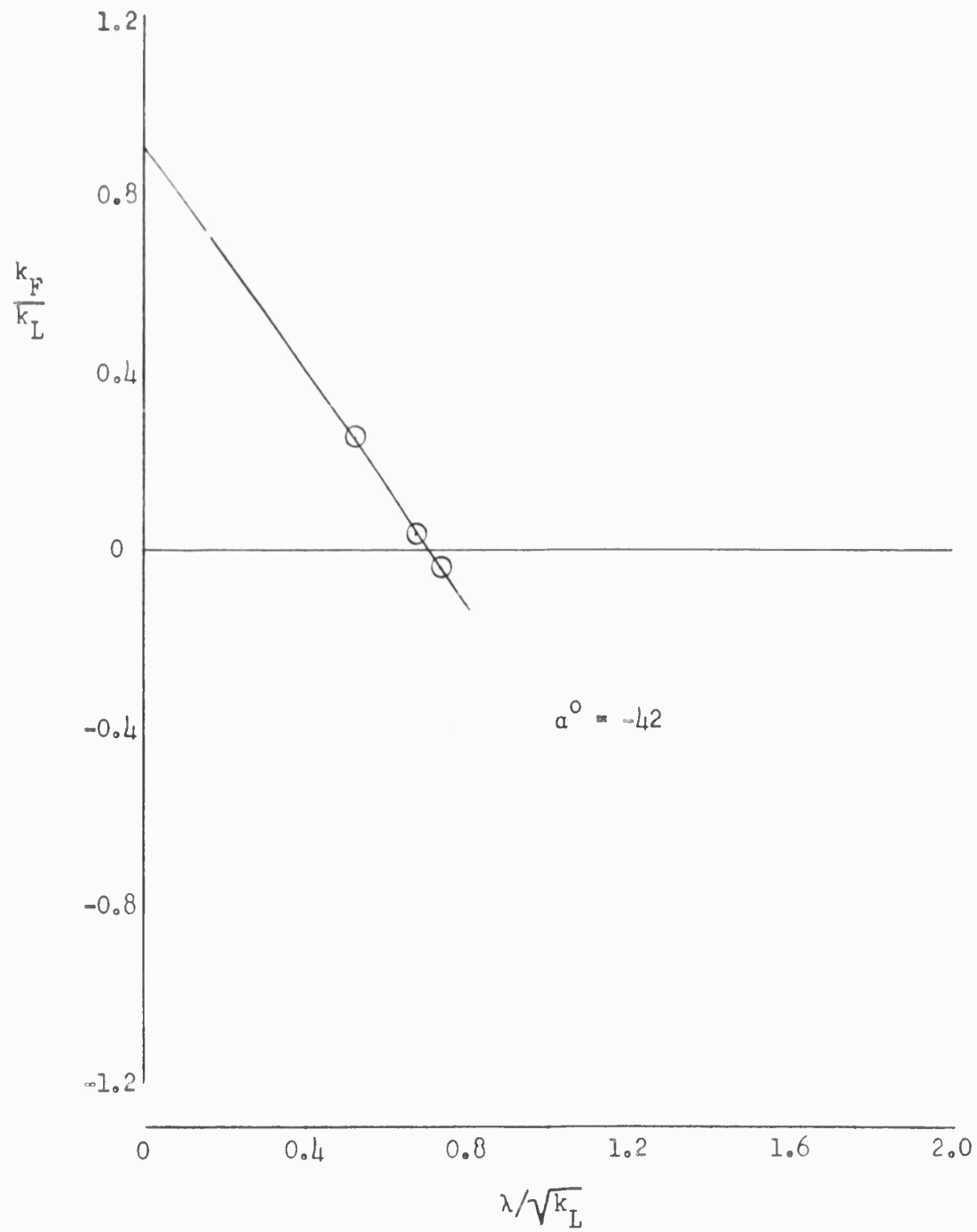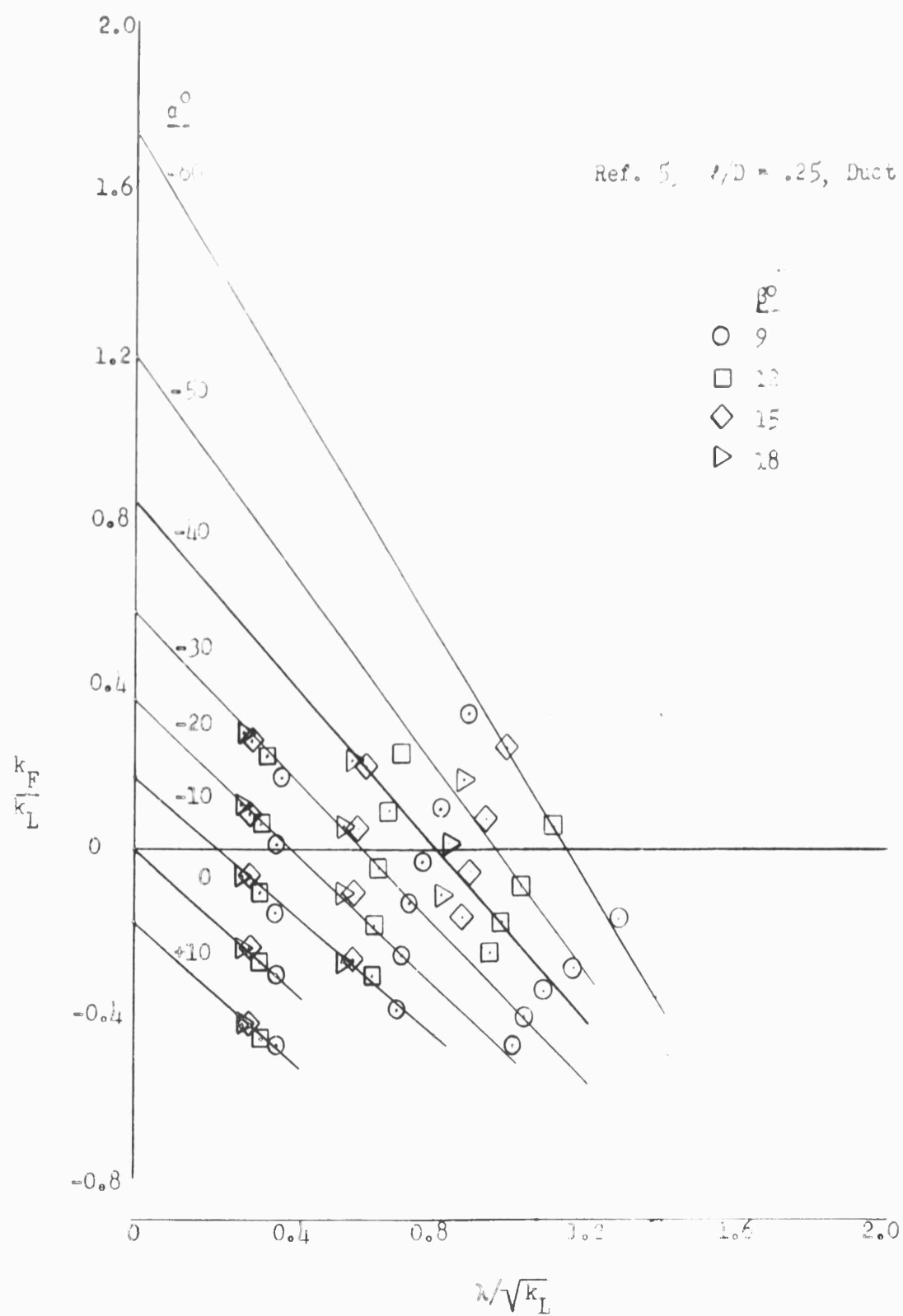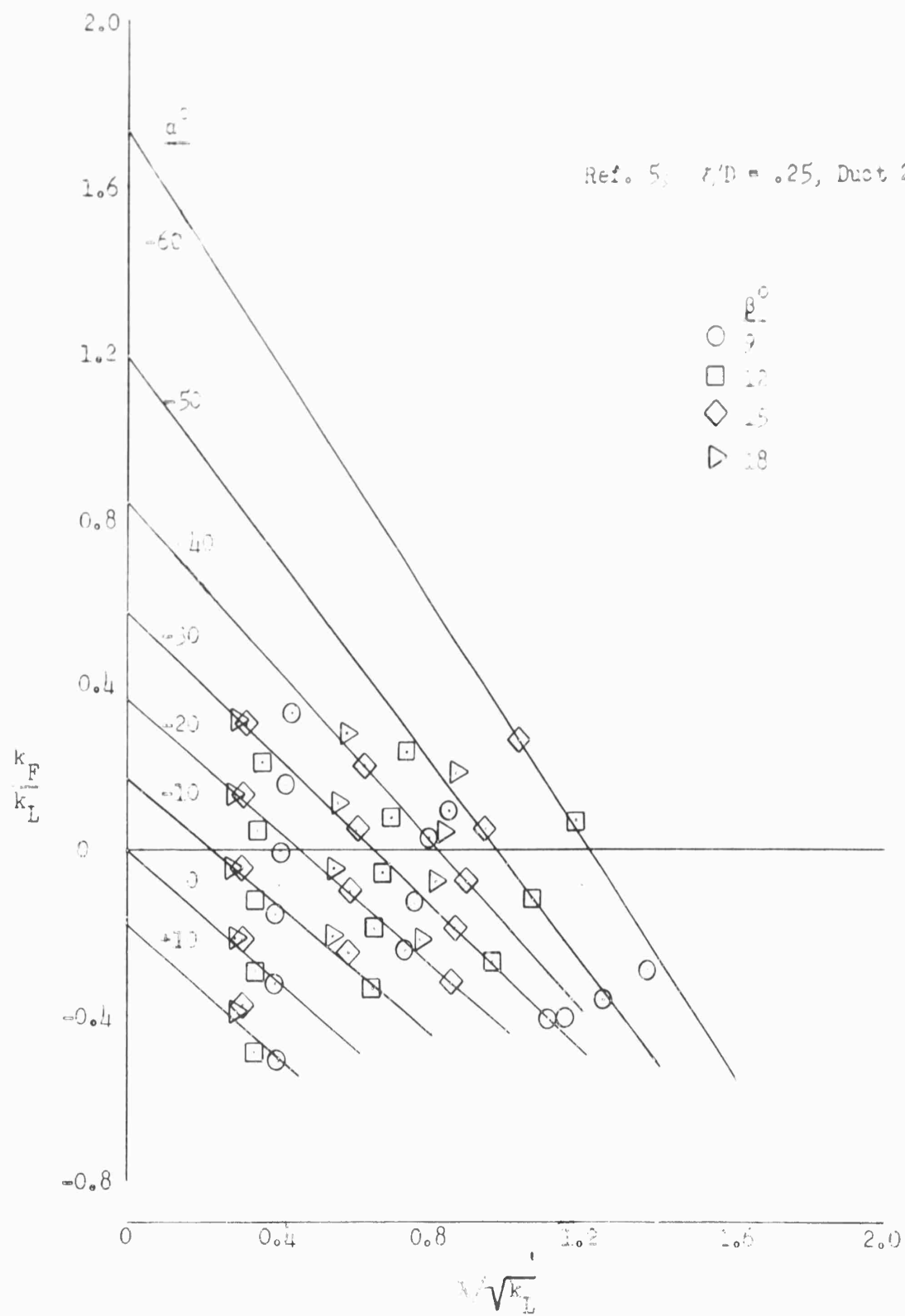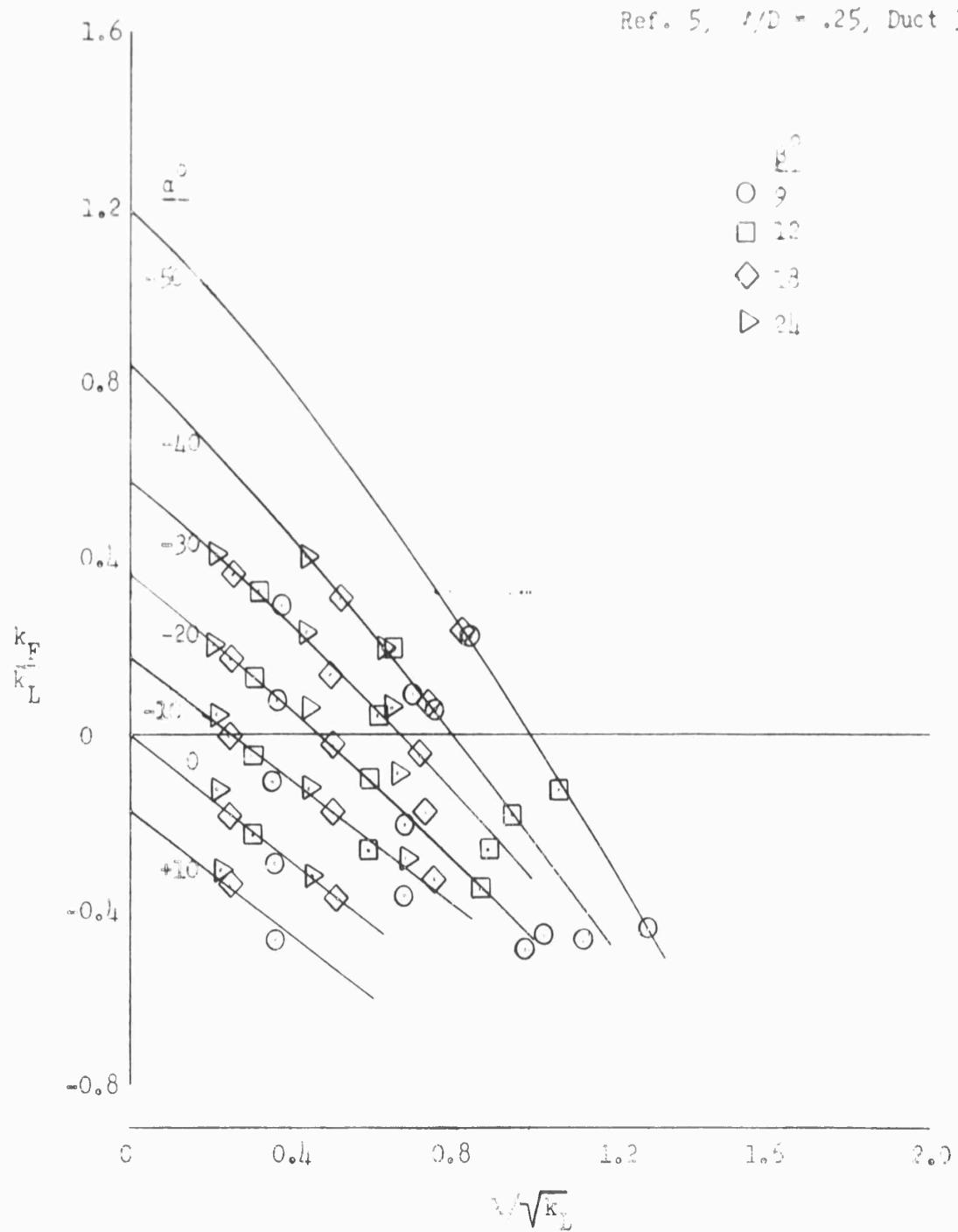
43

Ref. 1;  $l/D = .248$

$\beta^\circ$

○  5
□  8
◇  11

$a^\circ$

FIGURE 5(b)

44

Ref. 3;  $\ell/D = .284$

FIGURE 5(c)

45

FIGURE 5(d)

Ref. 5, l/D = .25, Duct 2

FIGURE

Ref. 5, $l/D = .25$, Duct 3

Ref. 5, $\gamma/D = .15$, Duct 4

$\frac{K_F}{K_L}$ vs $\sqrt{K_L}$

Ref. 19, l/D = .77

Ref. 2; $t/D = .68$

Ref. 13, $l/D = .75$

Ref. 23, $\prime/D = .229$, Duct 3

FIGURE 64(b)

Ref. 23,  t/D = .209, Duct 5

FIGURE 5(a)

FIGURE 3(c)

FIGURE

68

FIGURE 14(a)—PROGRESSIVE BOW DOWN PART DUE TO NONAXIAL FLOW

$\dfrac{k_F}{k_L}$

$\sqrt{k_L}$

$0.2$

$0.4$

$0.6$

$0.8$

$1.0$

$1.2$

$0$

$-0.4$

$-0.8$

$-1.2$

$-1.6$

$0$    $0.2$    $0.4$    $0.6$    $0.8$

$s/D$
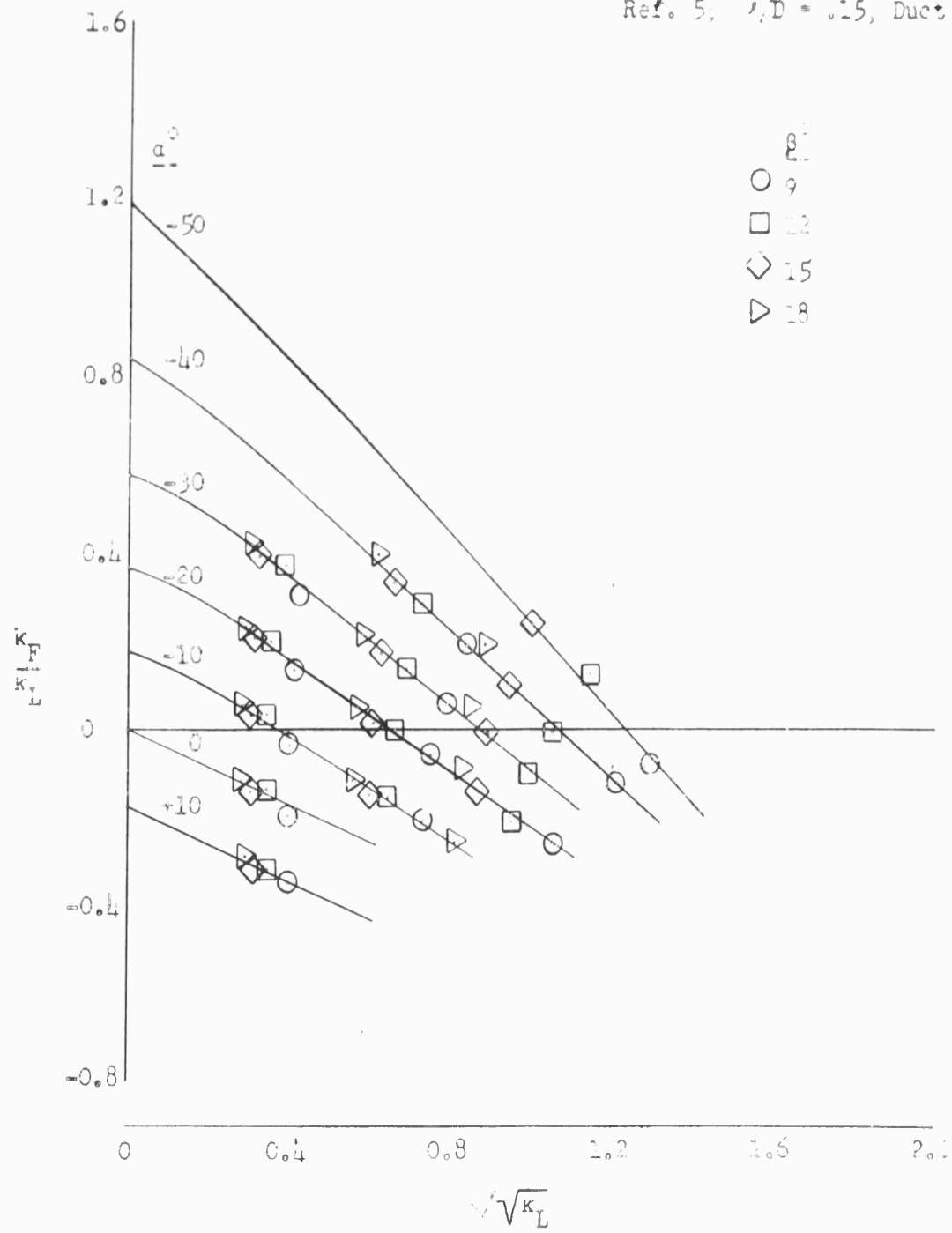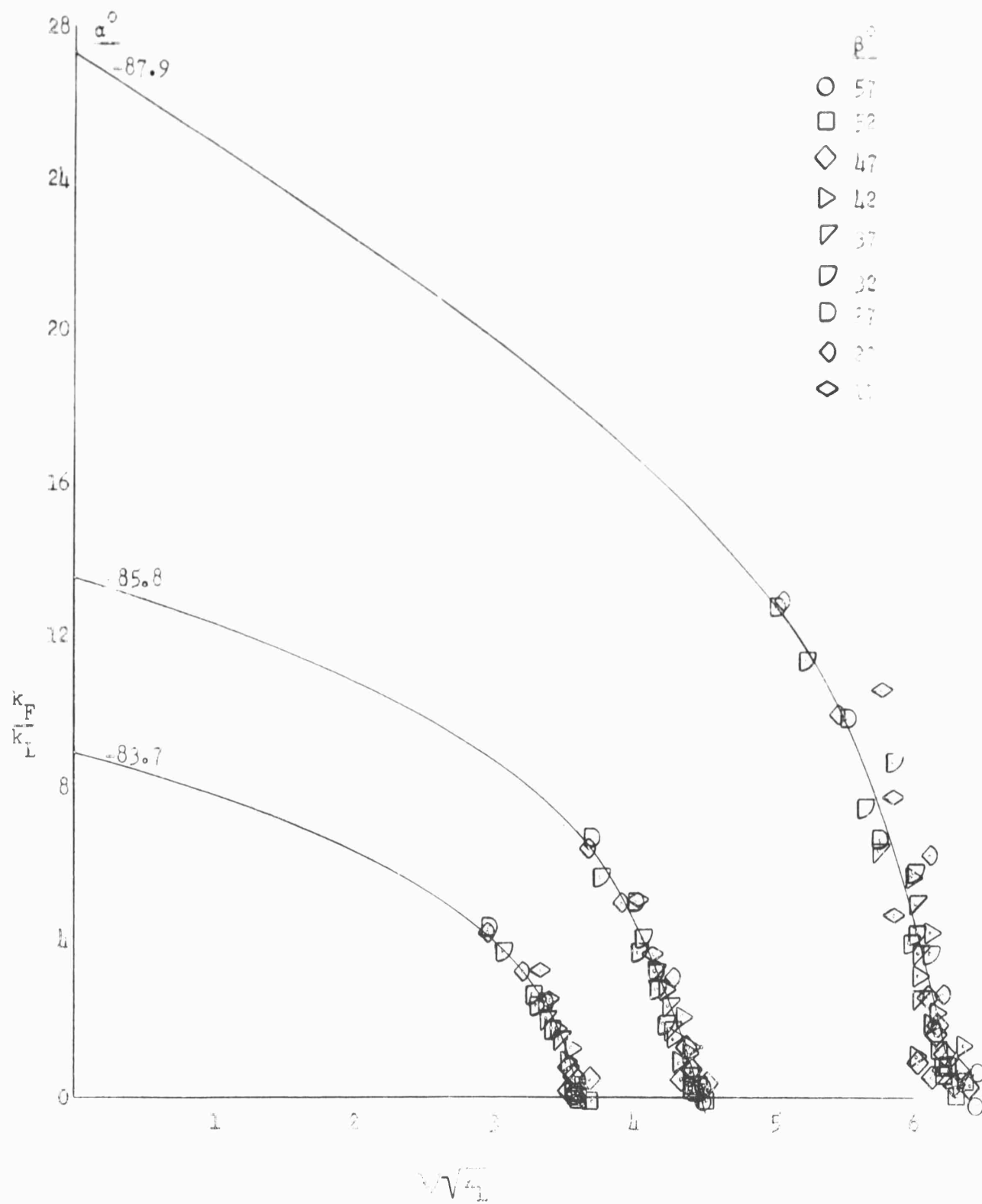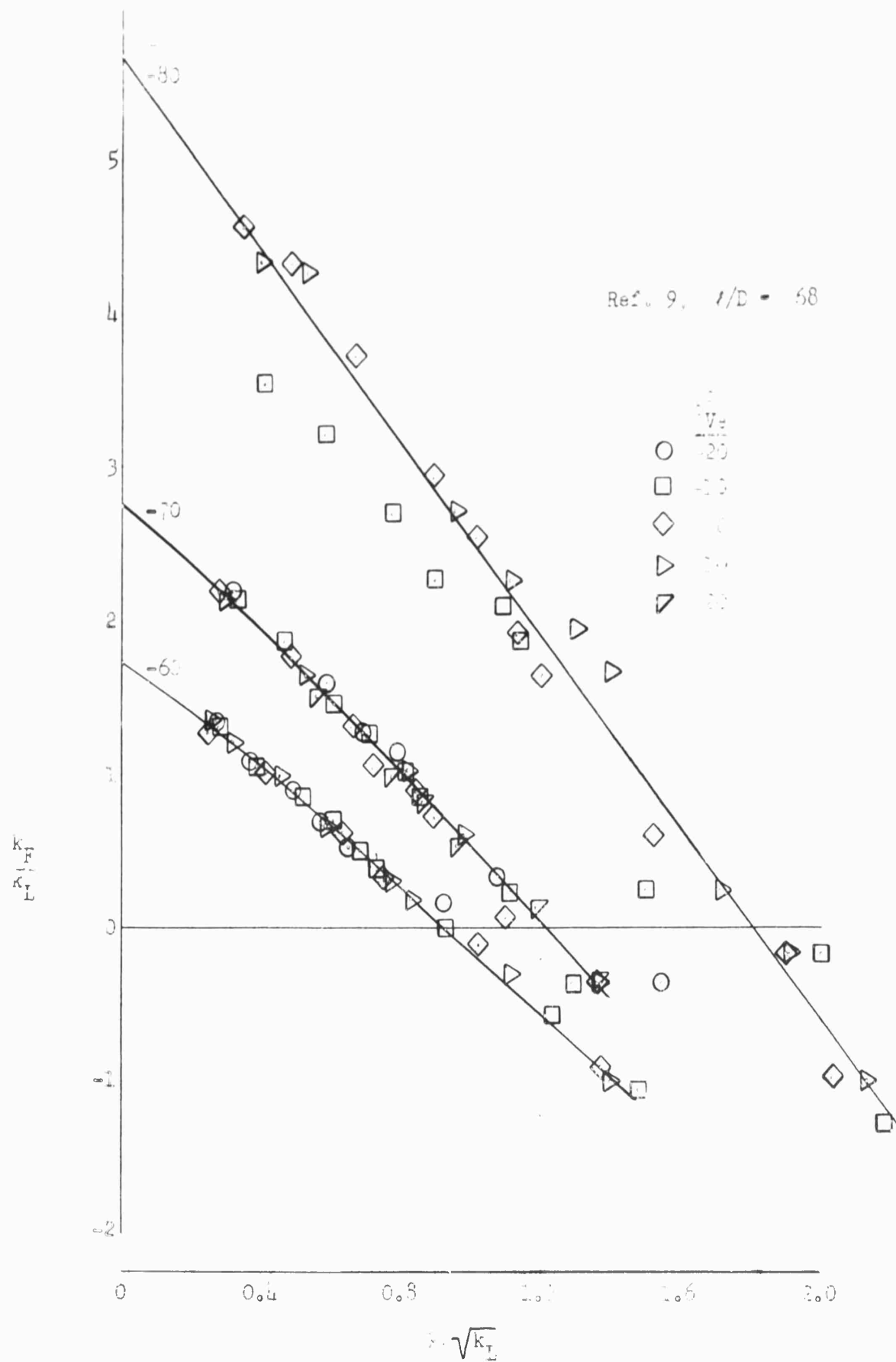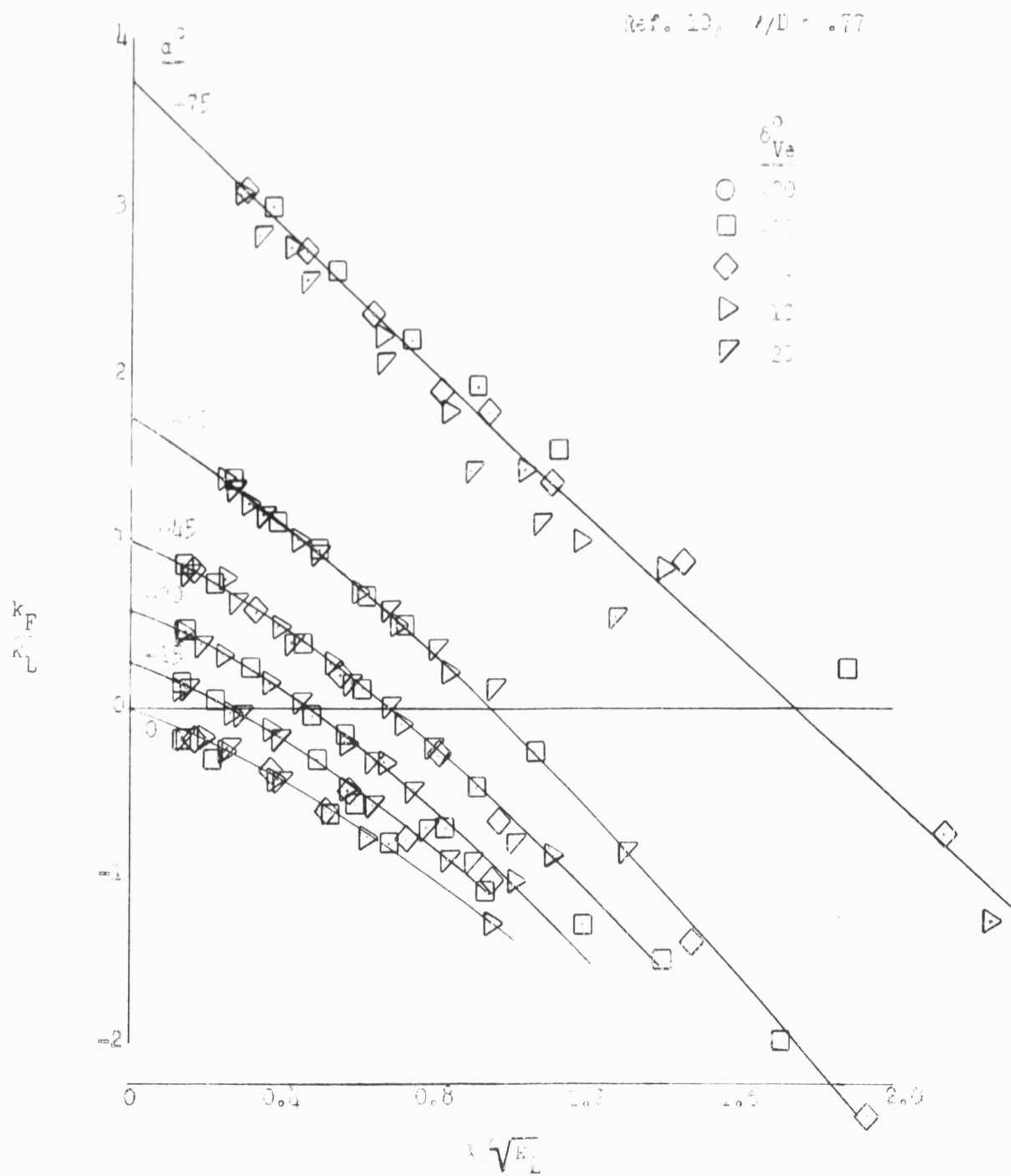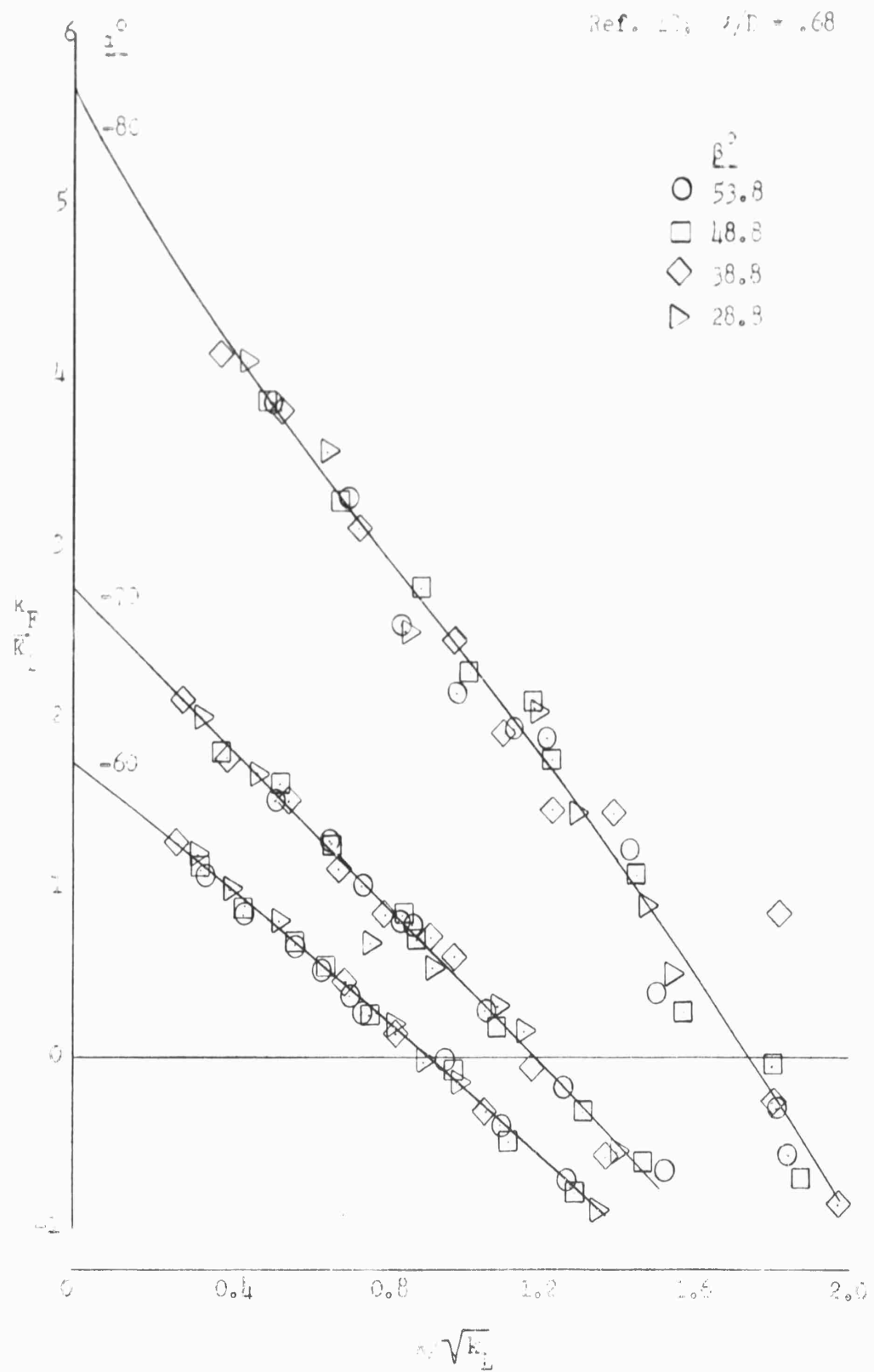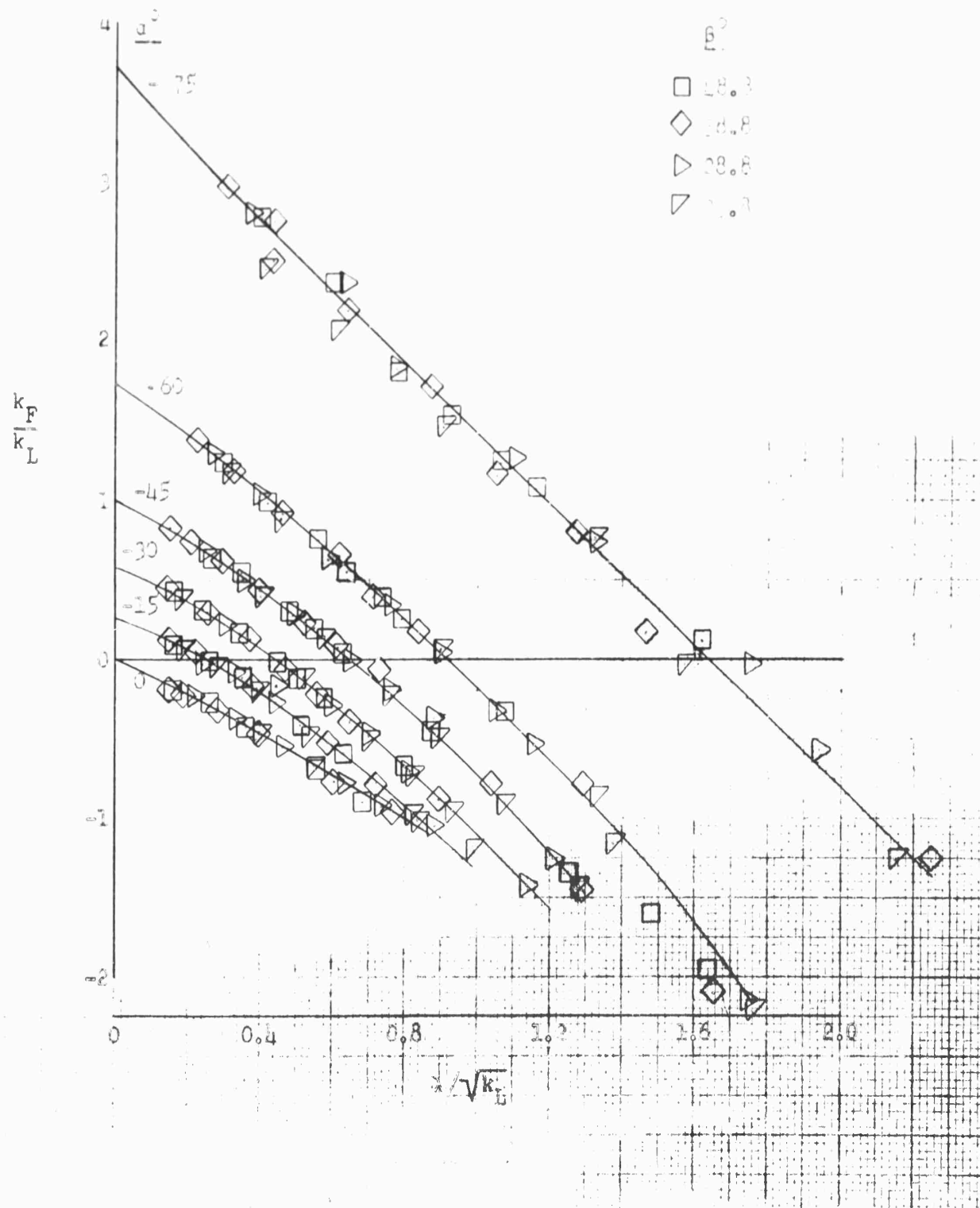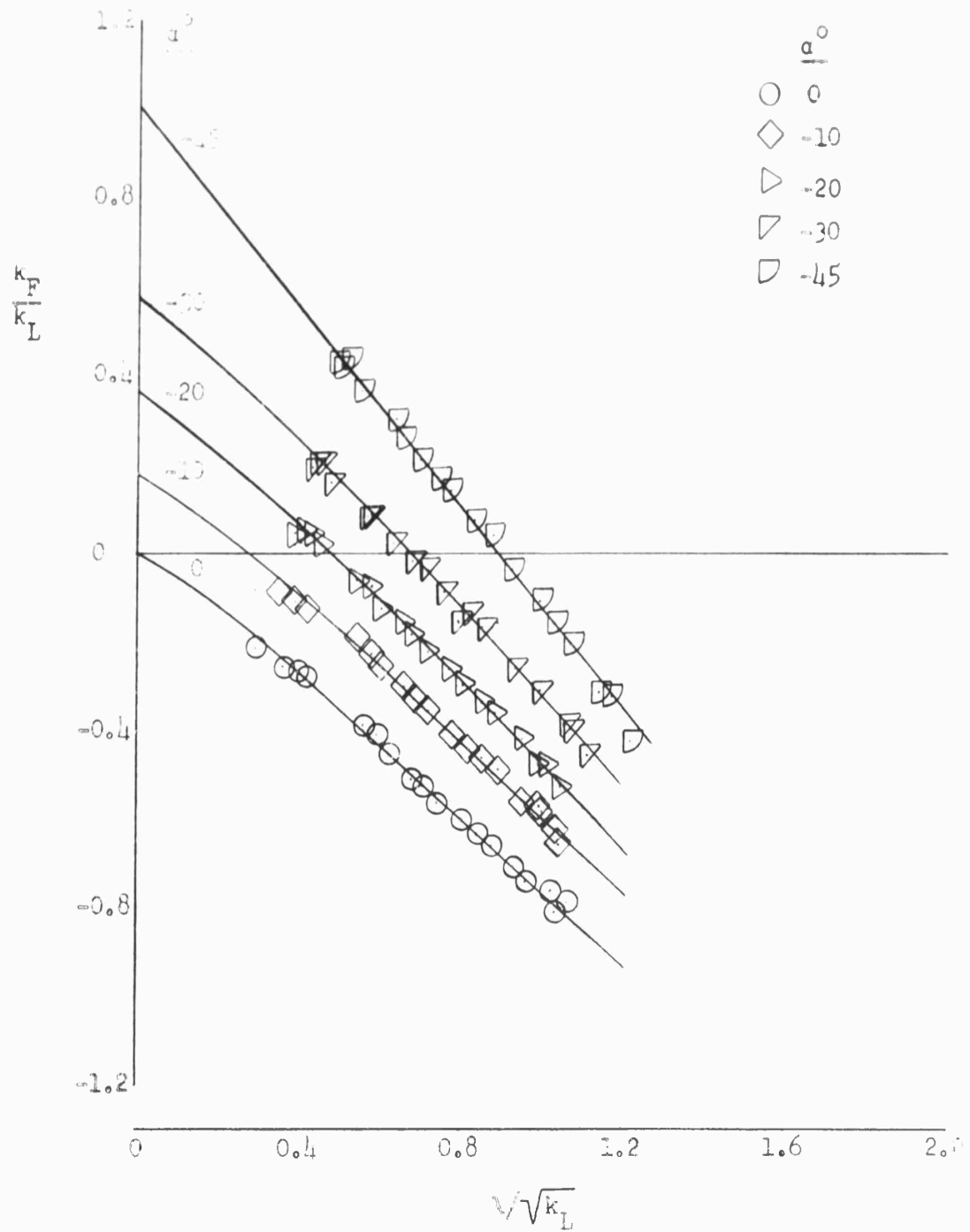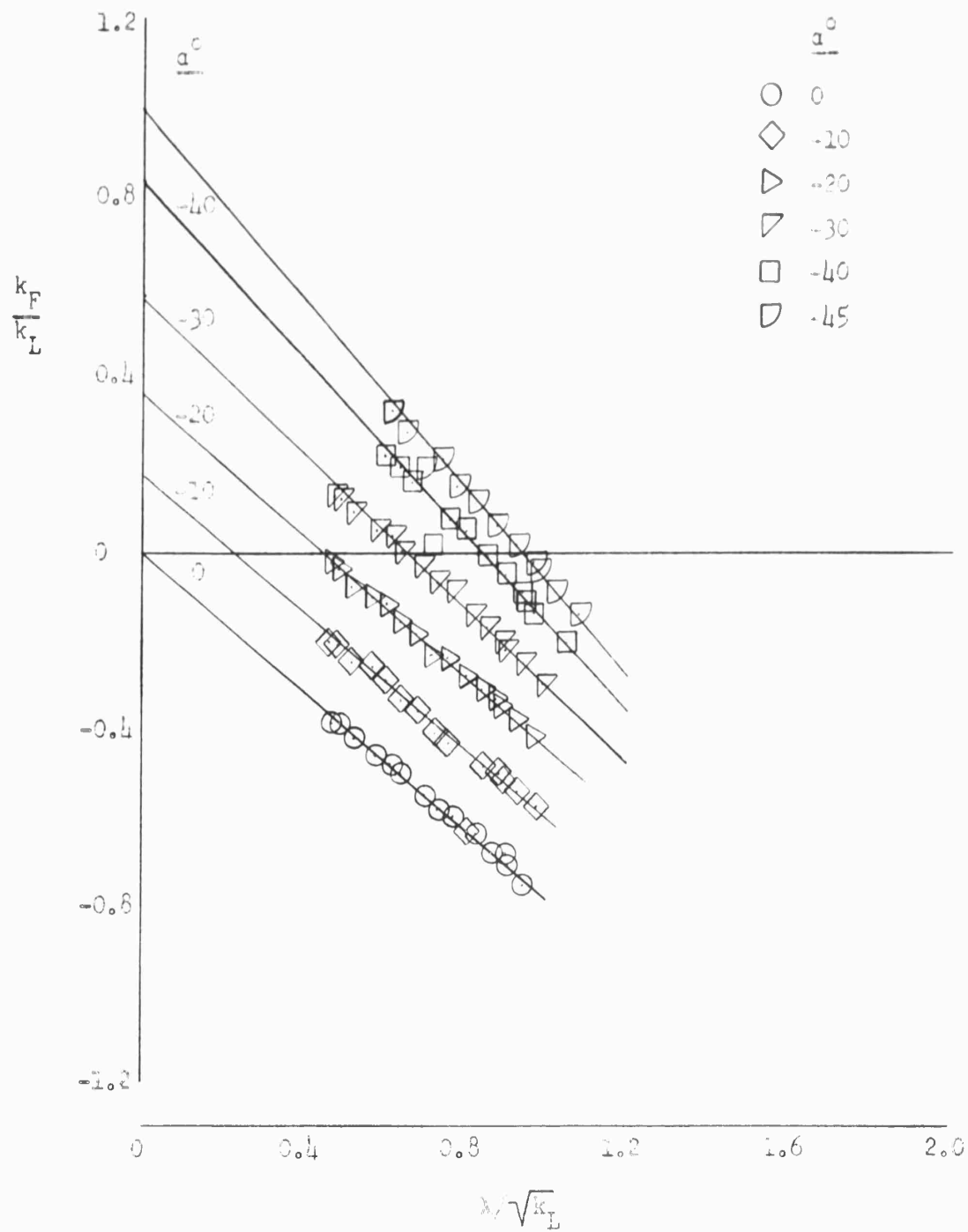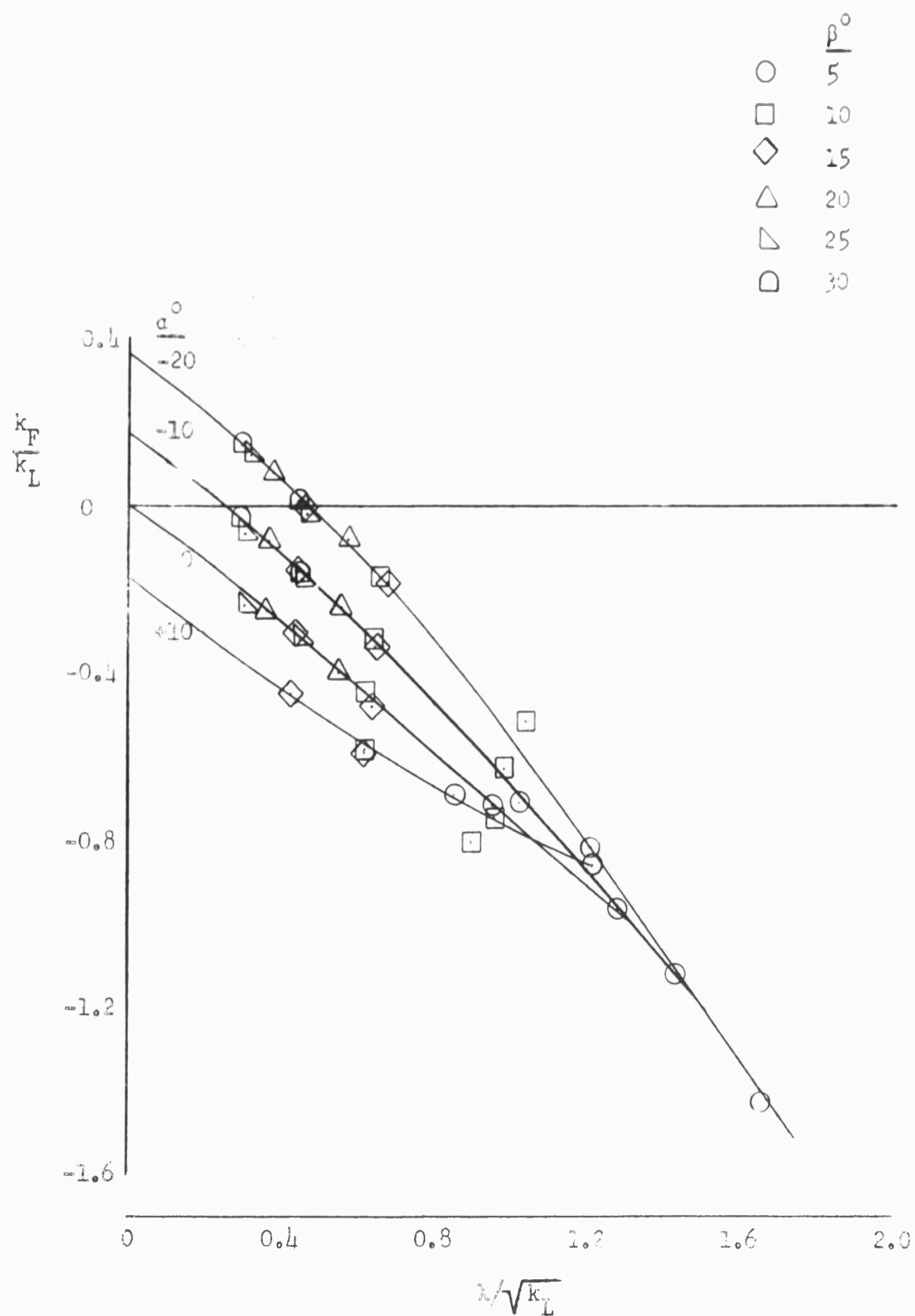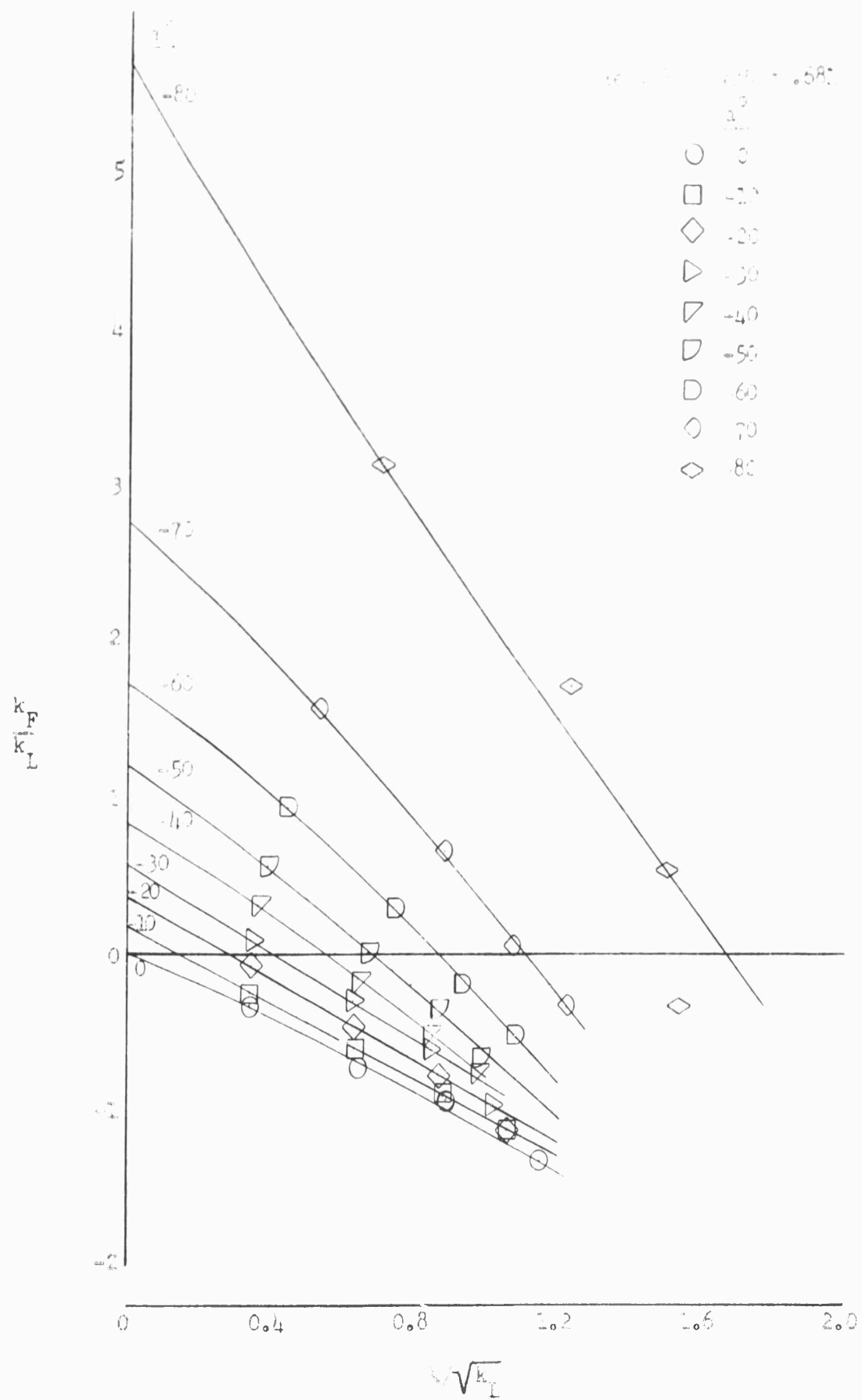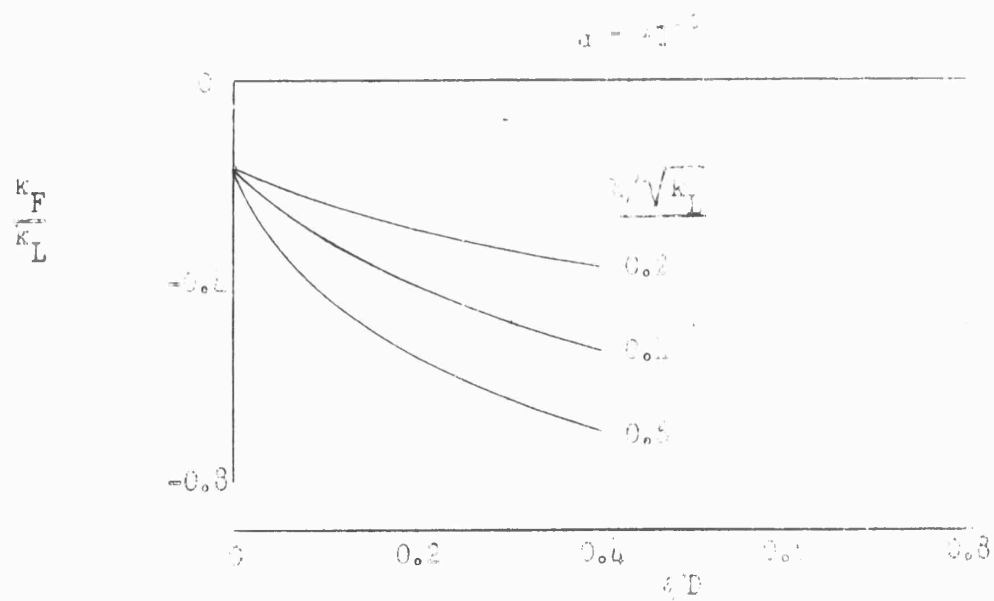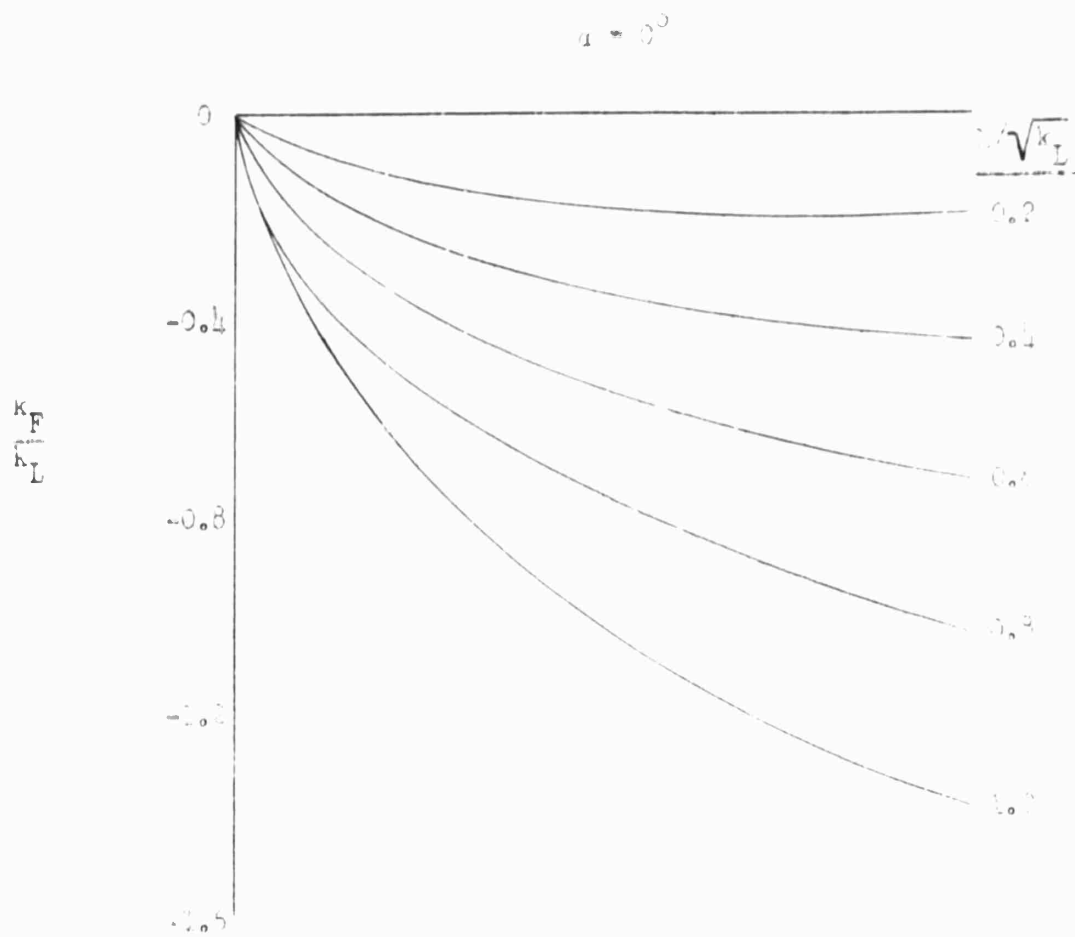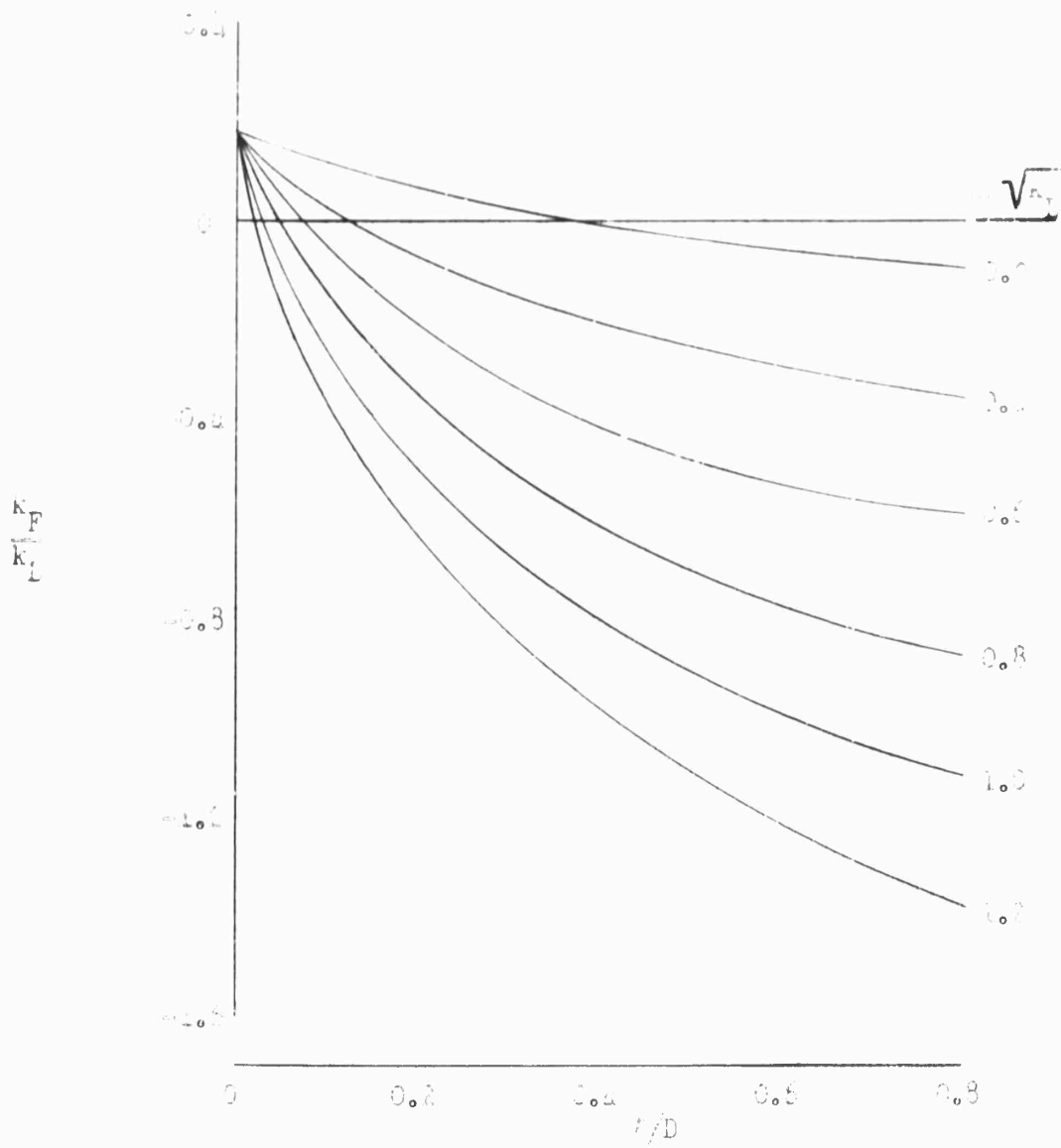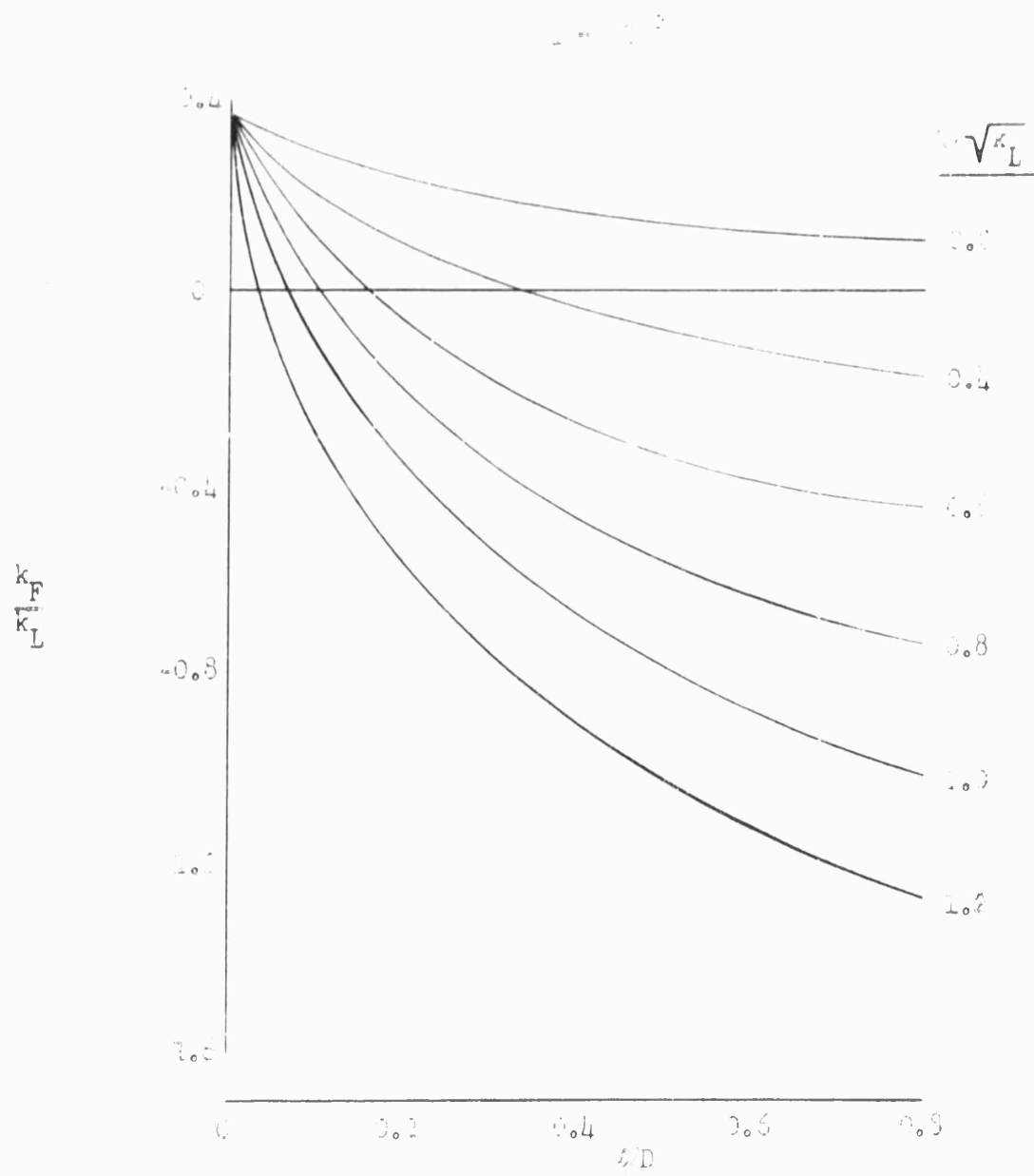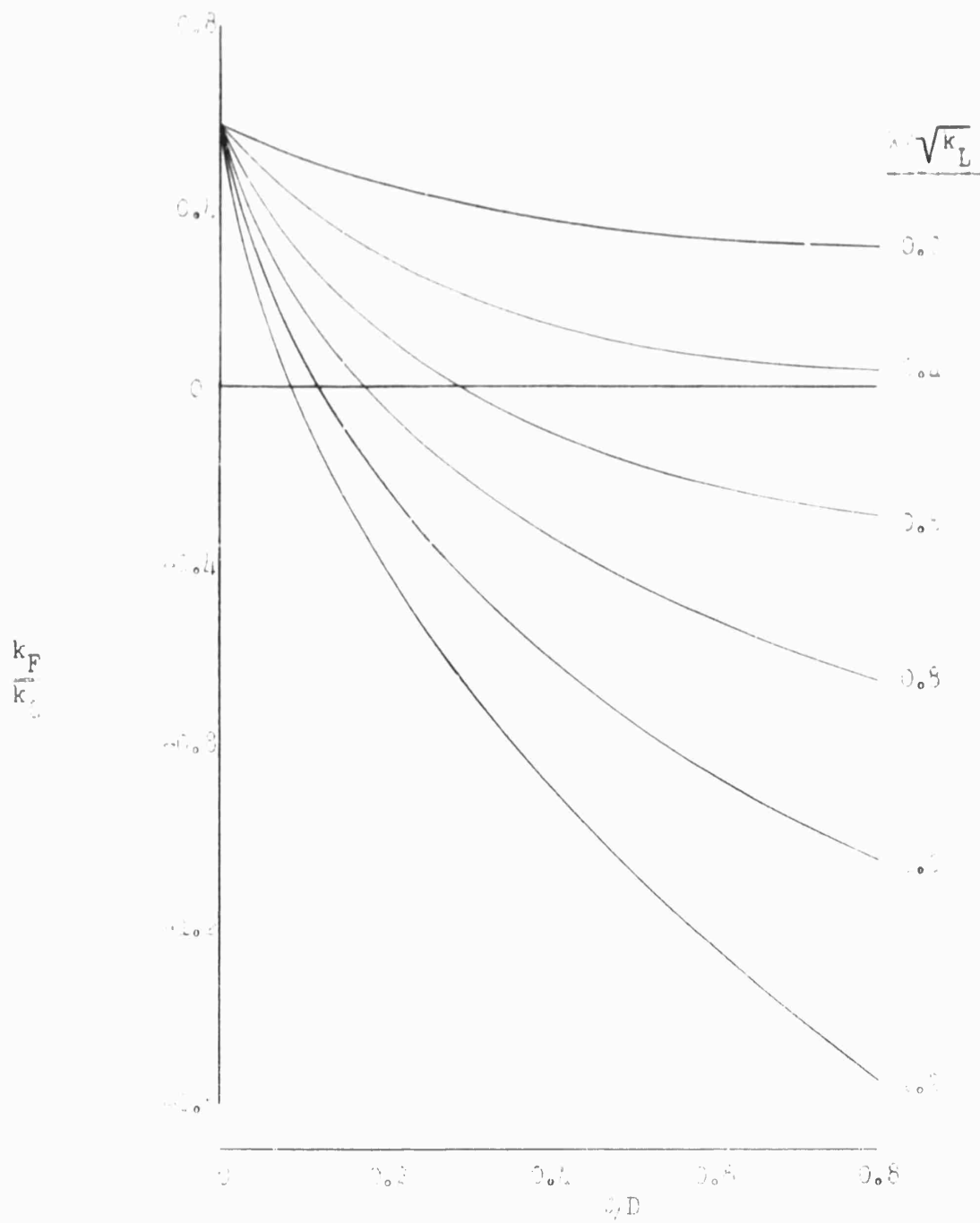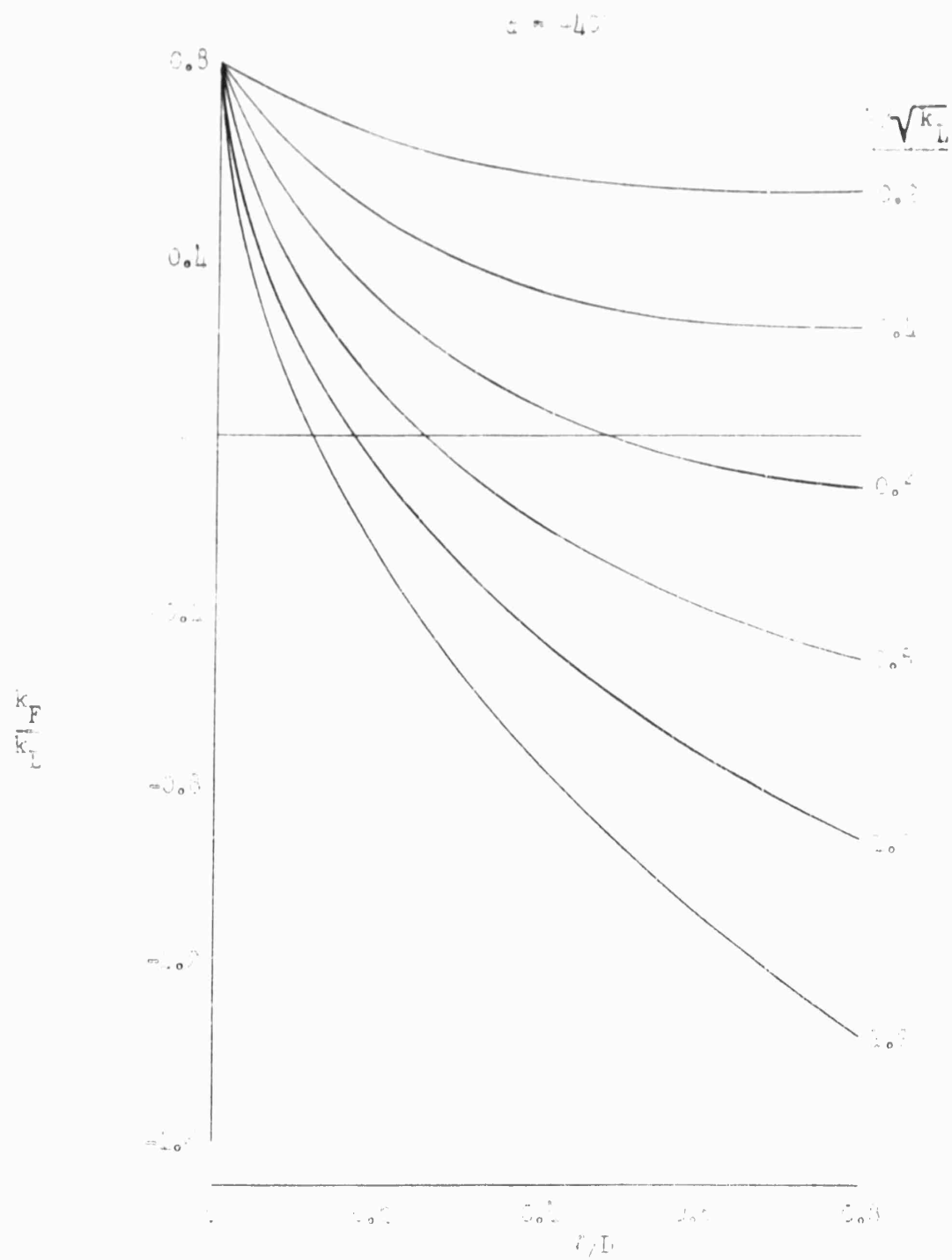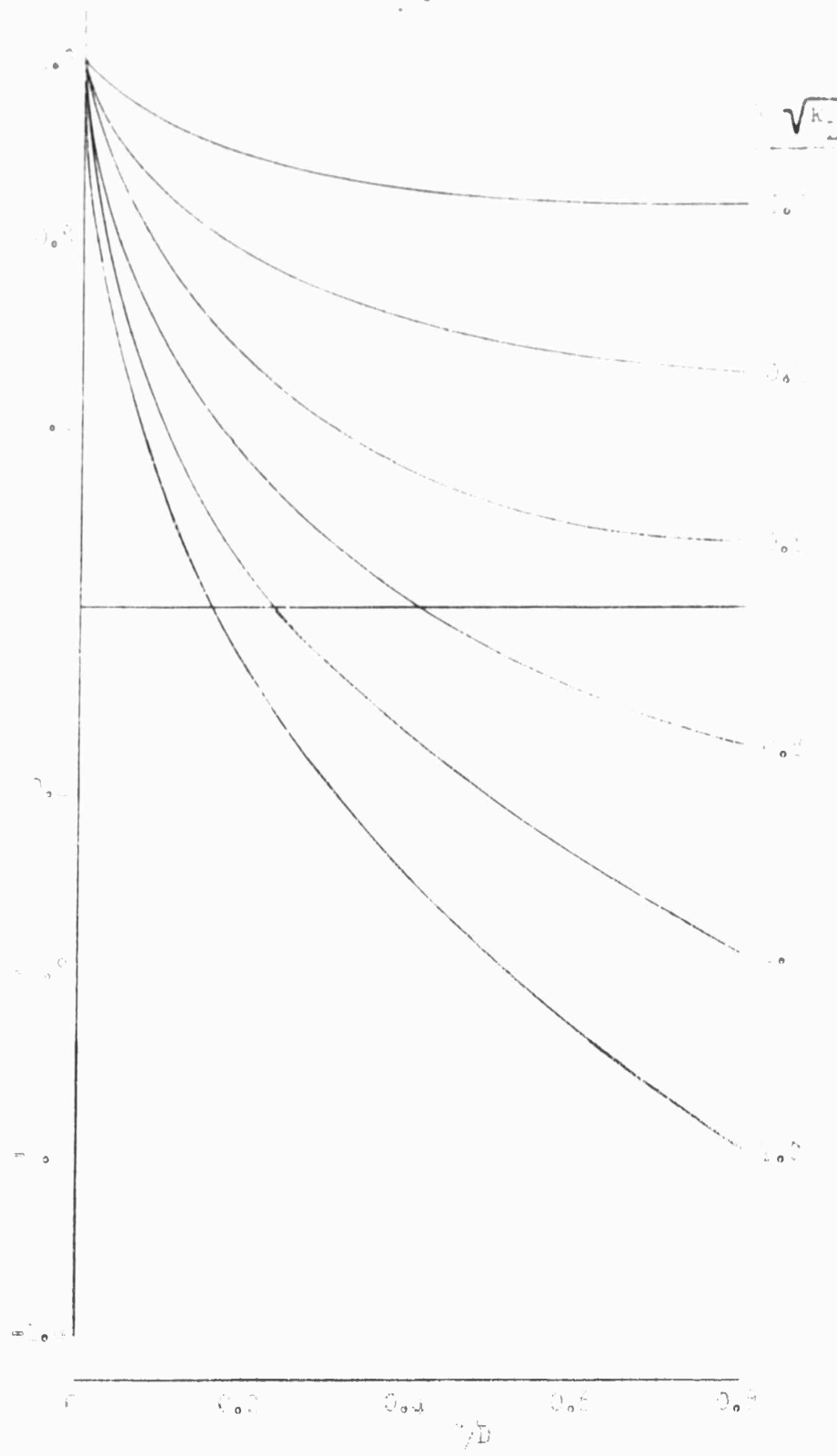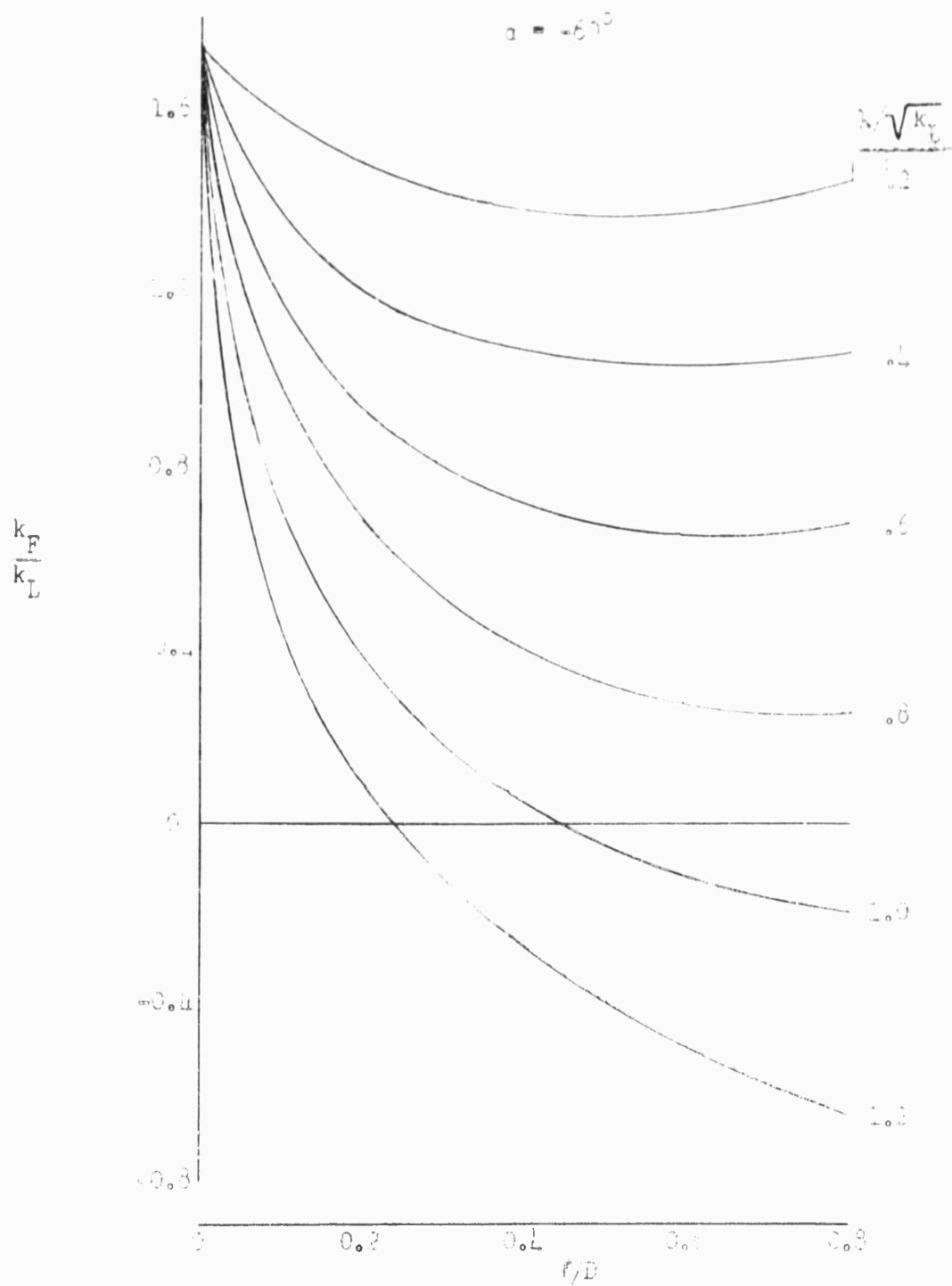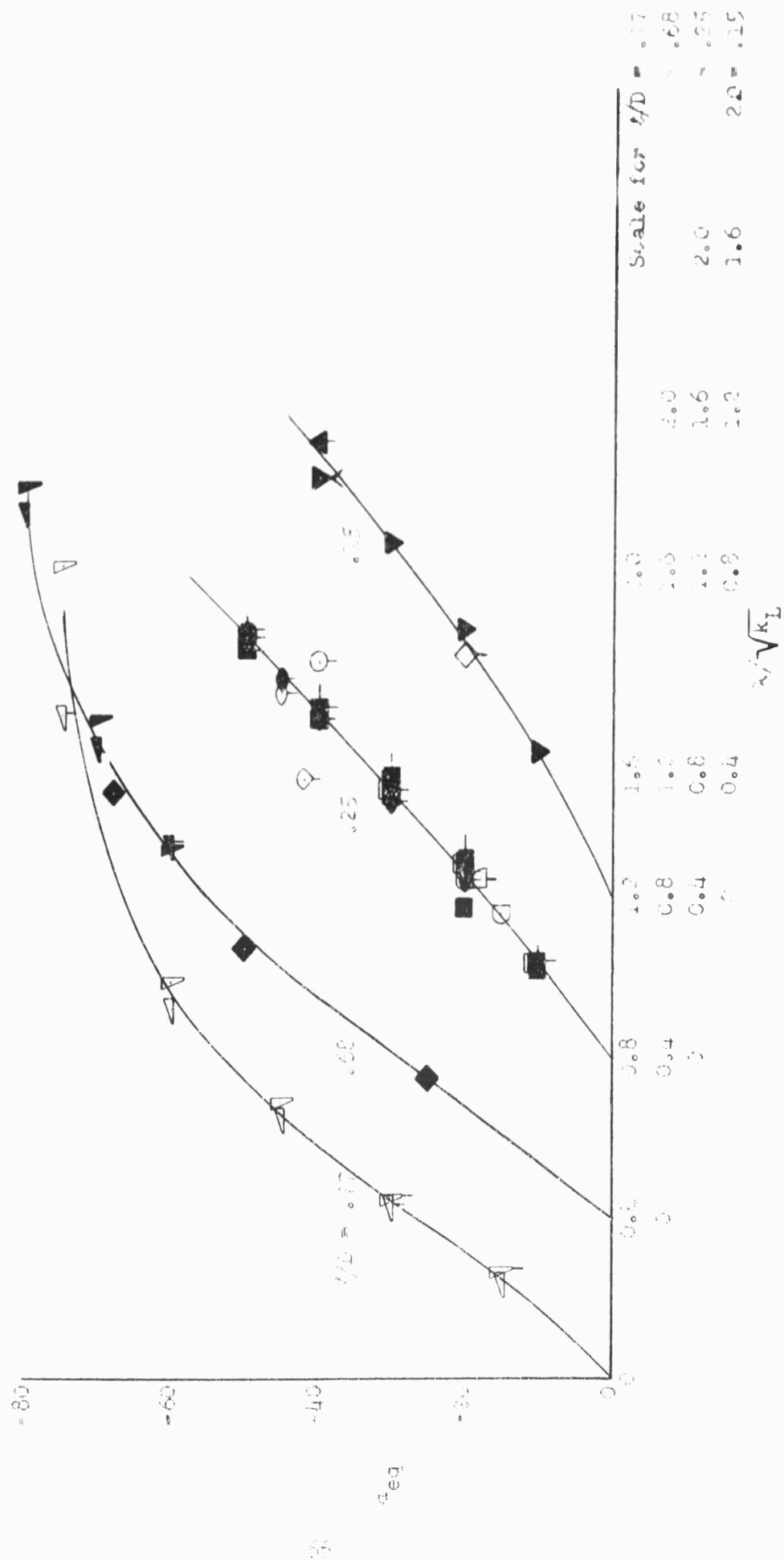
FIGURE 2: COMPARISON OF EQUILIBRIUM ANGLE OF ATTACK OF DUCTED PROPELLERS AT ...

$v / \sqrt{k_L}$

deg

Scale for $l/D = .77$
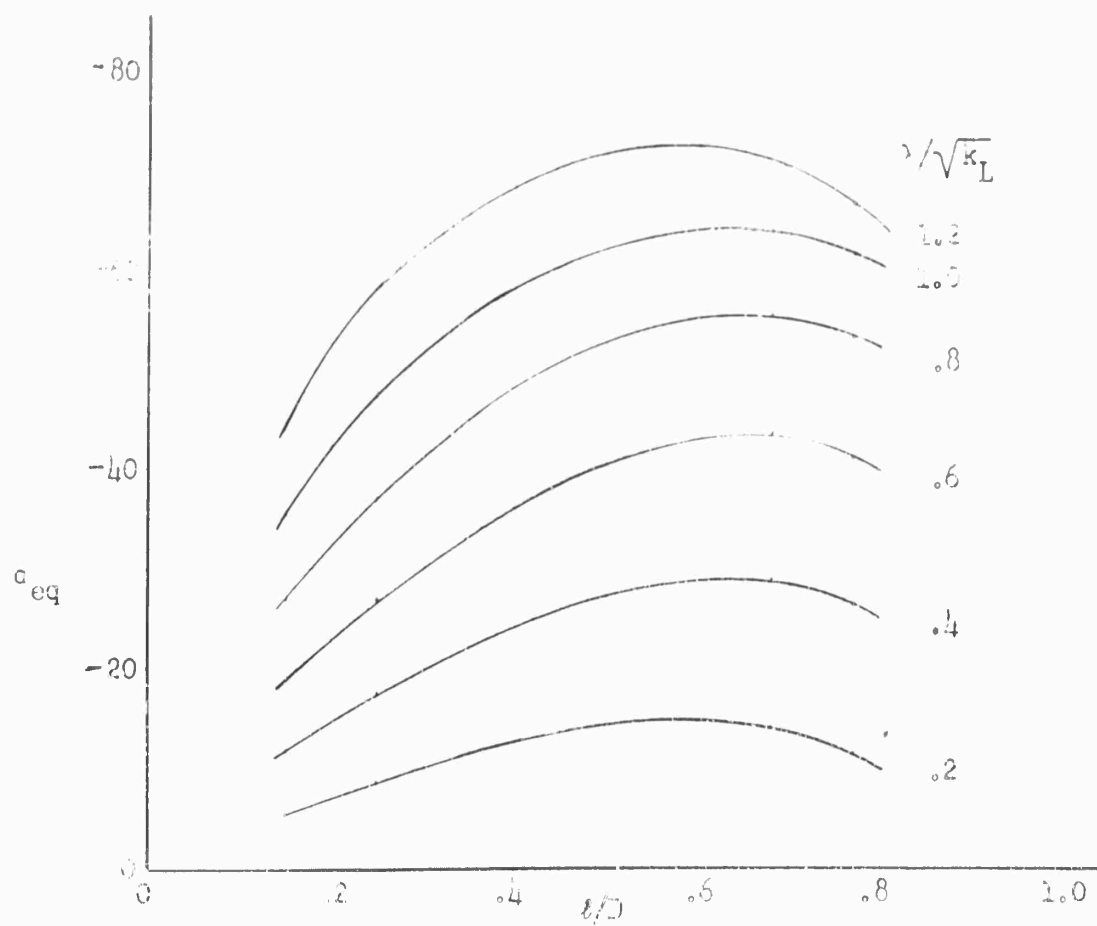
FIGURE 8: DUCTED PROPELLER EQUILIBRIUM ANGLE OF
ATTACK IN NON-AXIAL FLOW (F = 0)
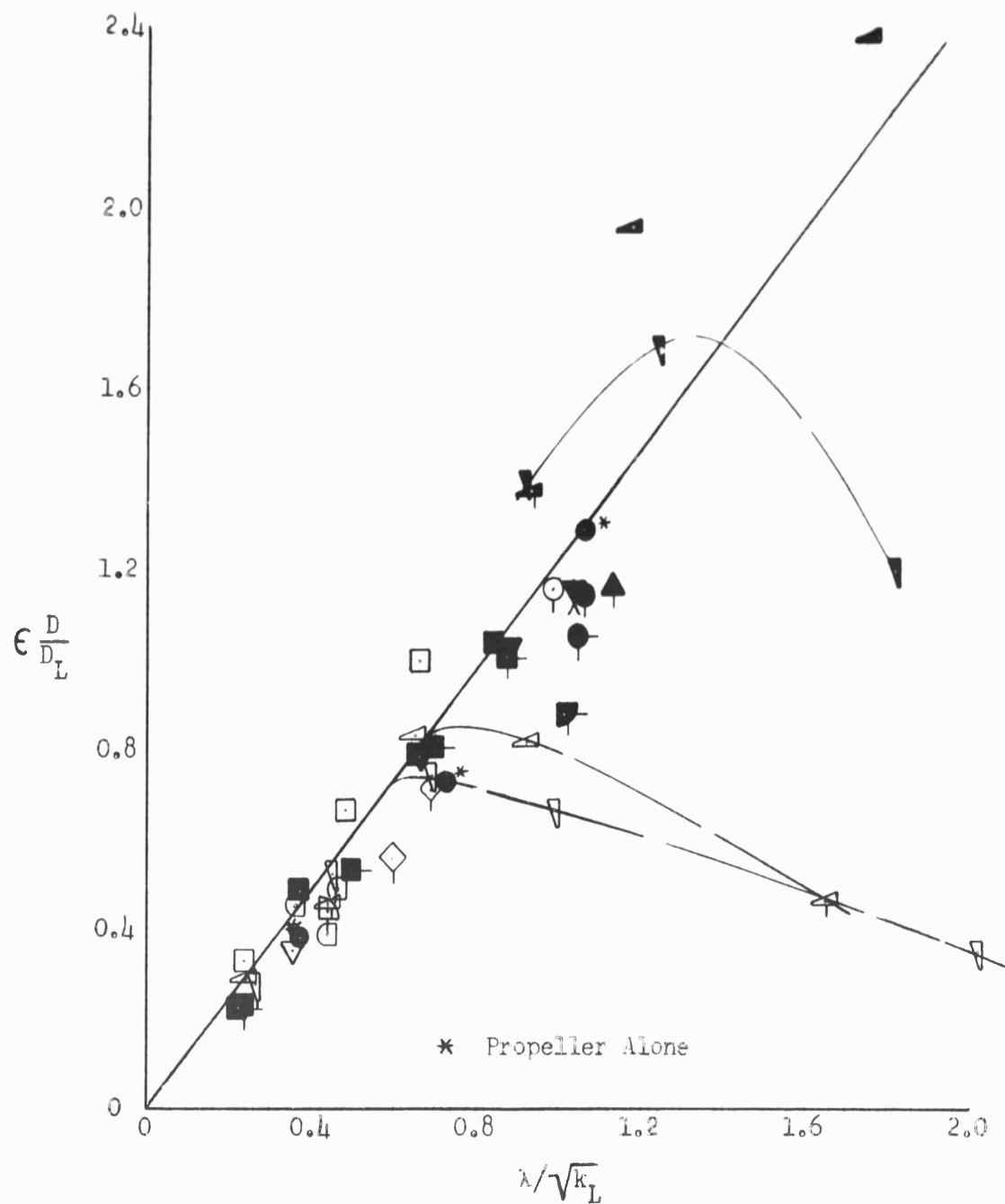
FIGURE 9: COMPARISON OF EQUIVALENT LIFT/DRAG RATIO OF DUCTED PROPELLERS IN NON-AXIAL FLOW AT EQUILIBRIUM (F = 0)
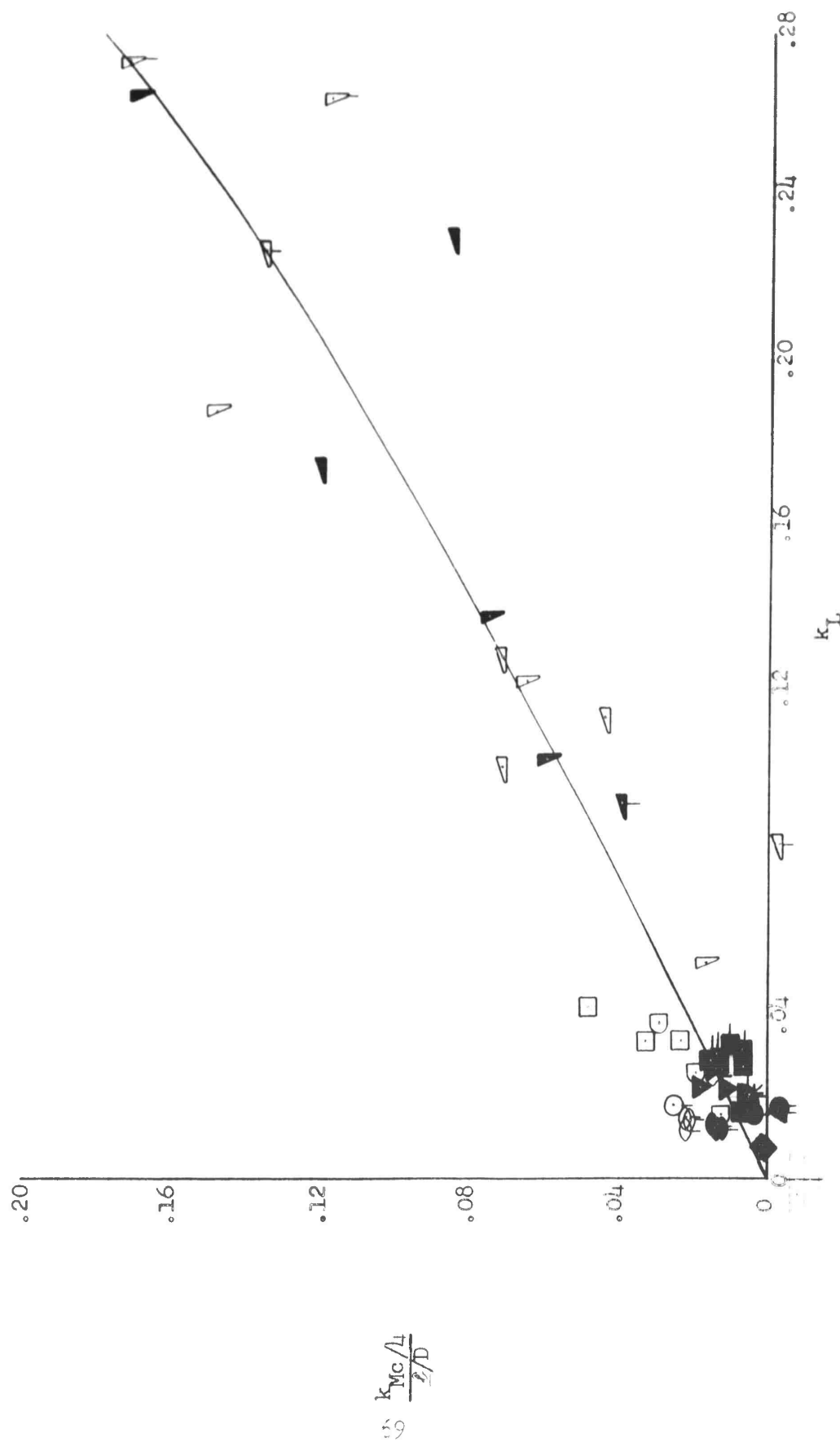
68

FIGURE 19 COMPARISON OF DUCTED PROPELLER PITCHING MOMENT COEFFICIENT AT EQUILIBRIUM (F = 0)

$$\frac{k_{Mc/4}}{\ell/D}$$

$k_L$
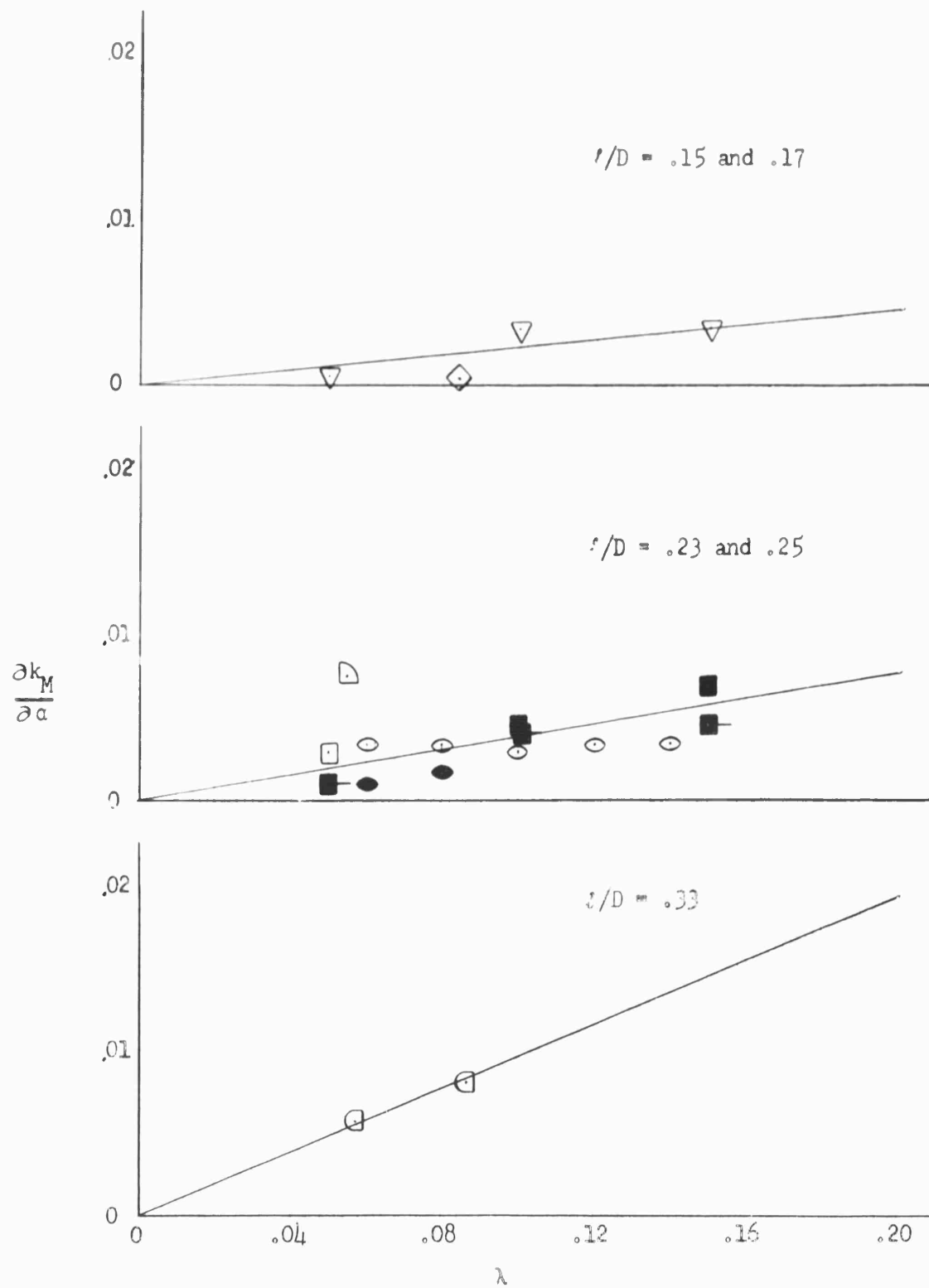
FIGURE 11(a). COMPARISON OF DUCTED PROPELLER AVERAGE
ANGLE-OF-ATTACK STABILITY DERIVATIVE

FIGURE 11(b)

$\frac{\partial k_M}{\partial a}$

$s/D = .77$
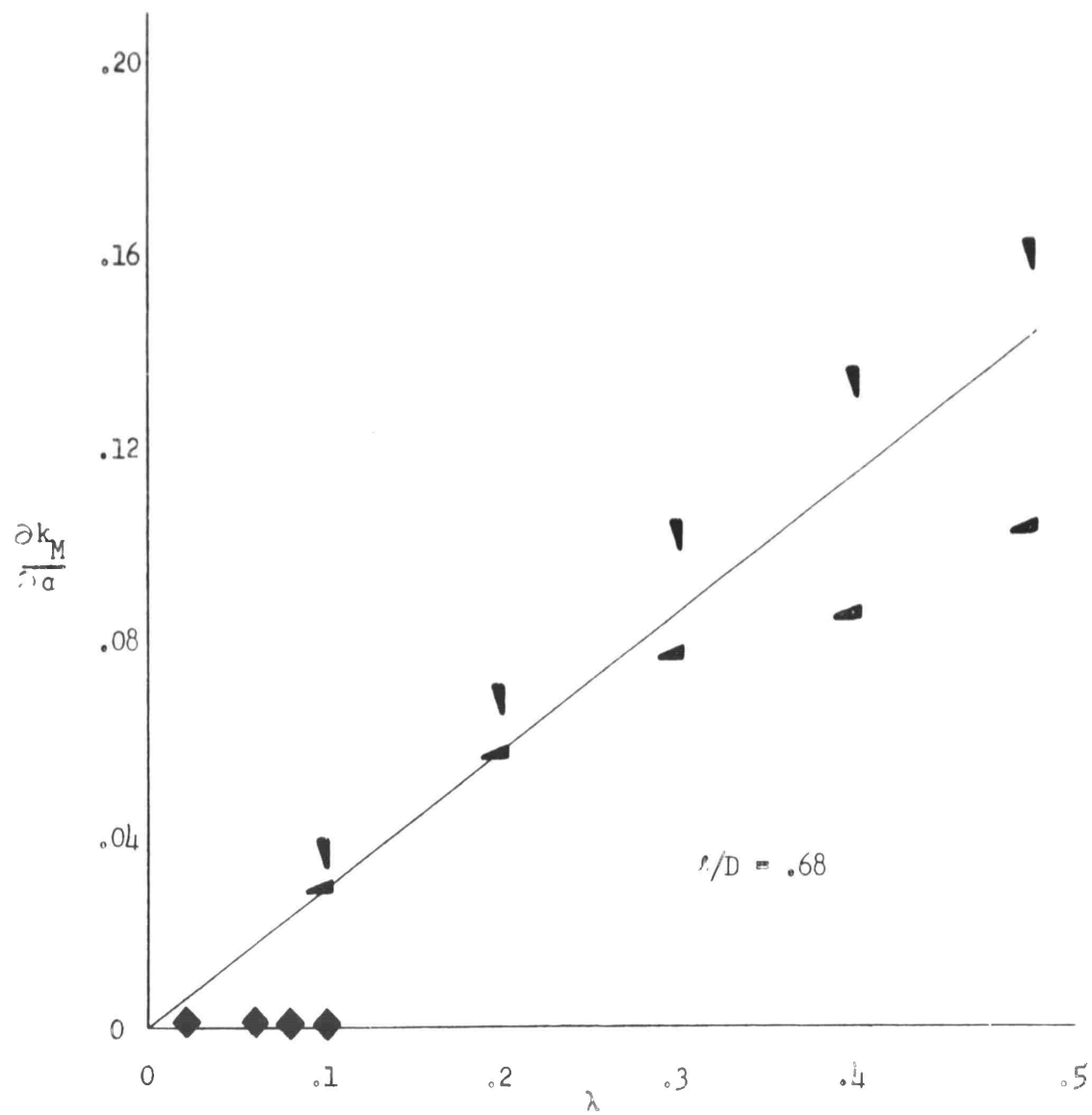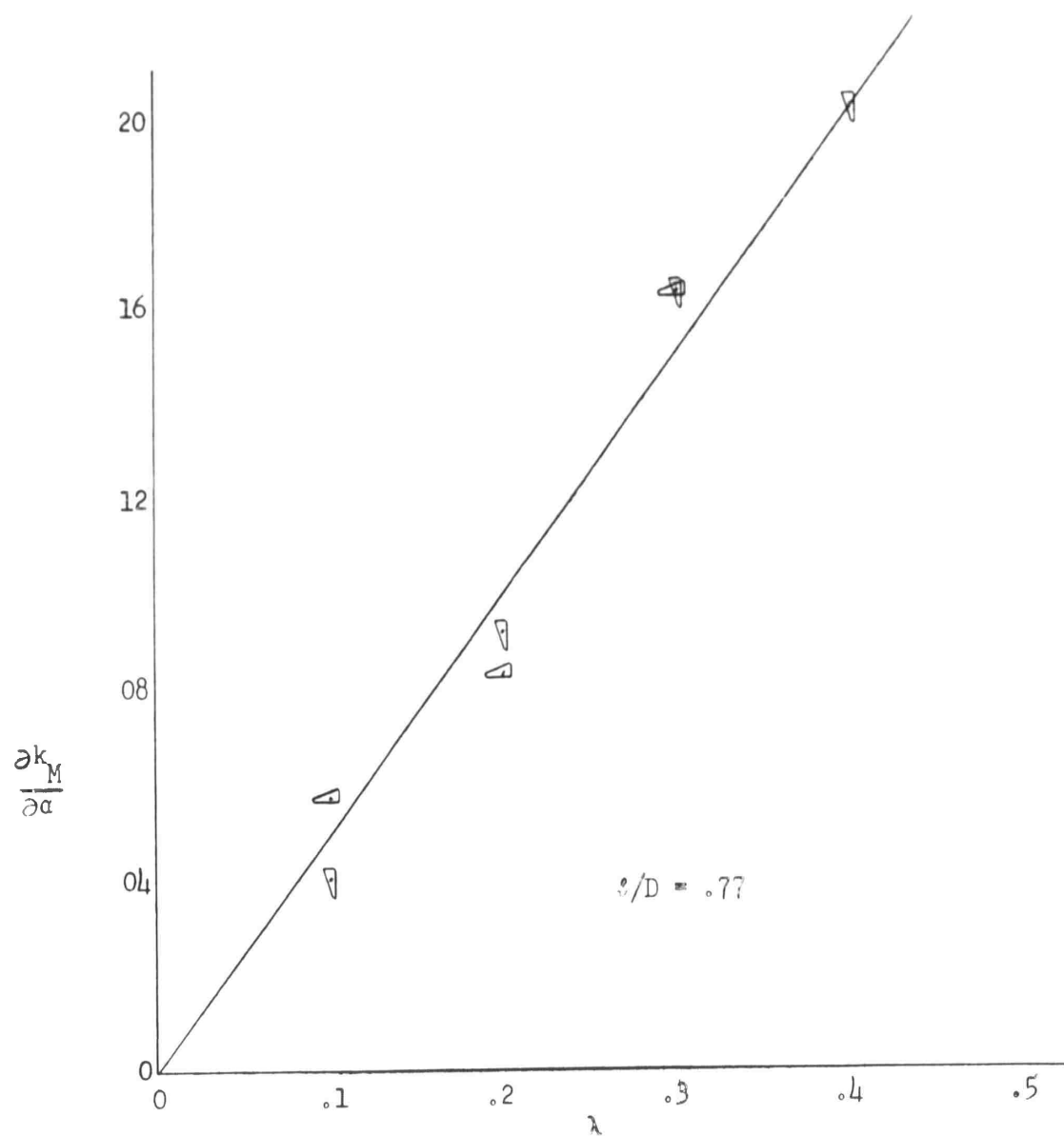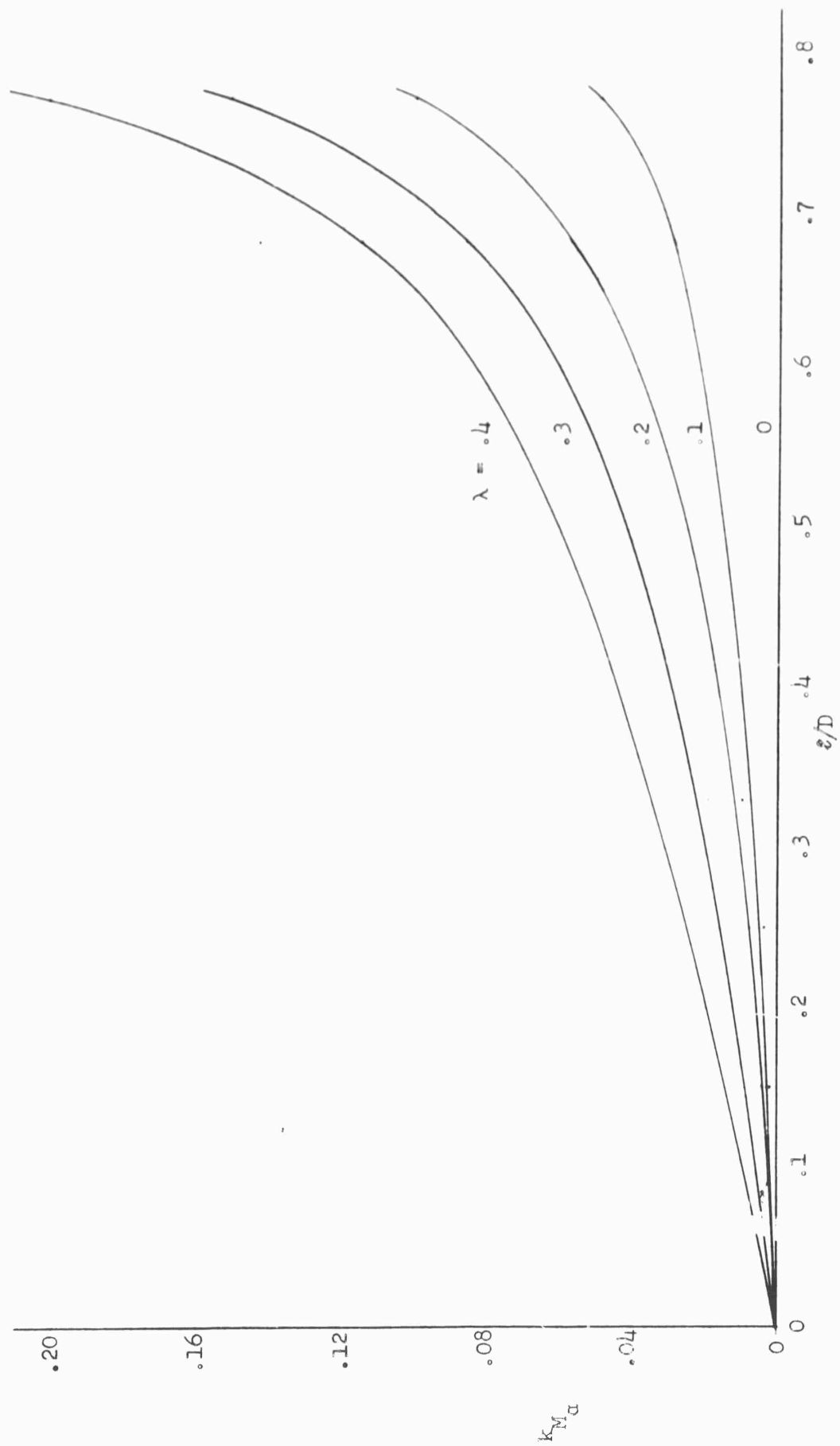
FIGURE 11(a)

FIGURE 12: DUCTED PROPELLER AVERAGE ANGLE-OF-ATTACK STABILITY DERIVATIVE
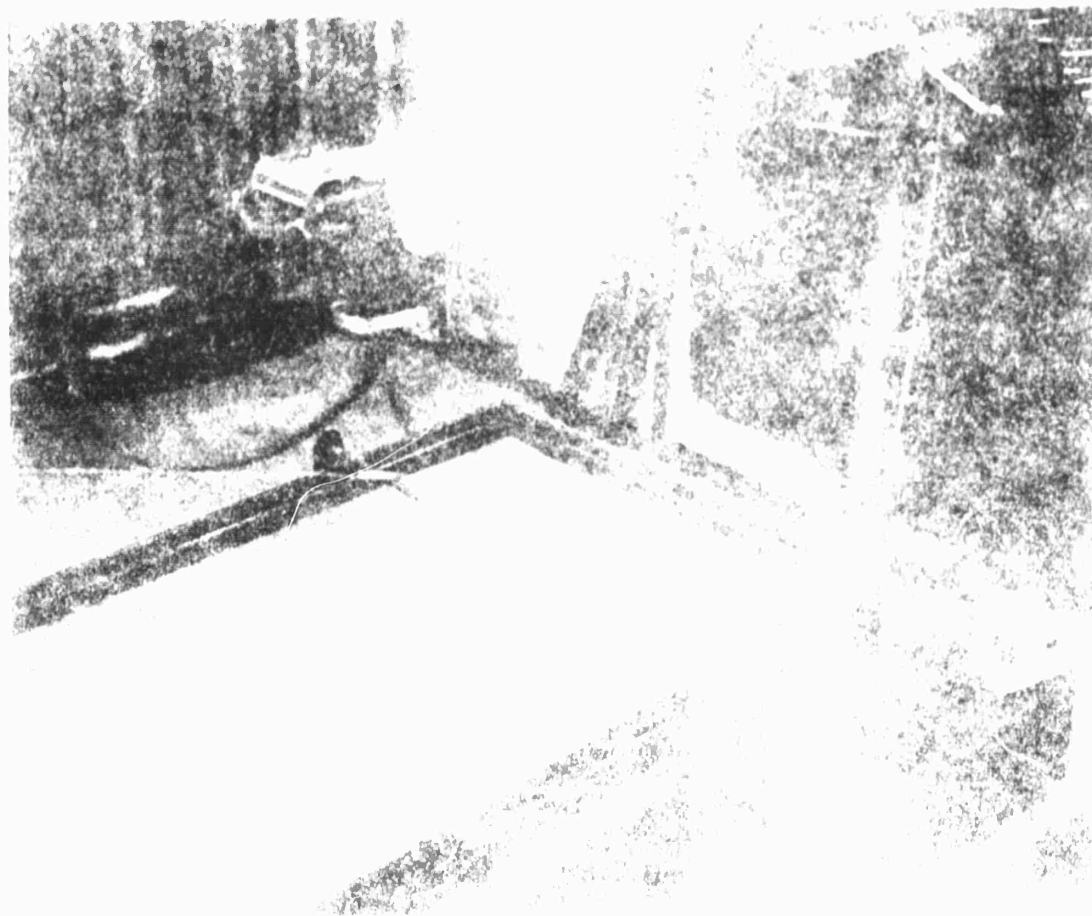
| Model | θ |
|-------|-----|
| 1 | 0 |
| 2 | 3 |
| 3 | 6 |
| 4 | 9 |
| 5 | 12 |
| 6 | 15 |
| 7 | 18 |
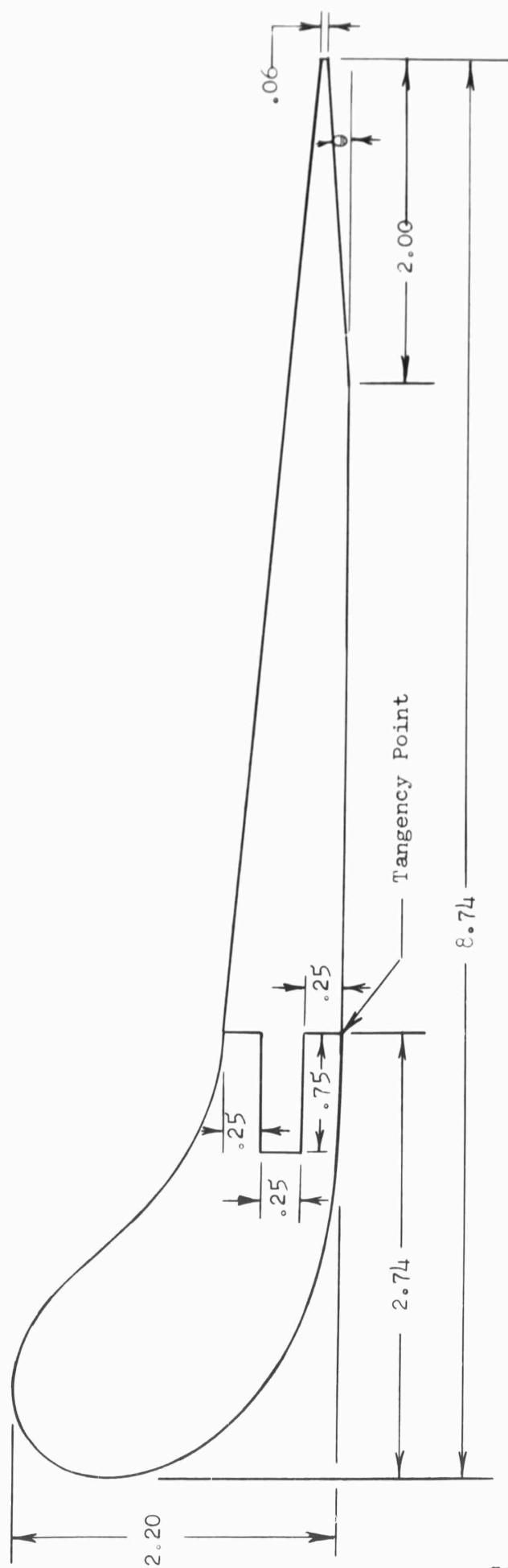
Model machined from
2.0 inch phenolic sheet.

FIGURE 14. PHYSICAL CHARACTERISTICS OF DUCTS FOR TWO-DIMENSIONAL STATIC MODELS
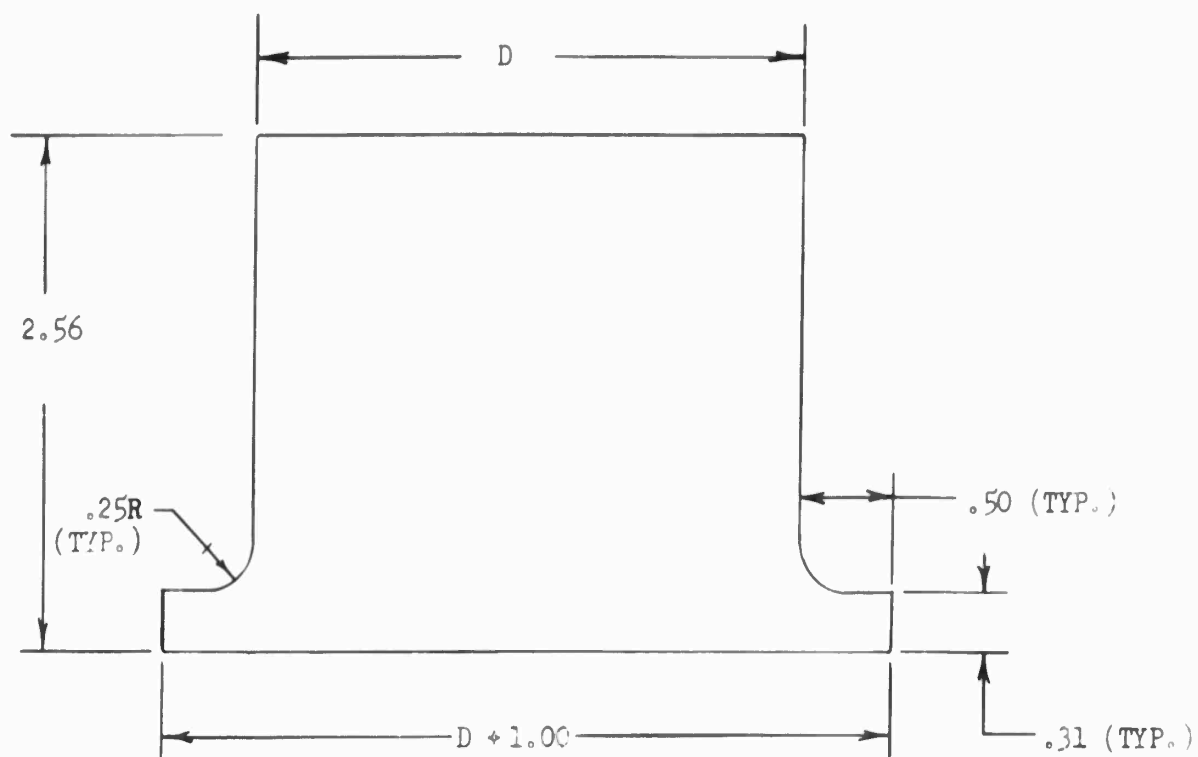
Blades machined from
0.060 transparent acrylic sheet

| Model | D |
|-------|---|
| A | 1 |
| B | 2 |
| C | 3 |
| D | 5 |

FIGURE 15: PHYSICAL CHARACTERISTICS OF IMPELLER BLADES
FOR TWO-DIMENSIONAL STATIC MODELS
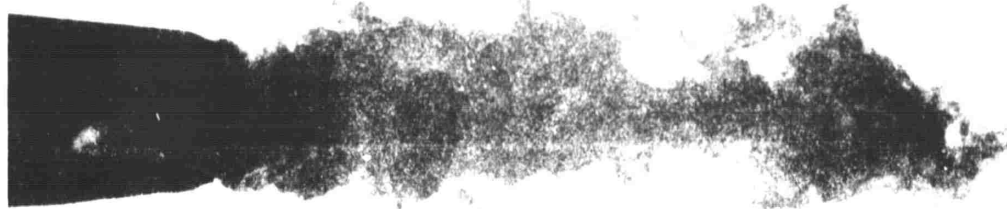
Duct 3

FIGURE 16(a): WAKE PATTERN ... ... ... ... PROPELLER
IN STATIC ...

Duct 6

Duct 6

FIGURE

Duct 2

Duct 3

Duct 4
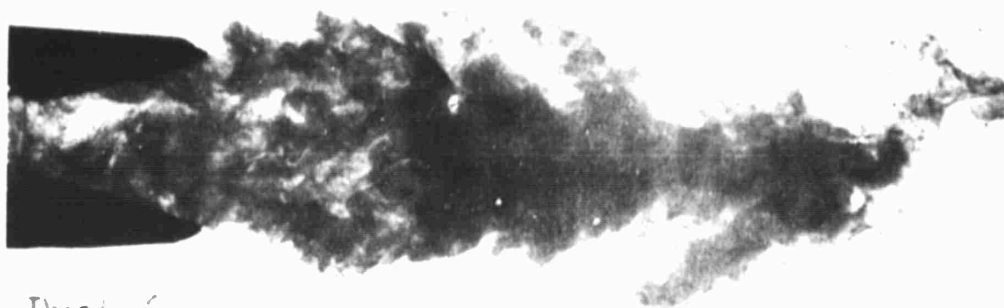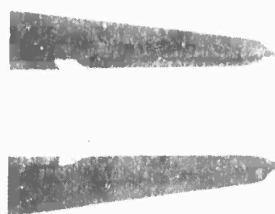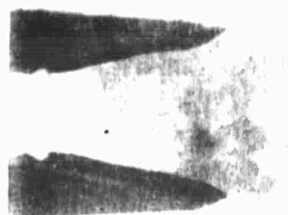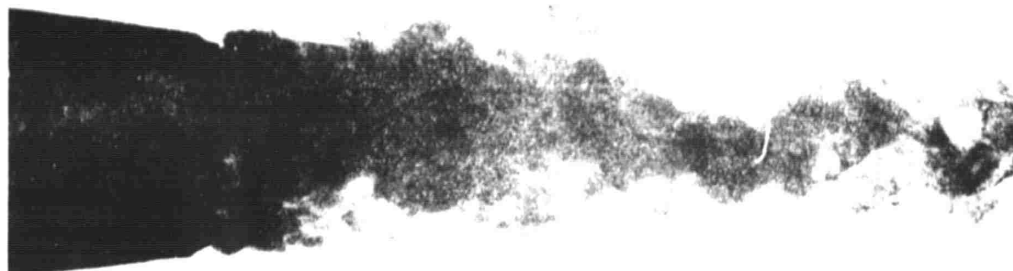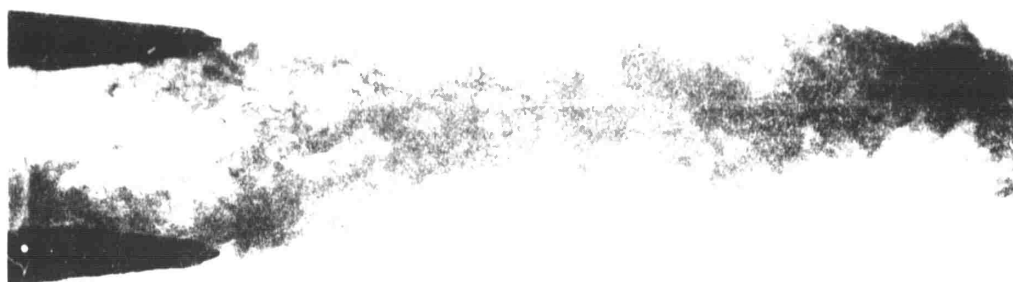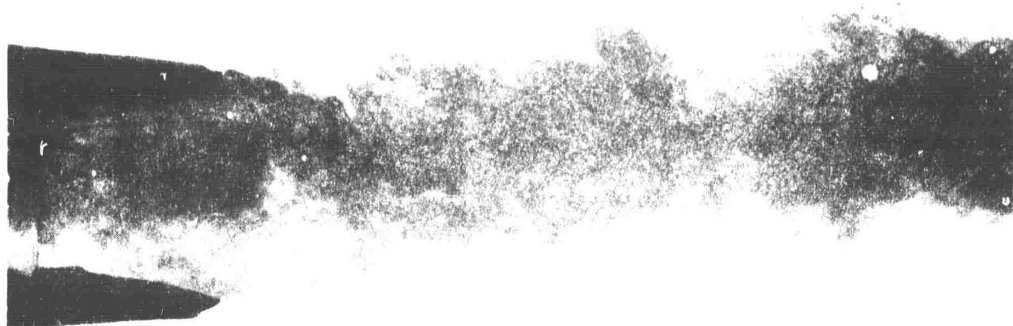
FIGURE 17(a): WAKE PATTERN OF SHROUDED PROPELLER
IN STATIC FLOW CONDITION
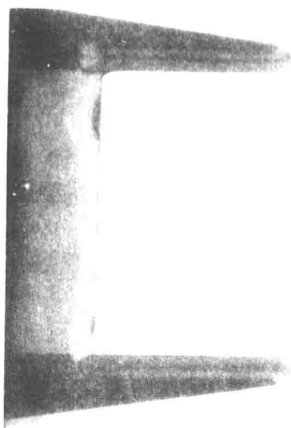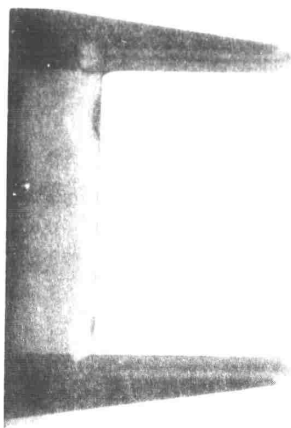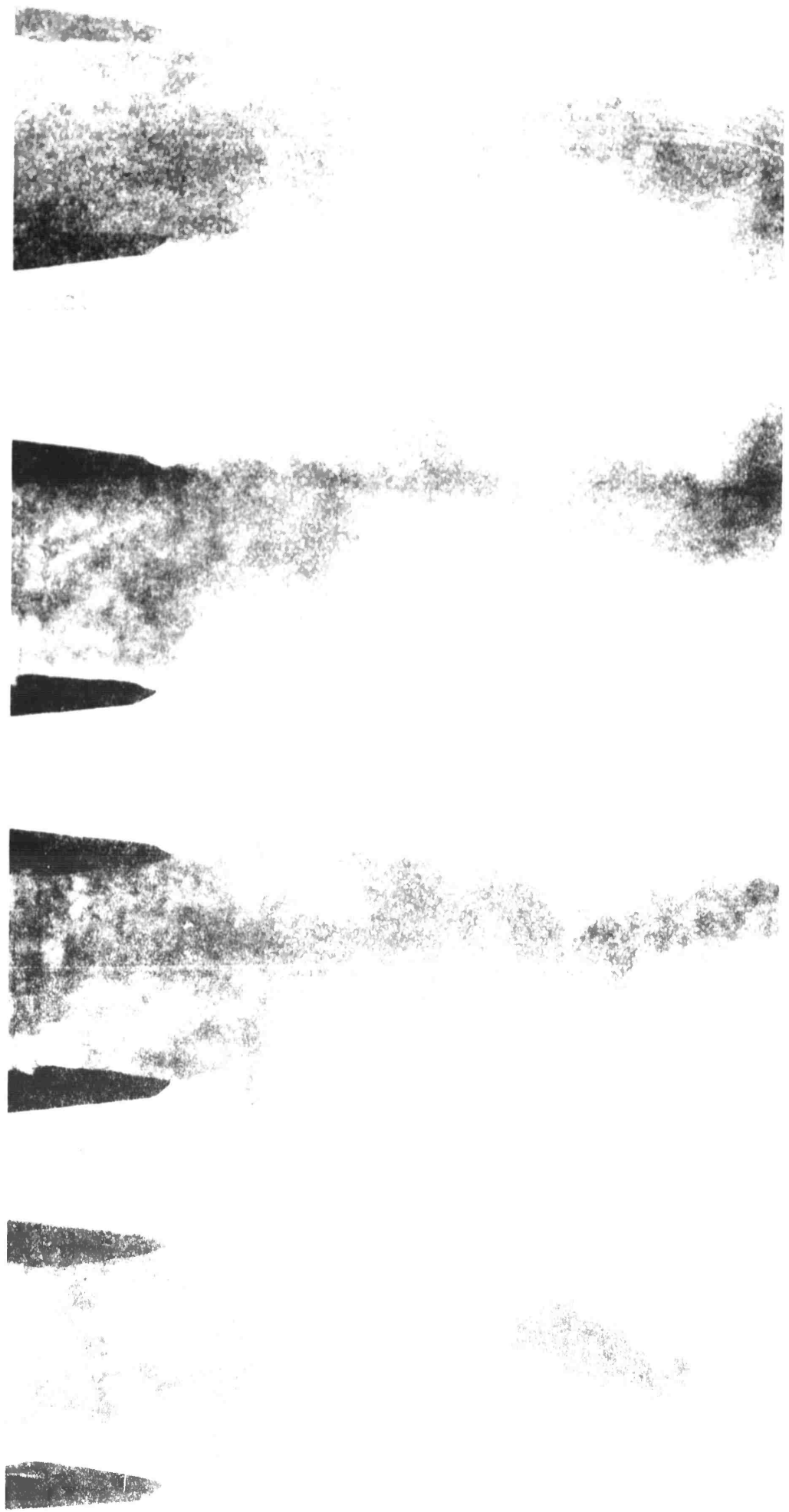
FIGURE 18(a): WAKE PATTERN                    PROPELLER
              IN ST
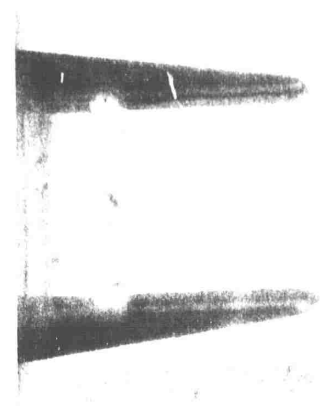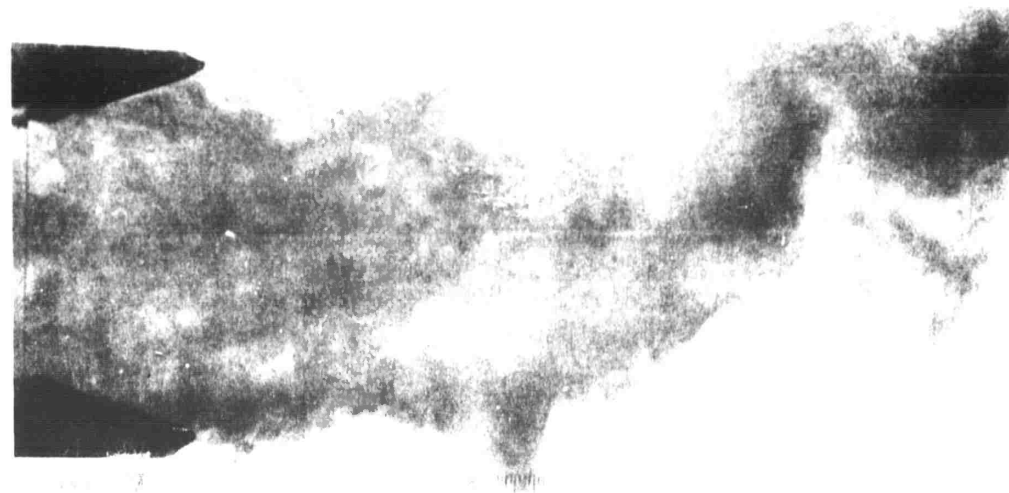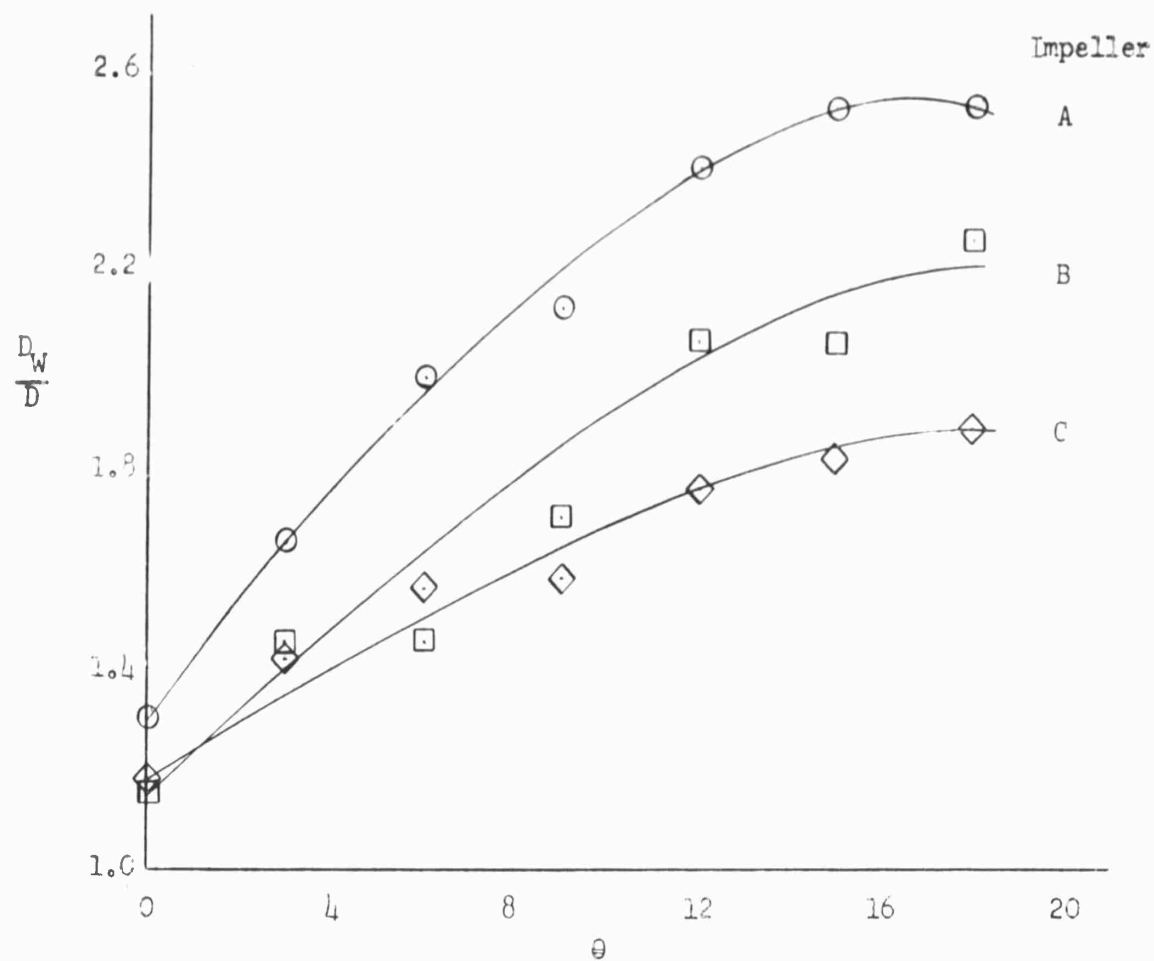
FIGURE 19: WAKE DIAMETER RATIOS OF VARIOUS TWO-DIMENSIONAL MODELS FROM VISUALIZATION WATER TESTS-STATIC FLOW

$1p/c = 1.00$

FIGURE 20:   EFFECT OF _____                    TWO-DIMENSIONAL
           _____                              _____ A        84
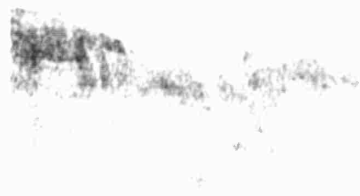
FIGURE 21:  WAKE PATTERN OF THE IMPELLER AT THE HUB IN AXIAL FLOW    85
            WITH IMPELLER 1
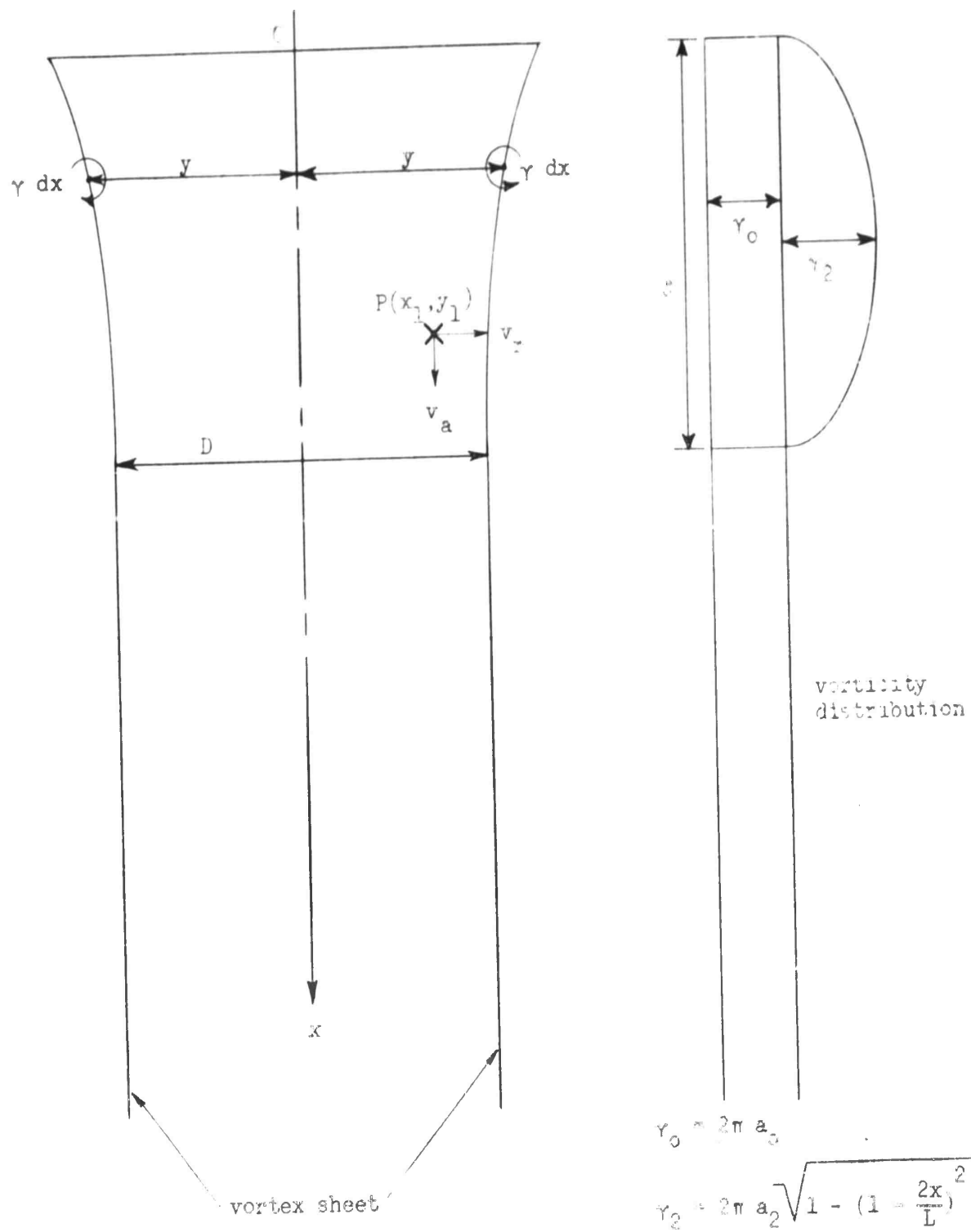
FIGURE 22: MATHEMATICAL MODEL FOR DUCT SHAPE AND
VORTICITY DISTRIBUTION

$$\gamma_0 = 2\pi a_5$$

$$\gamma_2 = 2\pi a_2 \sqrt{1 - (1 - \frac{2x}{L})^2}$$

vorticity
distribution

vortex sheet

$P(x_1, y_1)$

$\gamma\, dx$

$D$

$\gamma_0$

$\gamma_2$

$v_t$

$v_a$

$x$
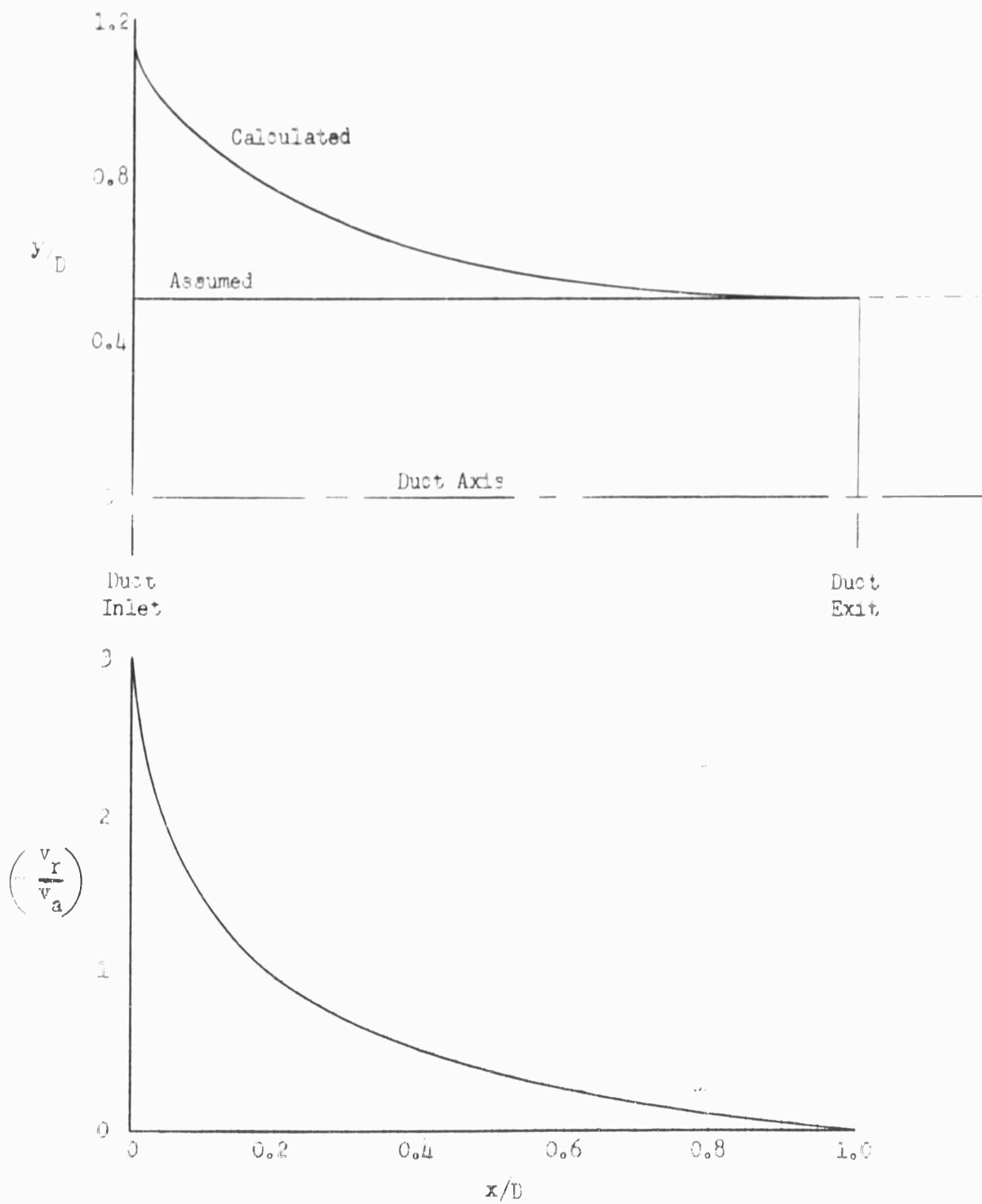
FIGURE 33: DETERMINATION OF DUCT SHAPE FOR CYLINDRICAL WAKE

FIGURE  INTERNAL SOLUTION

$\dfrac{x_p}{D} = 0.0$

Assumed

Calculated

$\dfrac{D_\infty}{D} = 1.0$

$y/D$

0.5

0.4

$\dfrac{D_\infty}{D} = 0.8$

$y/D$

0.5

0.4

$\dfrac{D_\infty}{D} = 0.2$

$y/D$

0.5

0.4

$x$
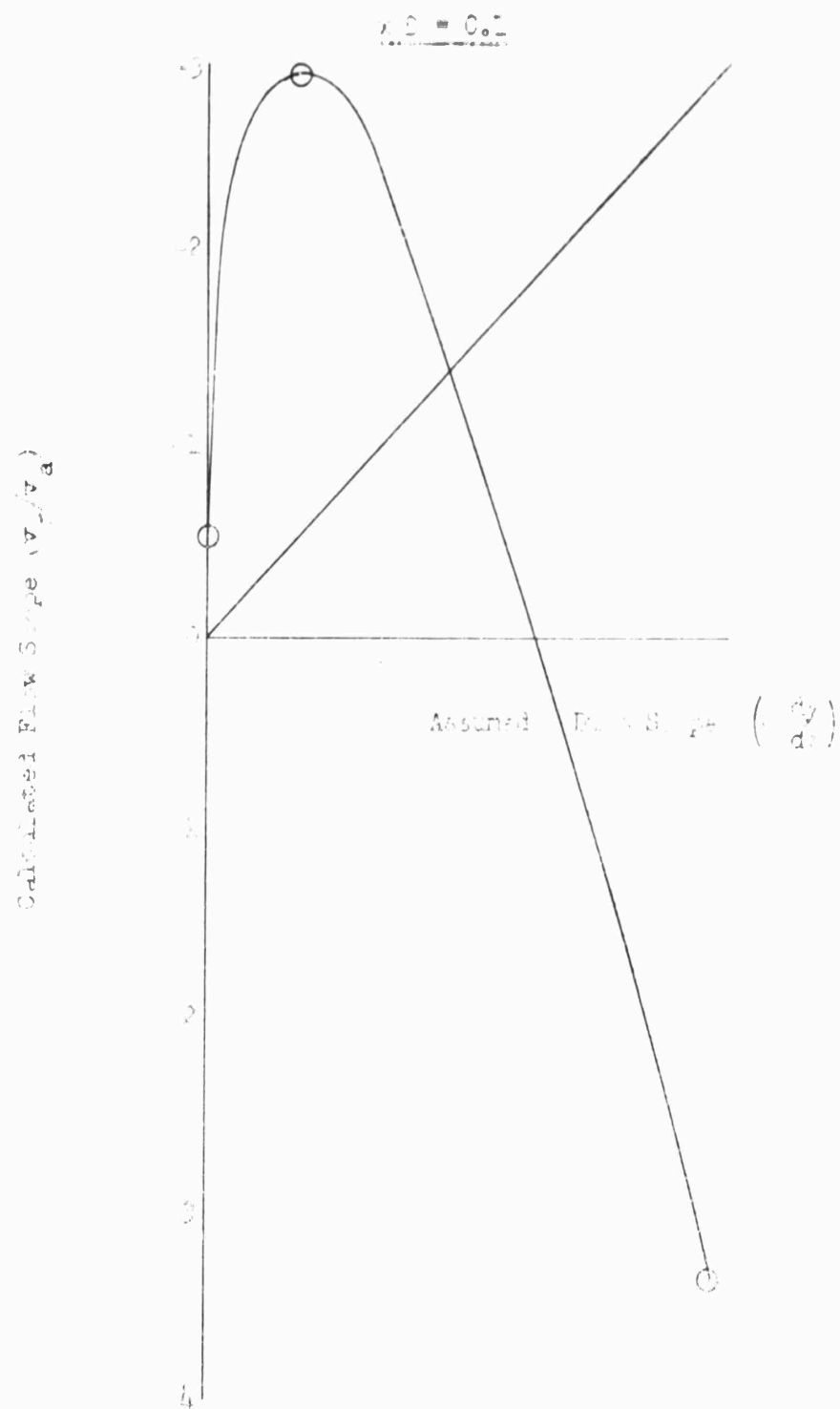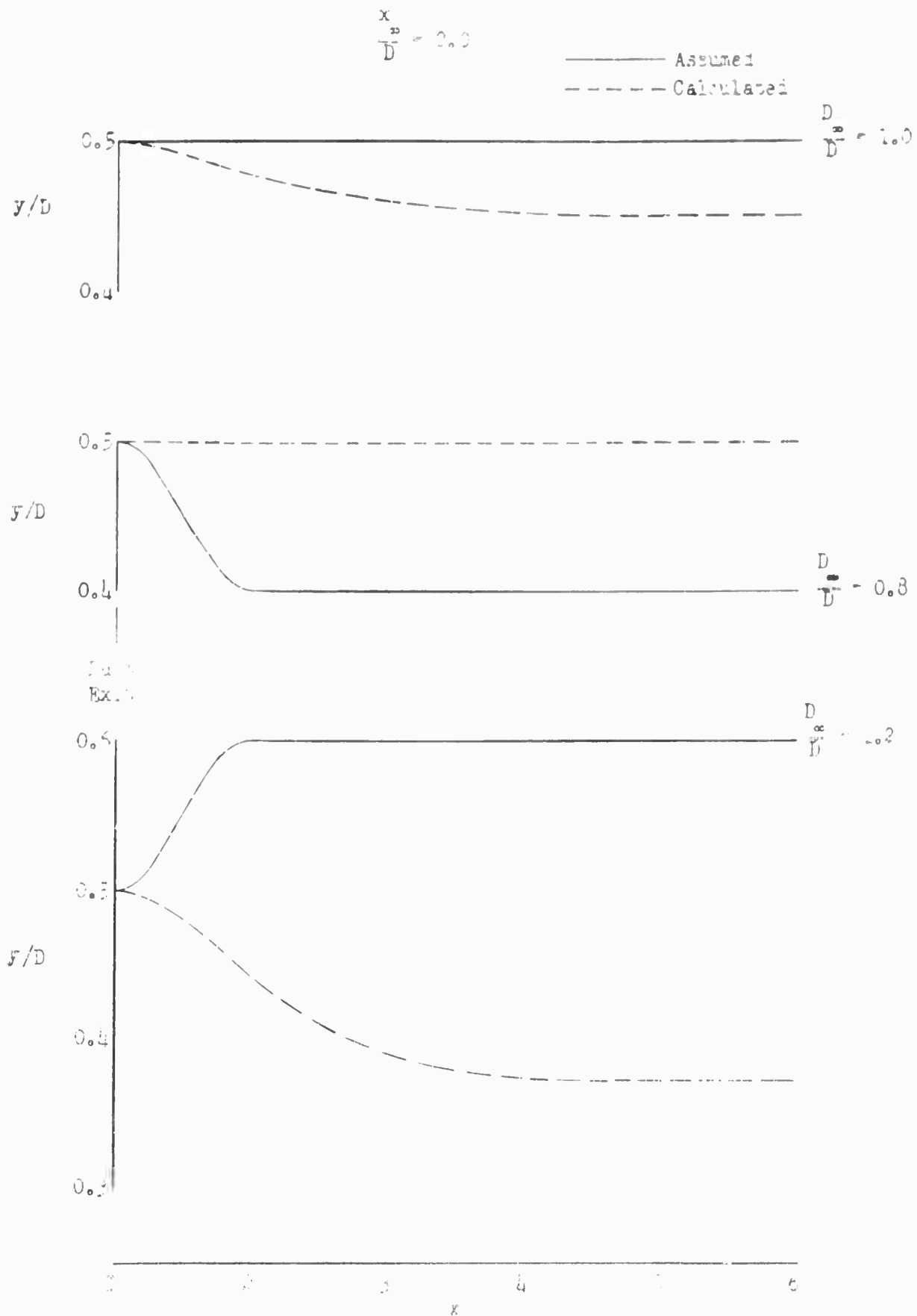
FIGURE     PRELIMINARY DETERMINATION OF WAKE SHAPE
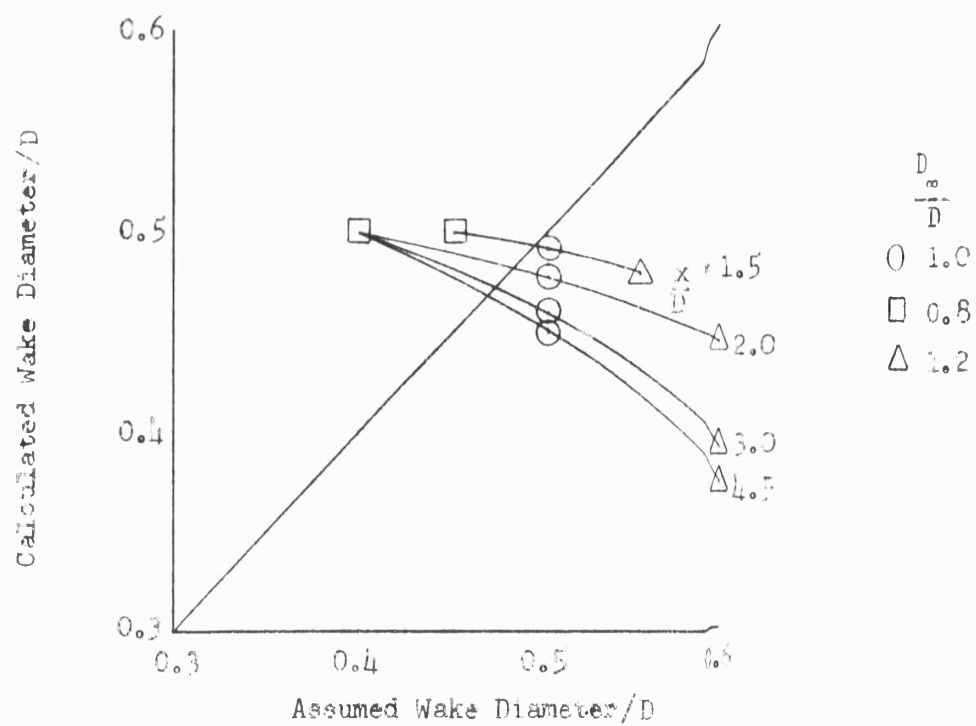FOR CALCULATED DRAG SHAPE FIGURE
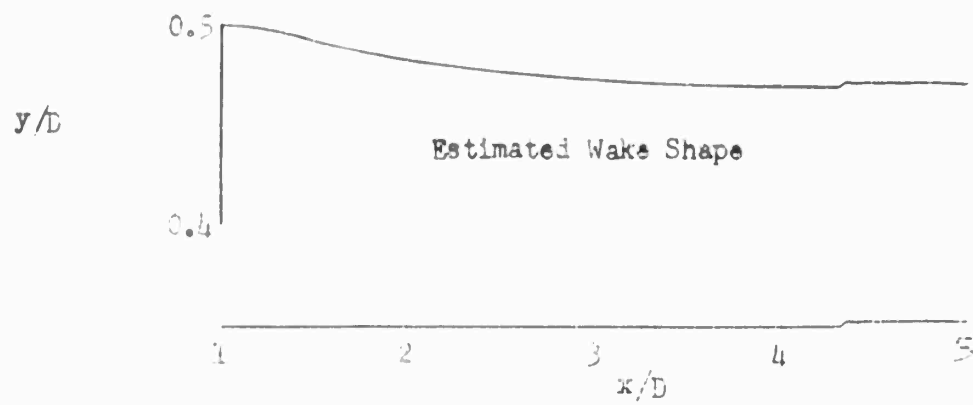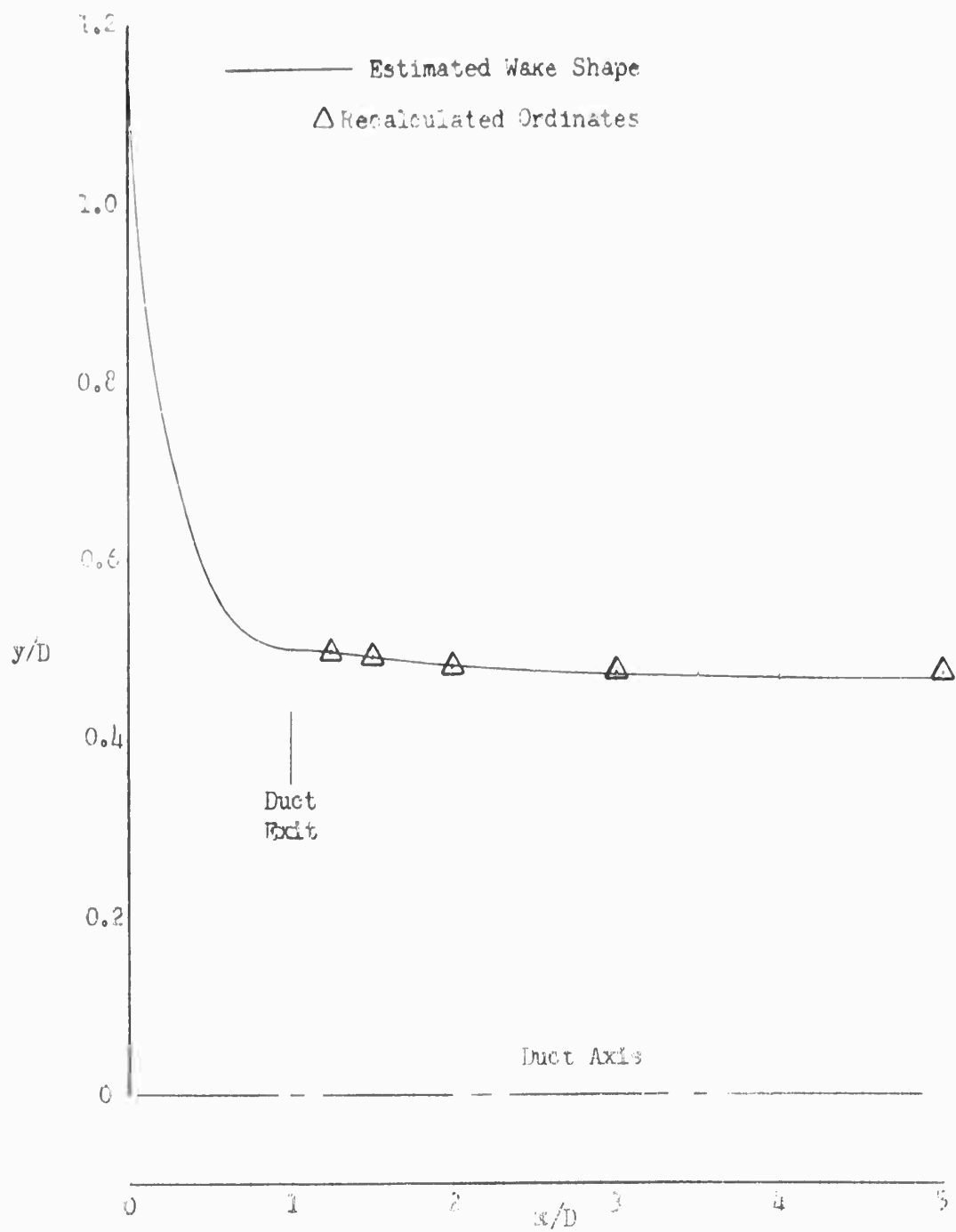
FIGURE 27:  ESTIMATION OF WAKE SHAPE

91

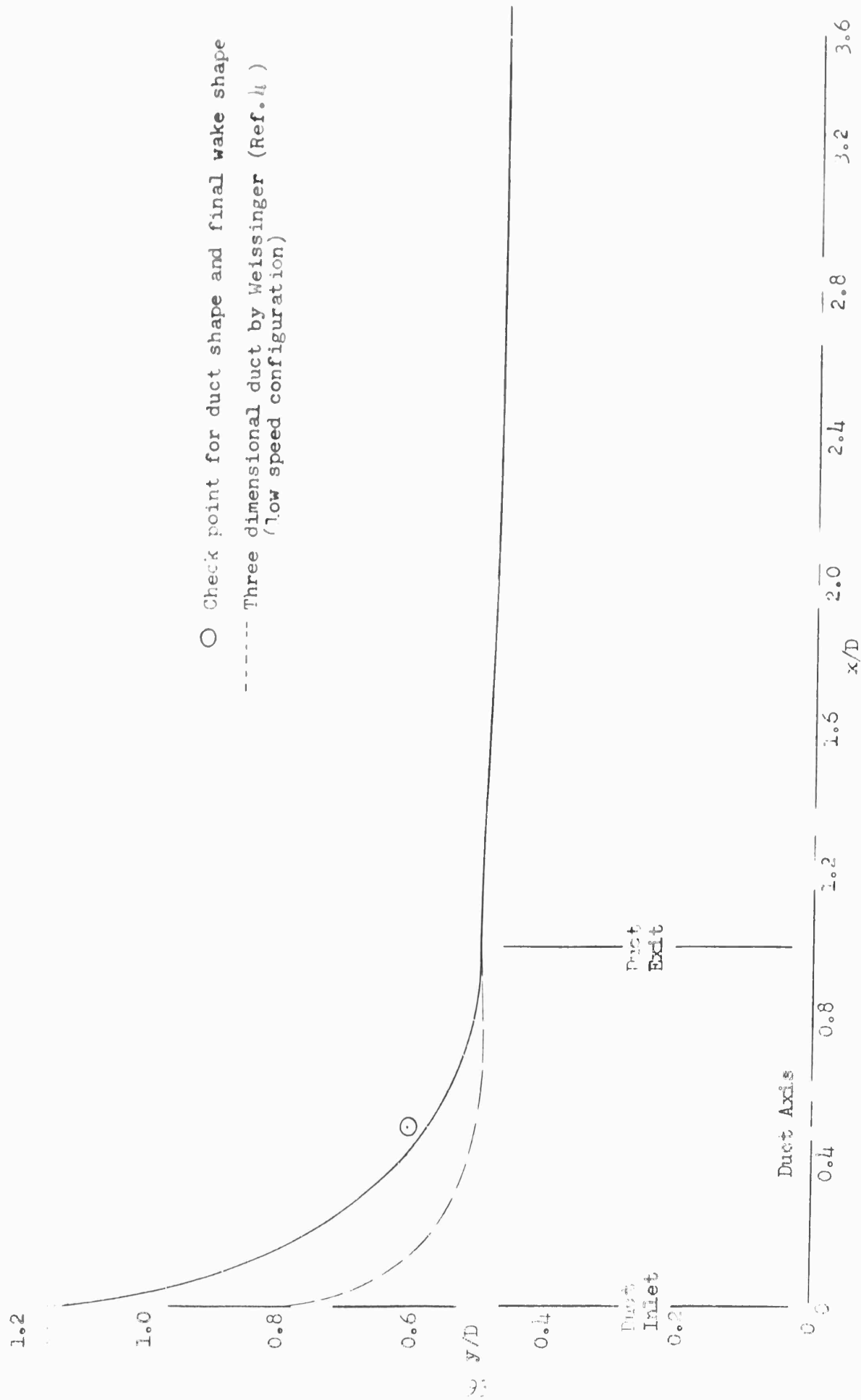FIGURE 28:  FINAL DETERMINATION OF WAKE SHAPE

FIGURE 29. REPRESENTATION OF CALCULATED DUCT SHAPE AND WAKE BOUNDARY LINE